Farm-wide Microgrid Decision Support System for the Australian Cotton Industry

by **Yunfeng Lin**

Thesis submitted in fulfilment of the requirements for the degree of

Doctor of Philosophy

under the supervision of

A/Professor Li Li

A/Professor Jiangfeng Zhang

School of Electrical and Data Engineering

Faculty of Engineering and IT

University of Technology Sydney

July 13, 2023

Certificate of Authorship / Originality

I, Yunfeng Lin, declare that this thesis is submitted in fulfilment of the requirements for the award of Doctor of Philosophy, in the School of Electrical and Data Engineering at the University of Technology Sydney.

This thesis is wholly my own work unless otherwise referenced or acknowledged. In addition, I certify that all information sources and literature used are indicated in the thesis. This document has not been submitted for qualifications at any other academic institution.

This research is supported by the Australian Government Research Training Program.

Signature: Production Note: Signature removed prior to publication.

Date: July 13, 2023

Abstract

According to Cotton Australia, energy costs in the cotton industry have increased by 350% from 2000 to 2014. Energy (electricity and diesel) costs for Australian cotton growers are expected to continue to increase by 2.9–7.2% annually until 2040. Diesel fuel provides at least 90% of the direct energy harnessed in farms. On average, irrigation accounts for 50–75% of the total direct energy consumption on-farm. An increasing number of alternative irrigation systems, for example, centre pivots and lateral move systems, in the future are expected to lead to highly significant energy costs associated with water pumping and machine operation. On the other hand, the costs of renewable energy continue to decrease, providing cotton growers with another option for energy supply. Renewable energy can be used to design the corresponding microgrids to irrigate cotton farms. The designed renewable microgrids can reduce these cotton farms' energy consumption costs and greenhouse gas emissions. This study aims to develop tailor-made renewable power planning and energy management plans for cotton-farm microgrids to secure power supply and reduce energy costs. In addition, we seek to optimize the microgrid's operation considering the uncertainty of environmental and demand factors on cotton farms to achieve cost savings for cotton stakeholders.

In this thesis, the first part presents an optimization model for cotton farm microgrid design, which explores available renewable energy sources (RESs) and energy storage options to ensure

a reliable power supply for cotton farms. By using the RES power supply, renewable energy is optimally utilized to satisfy the seasonal load demand, and the grid power is used as a backup power source. The objectives of optimization include investment cost, operating cost, and a simple payback period. A case study is undertaken using historical energy consumption data from a cotton farm in Gunnedah, New South Wales, to verify the applicability of the proposed approach.

The second part of this study presents a model predictive control (MPC) approach to the above designed cotton farm microgrid to minimize the water pumping operational cost while taking full advantage of renewable energy sources. The reason for using MPC is its ability to handle noise, disturbance, and real-time parameter changes. Microgrids at two different cotton farms are used for case studies to validate the proposed MPC methodology.

The third part of this study addresses the problem of optimizing cotton farm operating costs under uncertainties. An MPC approach is adopted to maximize the usage of renewable energy and minimize the overall water pumping cost during the cotton growth and irrigation period. To deal with the uncertainties in renewable generation, water demand, precipitation and evaporation, the operation problem of the cotton farm pumping system is formulated as a stochastic MPC problem to cater to real-time changes in uncertain weather conditions and irrigation demand. Static and dynamic scenario generation-reduction techniques are applied to obtain typical scenarios and the corresponding probabilities, which are further applied to formulate the stochastic optimization problem to deal with uncertainties.

Keywords:

Cotton Farm, Microgrid, Battery Energy Storage System, Renewable Energy, Planning and Operation, Optimization, Model Predictive Control, Water Reservoir, Uncertainty

Thesis Acknowledgements

First, I would like to express my heartfelt thanks to my two supervisors, Professor Li Li and Professor Jiangfeng Zhang, for their continuous support of my doctoral studies and research. They guided me with patience and enthusiasm, which helped me complete the research and writing of this thesis.

I would like to thank the Cotton Research & Development Corporation (CRDC) for the financial support of my study, and the General Manager, R&D Investment, Allan Williams, and his colleagues for their support and valuable advice.

I also sincerely thank my colleagues in the microgrid research group: Dr Kevin Wang, Dr Ali Azizivahed and Dr Amin Rajabi. They warmly and patiently accompanied me in discussing and solving the problems encountered in the study.

Finally, I would like to thank my family: my parents, wife and children, who have

been supporting and helping me spiritually and temporally during my study.

Yunfeng Lin

July 13, 2023

Sydney, Australia

List of Publications

Journal:

1. Y. Lin, J. Zhang, and L. Li, "A Model Predictive Control Approach to a Water Pumping System in an Australian Cotton Farm Microgrid," *Cleaner Energy Systems,* vol. 3, p. 100 026, 2022

Conference:

2. Y. Lin, J. Wang, J. Zhang, et al., "Optimal Investment Decision for Cotton Farm Microgrid Design," in *2021* 31^{st} *Australasian Universities Power Engineering Conference (AUPEC),* Perth, Australia, IEEE, 2021, pp. 1–6. doi:10.1109/AUPEC52110.2021.9597703

3. Y. Lin, J. Zhang, and L. Li, "A Model Predictive Control for Cotton Farm Microgrid Systems in Australia," in *2021* 31^{st} *Australasian Universities Power Engineering Conference (AUPEC),* Perth, Australia, IEEE, 2021, pp. 1–6

4. Y. Lin, J. Zhang, L. Li, et al., "A Model Predictive Control Approach for Cotton Farm Microgrid Operation Under Uncertainties," in *2022* 32^{nd} *Australasian Universities Power Engineering Conference (AUPEC),* Adelaide, Australia, IEEE, 2022, pp. 1–6

Journal (under review):

1. Y. Lin, J. Wang, J. Zhang, et al., "Microgrid Optimal Investment Design for Cotton Farms in Australia," *International Journal of Energy and Power Engineering,* 2022, (1^{st} round review)

2. Y. Lin, L. Li, J. Zhang, et al., "A Scenario-based Stochastic Model Predictive Control Approach for Microgrid Operation at an Australian Cotton Farm Under Uncertainties," *Energy,* 2022, (Under Review)

Collaborative Publications:

1. J. Wang, J. Zhang, L. Li, et al., "Peer-to-Peer Energy Trading for Residential Prosumers With Photovoltaic and Battery Storage Systems," *IEEE Systems Journal,* pp. 1–10, 2022. doi: 10.1109/JSYST.2022.3190976

2. J. Wang, J. Zhang, L. Li, et al., "Peer-to-Peer Energy Trading for Residential Prosumers with Battery Storage Systems," in 13^{rd} *International Conference*

on Applied Energy (ICAE2021), Bangkok, Thailand, 2021

Contents

List of Figures

List of Tables

List of Abbreviation

DMPC Distributed Model Predictive Control

ESS Energy Storage System

FIT Feed-in Tariff

IMG Islanded Microgrid

GA Genetic Algorithm

GMG Grid-connected Microgrid

MG Microgrid

PV Photovoltaic

RES Renewable Energy Source

SoC State-of-Charge

TOU Time-of-Use

VSD Variable Speed Drive

TDH Total Dynamic Head

Chapter 1

Introduction

1.1 Background of cotton farm and microgrid

The cotton industry is one of Australia's largest export earners in rural areas and provides thousands of job opportunities in Australia [1]. In 2019, more than 10,000 people were employed on Australian cotton farms, and cotton growers reported that they spent 93% of their business expenses in [2].

However, cotton cultivation is an energy-intensive industry, and the international cotton market is highly competitive and transparent. Therefore, the continuously rising energy cost has become a critical barrier to the cotton industry's development. In addition, conventional energy sources are unsustainable. In the last couple of decades, the prices of fossil fuel and electric grid energy have continued

to rise, which is the main reason for the rising costs of cotton products.

On the other hand, renewable energy is recognized as a cost-effective source of power generation. Renewable energy sources (RESs), such as solar, wind, and biomass, have the advantages of abundant forms of energy, less emission, low maintenance cost and lower ecological impact, Thus, they have increasingly been used in rural areas. Furthermore, renewable energy technology is more and more mature, and the investment cost is continuously reducing. As a result, the demand for photovoltaic (PV) and battery storage installation in Australia is also increasing. The number of microgrid (MG) systems composed of RESs, energy storage units and traditional energy sources is increasing in the Australian agriculture sector and has brought enormous benefits to agricultural development [1]. There are a number of initiatives in Australia to promote the use of MGs in the cotton farming industry. For example, the Cotton Research and Development Corporation (CRDC) has supported a number of projects focused on the deployment of MGs in the cotton industry. These projects have aimed to demonstrate the feasibility and benefits of MGs in the context of Australian agriculture, with the goal of encouraging wider adoption of MG technology.

In order to take advantage of these abundant natural resources, proper planning is essential for ensuring the sustainability of a cotton farm MG, and can help to

maximize the benefits of the technology for the cotton farm owners. However, the energy consumption of cotton irrigation is different from residential electricity consumption, as irrigation demand is not constant and occurs seasonally. Irrigation must match the growth period of cotton. In other words, this study needs to design a properly sized MG for cotton farms. Too large an MG will increase capital costs, while too small an MG will not help reduce operating costs. Therefore, it is essential to find an optimal size for the MG to accommodate the seasonal and high-power demands of cotton farm irrigation pumps. In addition, during the non-irrigation period, the reasonable use of excess energy to shorten the payback period also needs to be considered.

Although the MG can be equipped with renewable generations to reduce the fossil fuel-based energy cost, the overall MG must be properly operated in order to save more energy costs whilst meeting the cotton farm load demand. Furthermore, when the RES-based MG is properly operated, the RES can be used more efficiently, and more operating costs can be saved. The traditional irrigation method of most Australian cotton farmers is to pump groundwater or river water into a turkey nest dam and then use gravity (siphon) to flood irrigation into the cotton field [3]. The traditional operation of pumping water to the dam is based on the farmer's experience, which varies a lot from one person to another. There-

fore, the unit irrigation energy costs of different cotton farms are also different. When renewable energy-based MGs are built for these cotton farms, optimized MG operation will reduce the unit irrigation energy cost significantly. A variety of optimized operation technologies have been adopted to solve energy dispatch problems in order to save operating costs. To further reduce operating costs, advanced operation technologies are often required to properly operate the cotton farm MG.

Model predictive control (MPC) is a control technique that is used to optimize the operation of a system [4]. MPC can also be used to optimize the operation of the MG by properly dispatching controllable energy sources. MPC has several advantages over traditional control methods, including its ability to handle complex systems and constraints, and its ability to anticipate and react to changing conditions and disturbances.

There are also uncertainty issues to be considered in the optimal operation strategies of the cotton farm MG. A number of sources of uncertainty can affect the operation of cotton farms' irrigation systems, such as weather conditions, water demand for crop growth, and intermittent RES output. These uncertainties can make it difficult to predict irrigation needs accurately and optimize pump operation strategies. So, how to optimally operate the cotton farm MG given

various uncertainties coming from PV generation, rainwater, and irrigation demand is a challenging question. Scenario-based MPC is a control strategy that involves considering multiple possible future scenarios and choosing the control action that is optimal for the most likely scenarios. [5]. In scenario-based MPC, the prediction is based on multiple possible future scenarios, rather than a single scenario. The control action is chosen to be optimized based on the occurrence probabilities of each scenario. By considering a range of possible scenarios, the controller can adapt to changes in the system and provide robust performance under uncertainties. Scenario-based MPC also can optimize the control action over a longer time horizon to improve system performance. Thus, scenario-based MPC can be applied in cotton farm MG systems to improve the performance of MG under uncertain scenarios.

1.2 Research objectives and overview

This thesis aims to optimally design and operate an MG with renewable energy sources (e.g., PV, wind turbine, and/or battery storage system) in order to save energy costs and utilize renewable energy for sustainability and environmental protection purposes in Australia cotton farms.

The specific research objectives of this thesis are:

1. Optimally design an MG by integrating renewable energy resources to satisfy farmers' irrigation needs while keep investment and payback period minimum.

2. Apply the MPC approach to build a cost-minimization model for the above designed cotton farm MG under both the grid-connected and islanded operation modes, taking into account water irrigation needs, renewable energy sources, and grid feed-in tariff.

3. Propose static and dynamic scenario-based uncertainty models and apply the scenario generation and reduction techniques to minimize the operation cost of a cotton farm MG under uncertainties during an irrigation period.

1.3 Thesis organization

Chapter 2 provides a comprehensive review of the literature relevant to the overall aim. This includes different aspects related to the irrigation energy for cotton farms, optimal MG investment design and operation, MPC-based operation, and MG operation under uncertainty.

Chapter 3 solves the optimization problem of the cotton farm RESs planning. An irrigation pump model is presented for a cotton farm that is grid-connected.

A multi-objective methodology is designed to minimize the operational cost, the investment cost, and the payback period of a grid-connected MG.

This chapter leads to the following publications:

- Y. Lin, J. Wang, J. Zhang, et al., "Optimal Investment Decision for Cotton Farm Microgrid Design," in *2021 31st Australasian Universities Power Engineering Conference (AUPEC)*, Perth, Australia, IEEE, 2021, pp. 1–6. doi:10.1109/AUPEC52110.2021.9597703

- Y. Lin, J. Wang, J. Zhang, et al., "Microgrid Optimal Investment Design for Cotton Farms in Australia," *International Journal of Energy and Power Engineering,* 2022, (1st round review)

Chapter 4 proposes an MPC approach to operating a cotton farm MG to efficiently utilize RESs and achieve the minimal operational cost of irrigation pumps. Disturbance from evaporation, seepage and rain is studied to illustrate the robustness of the MPC approach. MGs at two different cotton farms are used for case studies to validate the proposed MPC methodology.

This chapter leads to the following publications:

- Y. Lin, J. Zhang, and L. Li, "A Model Predictive Control for Cotton Farm Mi-

crogrid Systems in Australia," in *2021 31st Australasian Universities Power Engineering Conference (AUPEC),* Perth, Australia, IEEE, 2021, pp. 1–6

- Y. Lin, J. Zhang, and L. Li, "A Model Predictive Control Approach to a Water Pumping System in an Australian Cotton Farm Microgrid," *Cleaner Energy Systems,* vol. 3, p. 100 026, 2022

Chapter 5 presents a scenario-based MPC approach to minimize the operational cost of a cotton farm MG under uncertainties. To deal with the uncertainties in renewable generation, water demand, precipitation and evaporation, scenario generation and reduction techniques are applied to obtain typical scenarios with their probability. Then an MPC approach is adopted based on the obtained static and dynamic scenarios to cater for real-time changes in uncertain weather conditions and irrigation demand.

This chapter leads to the following publications:

- Y. Lin, J. Zhang, L. Li, et al., "A Model Predictive Control Approach for Cotton Farm Microgrid Operation Under Uncertainties," in *2022 32nd Australasian Universities Power Engineering Conference (AUPEC),* Adelaide, Australia, IEEE, 2022, pp. 1–6

- Y. Lin, L. Li, J. Zhang, et al., "A Scenario-based Stochastic Model Predictive

Control Approach for Microgrid Operation at an Australian Cotton Farm Under Uncertainties," *Energy,* 2022, (Under Review)

Finally, Chapter 6 summarises the results and implications of this thesis and provides recommended directions for future studies.

Chapter 2

Literature Review

This chapter presents the literature review on the relevant background, optimal MG planning, and MG operation.

2.1 Cotton industry in Australia

Cotton is one of Australia's largest rural exporters and helps support the development of more than 152 rural communities [6]. In Australia, 77% of the cotton harvest was irrigated in 2016/2017, while the remaining 23% solely relied on rainfall [7]. Most cotton farms are located in Southern, Central, and North-Western NSW and Central and Southern Queensland, as cotton plants usually grow in zones with summer rainfall of 400–800 mm. Therefore, the traditional Australian cotton industry base is located between 45 degrees north latitude and 32 degrees

south latitude [6]. Cotton growers adopt conventional irrigation patterns to irrigate plants during their growing seasons. Fig. 2.1 shows the areas where cotton farms are concentrated in Australia.

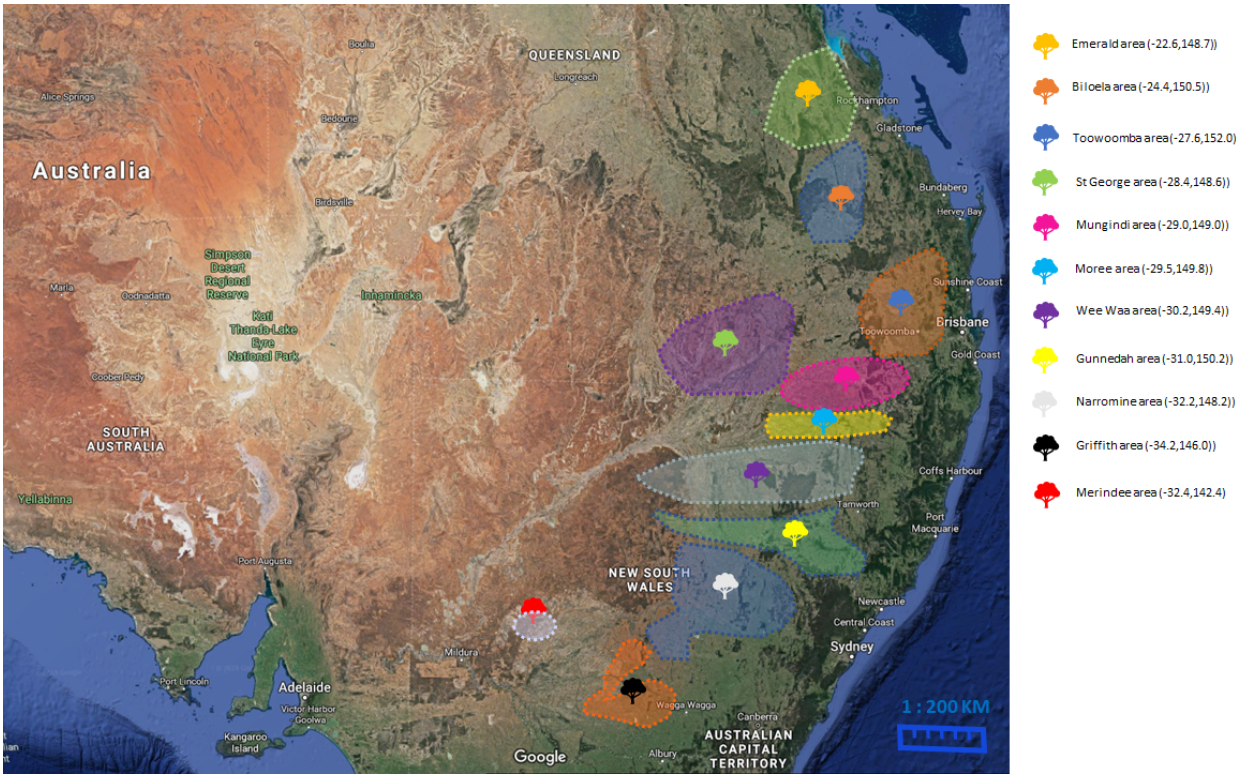

Figure 2.1: Concentrated irrigation map of Australian cotton farms (source from Google map) [6]

2.2 Energy use in the cotton industry

Cotton cultivation is a highly mechanized and high-energy input industry that relies on electrical power, diesel, fertilizers, and water. The CRDC has launched projects to meet the energy challenges of cotton production. On-farm direct energy use means energy is directly consumed on a cotton farm, and the sources include electricity, diesel, gas or liquefied petroleum gas, etc [8]. In the entire life

cycle of cotton growing, on-farm direct energy accounts for approximately 10% of the total energy consumption by cotton plantations. Of all sources, pumping water contributes to approximately 50%–75% of all on-farm direct energy consumption [8], which comprises a significant portion of cotton farm costs, whereas adopting renewable energy systems can bring more savings. Fig. 2.2 shows the itemized average energy use percentage per hectare at cotton farms.

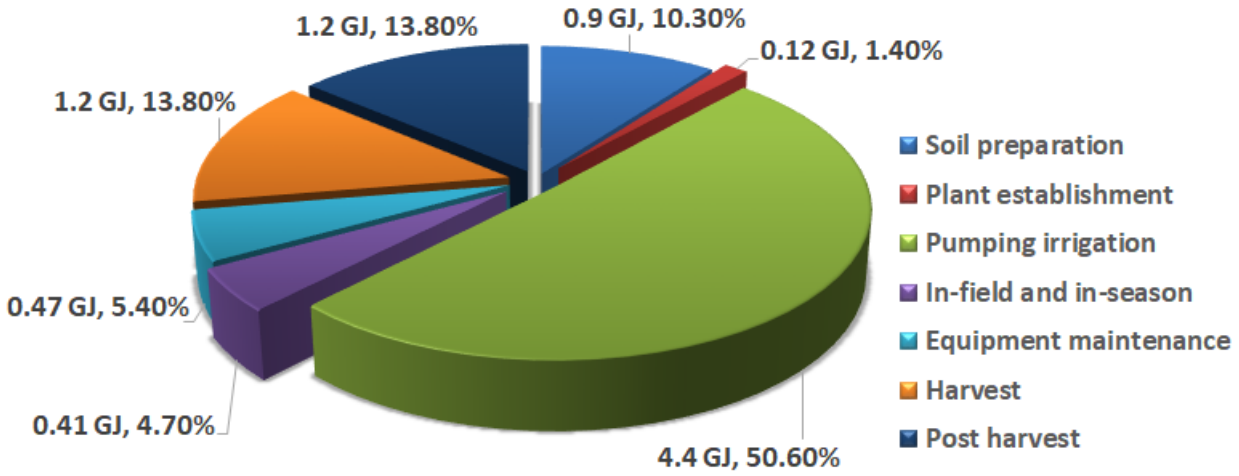

Figure 2.2: Direct on-farm energy usage components and percentage [9]

The chart above shows that 50.6% of the total energy is consumed by irrigation, whereas cotton farming practices before and after harvesting account only for 27.6% of energy consumption on average. The remaining farming processes for soil preparation, plant establishment, in-field pest spraying, in-season cultivation, and equipment maintenance account for 21.8% of the total energy consumption. Table 2.1 breaks down the individual components pertaining to average annual energy cost by energy source type for on-farm irrigation processes.

Table 2.1: Average annual irrigation energy cost breakdown by diesel and electricity energy [8], [10]

	Diesel	Electricity
Percentage of pumping irrigation	73%	27%
Energy usage (per 10^4 m^2)	3.2445 (GJ)	1.1755 (GJ)
Conversion factor from per unit energy source to GJ	0.0386 (GJ/L)	0.0036 (GJ/kWh)
Consumed volume (per 10^4 m^2)	83.5364 (L)	326.527 (kWh)
Unit price	1.5 (AU$/L)	0.26 (AU$/kWh)
Total cost	125.3 (AU$/$10^4$ m^2)	84.9 (AU$/$10^4$ m^2)

Cotton farmers are interested in MG investments for better revenue. In order to reduce the energy cost of the irrigation system, many studies have proposed different methods for retrofitting and optimizing the existing power systems and energy sources at the farms. Examples of these methods are listed as follows:

- In terms of improving water utilisation from the perspective of horticulture, an early work [11] proposes a method to schedule irrigation and increase water-use efficiency. Ref. [12] adopts the Monolayer method to reduce water evaporation. Technical and practical suggestions are proposed in [13] to improve irrigation efficiency, increase farm profits, and minimize environmental impacts through irrigation management; and

- Water pump performance improvement is also a significant factor in saving operational costs. Water pump overhaul or retrofit is a method to improve pump efficiency. A significant energy saving could be achieved when water pumps are appropriately operated [14]. Variable speed drives (VSDs) are an important energy-saving device for water pumps, which provide a variety of speeds so that the pumps can work at optimal rates [15]. Installing power factor correction devices can help electric pumps utilize energy efficiently and reduce maximum demand charges for the pumping system [16].

In addition, there are several traditional ways to save energy, such as establishing a reservoir or dam to manage irrigation [17] so that energy can be saved by pumping water to these storage facilities at cheap electricity tariff periods. Ref. [18] provides details to minimize evaporation and seepage and thus reduce the cost of water loss. Alternative irrigation systems adopt recent technologies, such as lateral move, centre-pivot irrigation systems and drip technology. They are used to save energy and improve water-use efficiency [19]–[21].

2.3 Optimal microgrid investment design for cotton farms

To optimally design cotton farm MGs, there have been many different approaches and methods in the literature which maximize the economic and social benefits of

MGs. In recent decades, RES planning optimization techniques have been widely adopted in agriculture; for example, advanced solar PV technology is applied taking advantage of grid connection and feed-in tariffs to achieve more incentives for cotton farms [22]. Ref. [23] proposes a hybrid power system combining solar, wind, and biomass technologies. This hybrid system is designed using a multi-objective optimization model to consider energy demand and renewable energy resource availability [23]. A methodology for determining the size of energy storage systems in standalone MGs is proposed in [24]. In [25], a sizing methodology using the non-dominated sorting genetic algorithm is developed to optimize for multiple objectives in the design of an autonomous MG for a rural area in Mali, and the results are the trade-off among renewable energy integration, system reliability, and operational cost. Furthermore, a PV-pumped hydro storage MG is designed in [26] by considering lifetime benefit and payback period in the economic feasibility study of MGs. The Emerald cotton farm's RES in Queensland, Australia, is analyzed in [27]. An MG is designed for this farm considering economic feasibility under a RES, and the cost savings are calculated using the HOMER software. Ref. [28] conducts an investment analysis of solar energy in a hybrid diesel irrigation pumping system in New South Wales, Australia, where the economic feasibility of incorporating solar energy and potential cost savings are studied. Table 2.2 summarizes the related literature on the optimal investment

design methodologies of hybrid renewable energy sources.

From these existing designs, it is noted that current research focuses on grid-connected microgrids (GMGs) and islanded microgrids (IMGs) with renewable energy resources, while the seasonal loads and intermittent nature of renewable power are not discussed for the particular MG design in cotton farms. Targeting these problems, Chapter 3 proposes a new MG design method for cotton farms considering the seasonal usage of water pumps and the intermittent solar and wind energy sources. The MG components will be chosen from PV, WT, and battery storage, and the MG will be connected to the utility grid to provide additional power support. The properly sized battery storage plays an essential role in peak demand management, RES power absorption, and load management under a time-varying feed-in tariff (FIT).

2.4 Optimal microgrid operation for cotton farms

Based on the aforementioned study, appropriate investment in MG can help cotton farm owners reduce their operational costs. However, only investing in the RESs of the MG cannot achieve the most savings in energy costs. MG control and operation are important in saving energy costs as well. When the hybrid renewable energy system is combined with optimal operation technology, the re-

Table 2.2: Microgrid planning methodologies of hybrid renewable energy sources

Microgrid components	Target of study	Novelty and contributions	Microgrid type	Reference
PV-Wind-Battery	Rural energy of South Africa	A hybrid power system is simulated; all the parts of the hybrid system are designed. The system controller is applied to different scenarios.	Islanded	[29]
PV-Wind-Battery-Diesel Generator	Minimizing hybrid power system investment costs in general remote areas	An approach is proposed for optimal hybrid power systems, and the genetic algorithm (GA) method is employed to solve the optimization problem.	Islanded	[30]
PV-Wind-Battery-Ultra Capacitor	Optimization of energy farm sizing in Key West, Florida	A GA approach is used to solve the optimization model for a hybrid energy system design for a farm MG	Grid-connected	[31]

Microgrid components	Target of study	Novelty and contributions	Microgrid type	Reference
Diesel Generator-PV-Wind-Battery -Converter	Renewable energy source and an assumed load simulation in Jntuk Vizianagram campus	A hybrid power system model is built, and then the HOMER software is used with the metrological data to solve the optimization problem.	Islanded	[32]
PV-Wind-Battery- Diesel Generator	Hybrid power system for rural mobile base transceiver station at Doka-Sharia of Kaduna state, Nigeria	A techno-economic analysis is presented for a hybrid energy source for a rural area telecommunication mobile-base station, and HOMER is used to compare two configurations.	Islanded	[33]
PV-Wind-Battery- Diesel Generator	Performance comparison of lithium-ion and lead-acid battery in different micro-grid scenarios	Optimal models for a islanded MG and grid-connection MG are designed through HOMER software. Four different configuration scenarios are compared.	both	[34]

Microgrid components	Target of study	Novelty and contributions	Microgrid type	Reference
Diesel Generator-PV-Wind -Battery	Rural family's energy usage in Sri Lanka	HOMER software is adopted to simulate the hybrid system configuration, and the renewable energy size for investment is discussed.	Islanded	[35]
PV-Wind-Battery-Diesel Generator	A sizing tool for a renewable energy and a case study at Bishopton village in Scotland	An empirical approach is employed for a hybrid energy system.	Islanded	[36]
PV-Wind-Battery	An MG sizing optimization approach for a PV/wind integrated hybrid energy system with battery storage	The simulated annealing algorithm is utilized to obtain an optimum size.	Islanded	[37]

Microgrid components	Target of study	Novelty and contributions	Microgrid type	Reference
Micro Turbine-PV-Wind -Battery-Grid	Multi-objective energy management of an MG	Multi-objective particle swarm optimization algorithm is adopted to obtain the optimal configuration of MG components. The emission reduction value and new operating cost can be calculated by this algorithm.	Grid-connected	[38]
PV-Wind-Battery	A renewable system to match the distribution load	The hybrid energy sources are integrated based on unutilized energy probability, relative excess power generated, deficiency of power supply probability, life cycle cost and life cycle unit cost.	Islanded	[39]
PV-Wind-Hydro-Biogas Energy Storage	Rural community'smrenewable energy source utilization in developing countries	A smart integrated renewable energy system is presented which includes multiple objectives of rural area energization. GA is used for the RES sizing optimization.	Islanded	[40]

newable energy source can be used more efficiently, and more operating costs can be saved. Once the MG planning investment model is established, optimized operation plays an important role in the energy-saving irrigation of cotton farms.

2.4.1 Optimal microgrid operation methodologies

In [41], a multi-agent method for MG system operation is proposed, and a model including several load agents, generator agents, and a single MG control agent is established. Ref. [42] builds a grid-connected DC MG model and also develops a practical lithium-ion battery degradation cost model with network constraints in order to optimize the battery scheduling of the MG. A method for rule-based operating strategies is proposed in [43], which operates the system with different operating parameters to maximize the system's self-sufficiency and net present value. The work [44] proposes an optimal pump size model for a grid-connected pump system and designs a closed-loop control operation model for the pump system to reduce energy costs and improve energy efficiency. The model proposed in [45] is embedded in the day-ahead energy management program of MG, and an optimal operation plan by minimizing the daily operational cost is evaluated to meet the power demand and thermal comfort requirements. In [46], different types of demand response programs (DRP) are modelled based on the price elasticity of demand and customer benefits, and renewable energy (wind and solar) operation

is simulated to study the impact of intermittent distributed generation devices. For decades, the predictive control technology has been used in many fields (e.g., improving transient stability performance of power systems [47], energy cost reduction of a building hybrid heating system [48], and control systems of nonlinear chemical reactors [49]. However, the above methodologies focus mainly on MG operations in residential or industrial areas, and the limited MG operation studies for the agriculture area focus only on improving equipment efficiency and reducing the water storage loss for the operational cost reduction. There are only very limited studies for optimizing the operation of MG systems in rural Australia to improve the operation efficiency of farm energy systems. The cotton farm MG is very different from the ordinary MG because it needs to consider the complex water demand during the cotton growth period. For example, water requirements can vary significantly during specific growing periods. In addition, the amount of irrigation water, evaporation and precipitation of the reservoir also need to be considered. In the operation of MGs, control methods can be very helpful. General control techniques are still popular, such as proportional-integral-derivative (PID) controls [50]–[54]. However, they are being replaced by MPC because of their reliability and stability in handling uncertainties [55]–[59]. Therefore, it is necessary to investigate if MPC can be applied in the operation of cotton farm MGs.

2.4.2 Operating principle of MPC

The basic idea of MPC is to build a predictive model, use a cost function to represent the behaviour required by the system, and minimize the cost function to generate actual control commands [60]. The main advantage lies in the feedback nature of MPC. In the MPC process, an optimal control problem is solved repeatedly over a moving finite prediction horizon, and only the first control element is executed after each iteration. In the next sampling interval, the new states of the system are sent to the prediction model, and the optimization process is repeated. In addition, output feedback and the repeated moving horizon optimization can provide a robust solution against uncertainties caused by external disturbances. Consider the example of the cotton farm MG. Excessive water is supplied due to the rainy season or the demand for water is increased due to temperature increasing, which can lead to uncertainties in water demand. In the MPC method, the updated data (e.g., water demand and PV generation) will be used to solve the optimization problem over each moving optimization horizon. That is, at time T, the optimization model is solved over the time period $[T, T+m]$ using the available data at time T. The obtained solution is implemented over a time period $[T, T+1]$. Then at time $T+1$, new system data will be fed back to the model, and the optimization problem is solved over the new time horizon $[T+1, T+m+1]$.

Then this process is repeated when T increases.

2.4.3 Summary of recent research in MPC methodologies

Table 2.3 shows the research related to MPC, including MG types, main methods, optimization objectives and algorithms.

2.4.4 Limitation of MPC methodology

We are particularly interested in the application of MPC to the MG system at Australian cotton farms, where the MG consists of a diesel generator, renewable generation, and battery storage to supply the water pumping system at cotton farms. In literature, MPC has been applied for pumping systems; for example, a water pumping station is operated using MPC in the energy resource allocation in [61]. Classic MPC approaches have been widely applied in the operation of MGs. For instance, MPC is used in [62] for the optimal operation of grid-connected wind farms, which have hydrogen-based ESSs and local load. From the aforementioned literature, the classic MPC can handle the optimization process in each closed-loop iteration. However, the irrigation mechanism of cotton farms does not only operate in an ideal mode but also faces different natural conditions, such as evaporation, rainfall and temperature changes. Consequently, the optimization results obtained only by the classic MPC method are inaccurate, and the disturbance

from nature uncertainty needs to be considered. Thus, Chapter 4 aims to propose an MPC approach to solve the cotton farm MG operation problem while taking into account the constraints of the Australian cotton growing industry, where the GMG and IMG model for a rural MG will be established, and weather condition changes are used to conduct robustness and operating cost analysis.

Table 2.3: Summary of the MPC methodologies in recent studies

Ref.	Microgrid type	Methodology	Objectives
[63]	Grid-connected	Stochastic inequality constrained closed-loop model-based predictive control	Wind turbine pitch control, motor speed and power generation
[64]	Grid-connected	MPC based on a dynamic discrete-time piece-wise affine model of a wind turbine	Optimal active power control of a wind farm, including power reference tracking and the wind turbine mechanical load minimization
[65]	Grid-connected	MPC optimization techniques for energy exchange with main grid	The operational cost and degradation issues

2.5 Microgrid operation under uncertainty

Due to the inherent randomness of natural phenomena, MG operations on cotton farms are affected by many uncertainties. In this study, sudden weather changes

Ref.	Microgrid type	Methodology	Objectives
[66]	Grid-connected and Islanded	Model predictive voltage control and model predictive power control for the interlinking converter control by using a State of Charge (SoC)–oriented charging scheme for battery energy storage	Voltage control in islanded mode and reactive power control in grid-connected mode.
[67]	Grid-connected	Distributed model predictive control for economic schedule optimization of a network of MGs with hybrid energy storage system (ESS)	To maximize economic benefit and minimize the degradation of each storage unit.
[68]	Grid-connected	Dual-mode distributed economic model predictive control for a nonlinear wind-PV-battery MG power system	To optimize the battery's SoC, and reduce the fluctuation of the power exchange with the grid
[69]	Islanded	A two-layer MPC method for MG operation	To optimize energy dispatch of future power profiles
[70]	Grid-connected	A hierarchical MPC approach to coordinate the wind generation and plug-in electric vehicles (PEV) charging in the MG	To regulate the PEV charging load to follow the wind generation and adjust the wind generator power output to match the PEVs charging demand

Ref.	Microgrid type	Methodology	Objectives
[71]	Grid-connected	Economic MPC for the management of a smart MG system connected to an electrical power grid.	To minimize the costs of production and distribution, and guarantee energy availability
[72]	Islanded	An MPC method for a real-time optimization to maximize the power from RES to a building	To minimize the use of backup energy and maximize the amount of RES power directly consumed by the load
[73]	Grid-connected	An MPC approach for achieving economic efficiency in MG operation management	To maximize generated power in a flap-type wave energy converter model.

cause uncertainty, including PV generation, rainfall, and dam water evaporation. In addition, water demand uncertainty for irrigation is based on the cotton growing stage combined with weather conditions. In order to reduce the influence of uncertainty on the system operation, various methods for dealing with uncertainty have been proposed in the literature. Ref. [74] solves the MG planning problem by decomposing it into an investment master problem and an operation sub-problem; in the operation sub-problem, the optimal operation in the worst case under uncertain conditions is calculated. Ref. [75] uses scenario-based techniques to model the uncertainty of PV system and wind turbine output power, load demand forecast errors, and grid bidding strategy for the optimal energy management of an MG. In order to classify the relevant literature on MG uncertainty analysis, Table 2.4 lists the applications and methods of uncertainty modelling. However, in the

aforementioned studies above, there is no relevant description of the application of MPC for reducing agricultural operational costs under the influence of various real-world uncertain conditions, especially for cotton farm irrigation conditions that have multi-input uncertainty parameters, such as cotton farm MG under uncertain RES generation and weather changes. Therefore, the motivation of Chapter 5is to design an optimal MG system operation under uncertainties for Australian cotton farms.

2.6 Summary

Based on the aforementioned literature review in this chapter, operational cost reduction for cotton farms in Australia can be achieved in the following steps:

- Through the optimization methodology, and based on the scale of the farm size and the historical data of energy consumption, the investment cost and simple payback period of the cotton farm MG can be planned.

- Based on optimal control of the MG operation, the utilization rate of RESs is improved, and the operational cost can be further reduced.

- By considering the influence of the uncertainty in the natural environment and water demand on the MG operation, the optimal MG operation approach

can be adopted, and the expected value of the operational cost will be more accurate and reliable.

Table 2.4: Review of uncertainty modelling methods and applications

Ref.	Uncertainty source	Methodology description
[76]	Leveled cost of energy and reliability parameters	Uncertainty of renewable distributed generations (DGs) is modelled based on Monte Carlo simulation, and then the optimal size of DGs is considered as an optimization problem under technical and economic constraints which is solved by a genetic algorithm.
[77]	Solar radiation, wind speed, water flow of a river, load consumption, and electricity price	A modified Metropolis–coupled Markov chain Monte Carlo simulation is proposed to predict the stochastic behaviour of different uncertainty sources in the planning of a stand-alone renewable energy-based MG.
[78]	Wind, solar and load	A hybrid energy systems model is built based on solar and wind energy combined with energy storage units under uncertainty, and the Monte Carlo simulation and Cuckoo search algorithm provide a reliable and cost-effective solution.

Ref.	Uncertainty source	Methodology description
[79]	Load, PV and wind	Through the two-stage stochastic programming, a more robust schedule is derived that minimizes the risk of uncertainty effects, and the MPC can effectively optimize the objectives, and further compensate for the uncertainty in the MG through the closed-loop mechanism.
[80]	Load	A two-layer stochastic MPC is proposed for the energy management of grid-connected MGs. A stochastic MPC regulator is used at the lower layer to compensate for the uncertainties and maintain the total energy exchange with the network.
[81]	Fluctuating demand and generation from RESs	Uncertainty is modelled using a scenario generation and reduction approach. A two-stage stochastic programming method is proposed to optimize MG operations. MPC is used to further compensate for the uncertainty.
[82]	PV, wind and load demand	A battery operating cost model is proposed that treats the battery as an equivalent fuel-run generator to allow it to be incorporated into the unit commitment problem, the uncertainties in renewable energy and load demand are also considered in the unit commitment and economic dispatch problems using a probabilistic constrained approach.

Chapter 3

Microgrid Optimal Investment Design for Cotton Farms in Australia

3.1 Introduction

As one of the largest exporters in rural areas, the cotton industry in Australia creates thousands of jobs every year [83]. With more than 427 thousand hectares used to plant cotton among over 1400 cotton farms, the overall revenue in the cotton industry hit a record of AU$ 2.3 billion in 2017/2018 [84]. As an industry with high energy demand, the revenue of the cotton industry is highly sensitive to energy costs. Therefore, reducing operating costs plays an important role in improving the competitiveness of Australian cotton products. This chapter aims to reduce cotton farm energy costs by designing the relevant microgrid (MG)

equipped with photovoltaic (PV) units, wind turbines (WT) generators, and battery storage. In order to design a more suitable MG for cotton farms, this chapter takes operation cost, investment cost and simple payback period as the optimization objectives, and considers the constraints of the cotton farm such as seasonal irrigation demand, water reservoir, water evaporation, etc. The underlying problem is then transformed into a single-objective optimization problem by summing the normalized objective functions with corresponding weighting factors. Sensitivity analyses of various key impacting factors, including weighting factors, tariffs and weather conditions, are conducted.

The Australian cotton farming region is rich in natural resources. The yearly average solar global horizontal irradiation is 4.86 kWh/(m^2· day), the annual average wind speed at 50 m height is 4.2 m/s, and the annual average temperature is 16.04 °C. In the literature, many studies on renewable energy generation have been proposed in agricultural areas. For example, Ref. [27] illustrates a standalone MG case study in which a hybrid power supply system was implemented in a cotton farm at Emerald, Queensland, and the optimal design of irrigation pumps in a cotton farm was achieved by the software Hybrid Optimization of Multiple Energy Resources (HOMER). In [28], an off-grid MG was investigated for a cotton farm in Australia, and HOMER was used to obtain the optimal investment results for

energy cost reduction. In the case study of [85], thirteen hybrid MG projects were evaluated, and a sustainability assessment was performed in terms of the institutional, technical, environmental, and socio-economic impact on rural Venezuela. Furthermore, rural MGs can be divided into two categories per operation mode: grid-connected and off-grid MGs [86]. Several papers present an off-grid MG system based on renewable energy sources (RESs) and conventional energy sources. Ref. [87] developed a viable MG system including PV, small hydro, battery storage, and diesel generators for rural electrification in Southern Cameroons. Ref. [88] proposed a methodology based on the energy balance evaluation for a given design period to determine the size of the electrical energy storage in standalone systems. In [89], a hybrid AC/DC off-grid MG planning model was proposed to help select the best technology for each device from the candidate list.

Grid-connected MGs are often applied in rural areas. For example, a grid-connected hybrid MG with PV and wind turbine was reported in [90], which can meet the energy needs of 15 residential houses in rural communities in Chile. A grid-connected MG was recently established in a remote area of Uttar Pradesh, India, and the installed PV and battery storage can support the loads in case of insufficient power from the grid [91]. These MG design results are not directly applicable to the MG of cotton farms because of the seasonal energy demand of

water pumping: water needs to be pumped only during irrigation periods, and there is not any water pumping load at non-irrigation periods. Due to this extraordinary characteristic, the scale of the designed MG needs to be appropriately decided for the cotton farm: an MG of a too large size increases the capital cost, while an MG of a too small size leads to instability issues and does not contribute significantly to reducing the operational cost. To solve the aforementioned issue, this chapter will study the optimal sizing problem of a cotton farm MG tailored to the irrigation characteristics of cotton farms. Furthermore, the charge from the grid for the maximum demand will be modelled to match the actual situation of the Australian cotton industry [92]. In literature, many existing studies minimise energy costs under the time-of-use (TOU) electricity tariff and charge for the maximum demand. For example, an optimal load shifting strategy is presented in [93] to minimize the operation cost of the conveyor belt systems of a colliery, and a closed-loop optimal control technique is presented in [94] to reduce the TOU cost and maximum demand charges for a water pumping system. Moreover, a multi-agent mathematical model is presented in [95] for energy cost reduction through demand-side management. The results show that the proposed method can significantly reduce domestic energy consumption. A demand-side management model is introduced in [96] for an MG equipped with PV and battery storage to reduce residential energy costs.

However, it is difficult to shift the irrigation pump load for cotton farms, especially in the water high-demand season in which cotton needs to be irrigated continuously for at least two to three weeks, and the pumps are kept running for these weeks. To resolve this issue, the most common method is reducing the maximum demand cost by energy storage, which can be considered for power management and peak demand reduction in the grid-connected MG system. Ref. [97] showed that battery size optimization can ensure a smooth power flow in the MG and reduce peak load demand. Ref. [98] takes advantage of the particle swarm optimization method to minimize the MG's total energy and operating cost by optimally adjusting the control variables to satisfy various constraints. Ref. [99] reviewed the control strategies of different types of energy storage devices and the corresponding working principles and limitations. Consequently, battery storage can be considered for power management and peak demand reduction in the grid-connected MG system in [100]. By 2020, Australia will have over 15,800 cotton farms and other agricultural consumers connected to the electricity grid [27]. Therefore, the choice of electricity price plays a critical role in shortening the investment payback period for a grid-connected MG. An electricity cost reduction demand side management model based on MG supply chain and TOU tariff was proposed by [101], where end-users are equipped with energy storage. A model was developed in [102] to evaluate the effectiveness of demand response strategies

using TOU tariff combined with regional thermal control. Ref. [103] proposed a model to reduce residential electricity demand by considering price elasticity and solar PV power, where Monte Carlo simulation for power flow analysis in low-voltage distribution networks was applied. However, these models have not considered the situation in that power utility purchases energy from MGs. A feed-in tariff (FIT) is one of the incentive schemes envisaged by the Australian government for RES installation. Nevertheless, Australia's Small-scale Renewable Energy Scheme (SRES) limits PV installation to no more than 100 kW and wind systems to a capacity of no more than 10 kW. In this study, the FIT scheme is considered in the objective function to reduce operational costs. Meanwhile, FIT can shorten the payback period for the grid-connected MG during off-irrigation seasons.

For the MG optimization modelling, Ref. [104] developed a model for energy storage management in the distribution network, which can reduce operational costs and improve voltage stability. A stochastic techno-economic MG model was proposed in [105] for a rural MG to assess technical design decisions and financial conditions. Ref. [106] modelled a hybrid energy system and obtained the optimal configuration with the help of life cycle cost minimization. Furthermore, Ref. [107] established a pump storage model based on the hybrid solar-wind system to

do the techno-economic optimization for a rural MG.

The aforementioned literature paid attention to the RES integration and management method for rural MGs, but none of them discussed the case that both seasonal pumping loads and intermittent renewable sources appear simultaneously in the same MG. Motivated by the problems mentioned above, this chapter presents a new cotton farm MG design method, where the seasonal water pumping demand and intermittent PV and wind power generation are considered. The proposed cotton farm MG is structured with PV, WT, and battery storage. In addition, the proposed MG is assumed to be connected to the power grid to ensure enough power supply for irrigation. PV and wind turbines are energy generators in this MG, and the battery is essential for energy demand management under time-varying FIT. However, the corresponding investment cost is expensive and should not be ignored. Considering all these factors, this study proposes a multi-objective optimization problem to minimize MG's operational cost, investment cost, and payback period. A grid-connected MG cotton farm case study is simulated to validate the design results. Furthermore, the impact of numerical research results in different situations is considered from the perspective of cotton farm stakeholders.

The main contributions of this study are given below.

1. A multi-objective MG optimal design model is proposed for cotton farms that are able to handle seasonal water pumping loads under various weather conditions, Australia's renewable energy policies, electricity prices, and FITs.

2. The relationships among pump energy consumption, water storage and irrigation water demand during cotton planting cycles are modelled in the MG design.

3. Using an actual cotton farm for the case study, the impact of grid electricity tariff and FIT on the initial investment and routine operational costs of the MG is discussed. The case study also indicates that the capacity of the WT should be limited by 10 kW in order to be economically viable.

The rest part of this chapter is organized as follows. Section 3.2 introduces the RES components of MG for Australian cotton farms and establishes design objectives and constraints of RESs and cotton irrigation. Details of a case study are given in Section 3.3. In Section 3.4, the Yalmip toolbox [108] is used together with MATLAB fmincon optimization tools to solve the normalized multi-objective MG optimization problem. The numerical results and the economic impact are also discussed in this chapter. Section 3.5 summarizes the chapter and draws conclusions.

3.2 Optimal design of cotton farm microgrid

This section briefly reviews the energy models of key MG components.

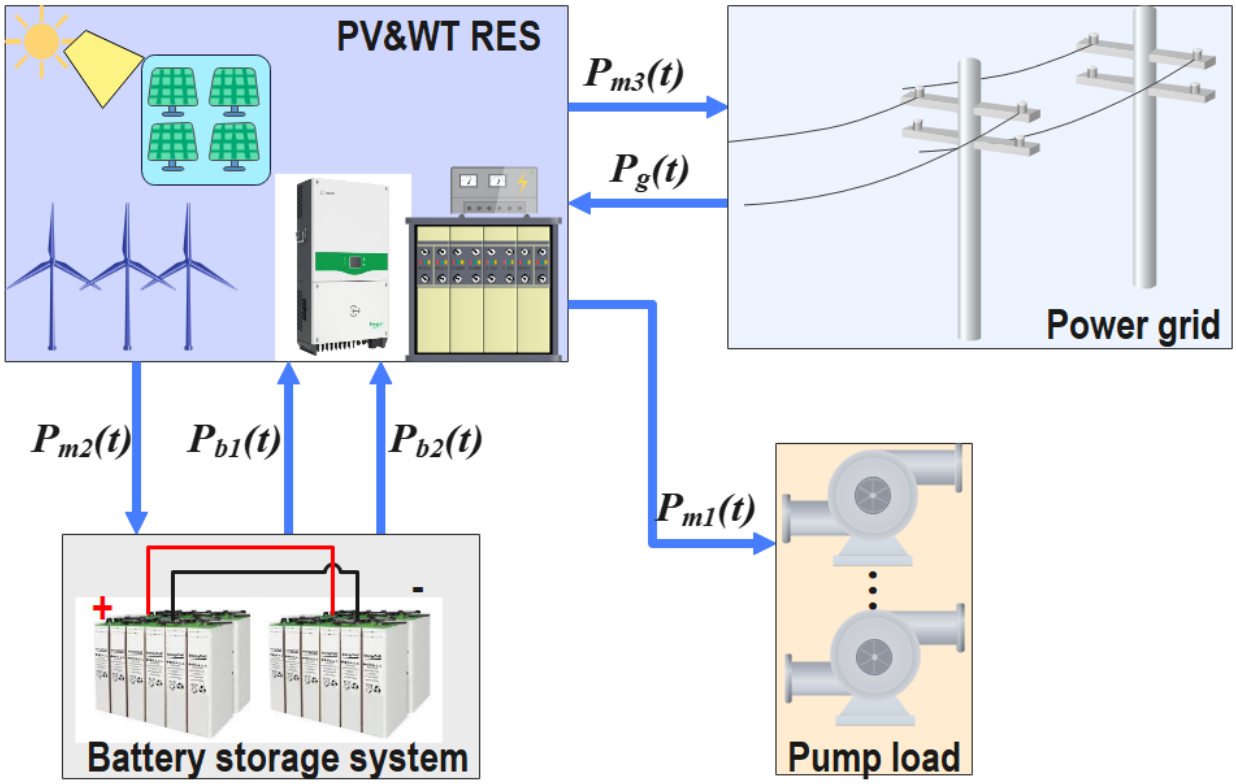

Figure 3.1: Grid-connected microgrid

Figure 3.1 shows the power balance within the MG. The power of water pumps is supplied by the grid, battery storage, PV and WT. In Figure 3.1, notation $P_g(t)$ represents the amount of power purchased from the grid at time t, i.e., the t^{th} hour since the time is sampled each hour; $P_{m1}(t)$ is the power flowing from the PV and WT to the water pump at time t; $P_{b1}(t)$ denotes the power discharged by the battery at time t to supply the load. Excess power from the PV and WT can be sold to the grid or charged to the battery storage. The notation $P_{m2}(t)$ denotes

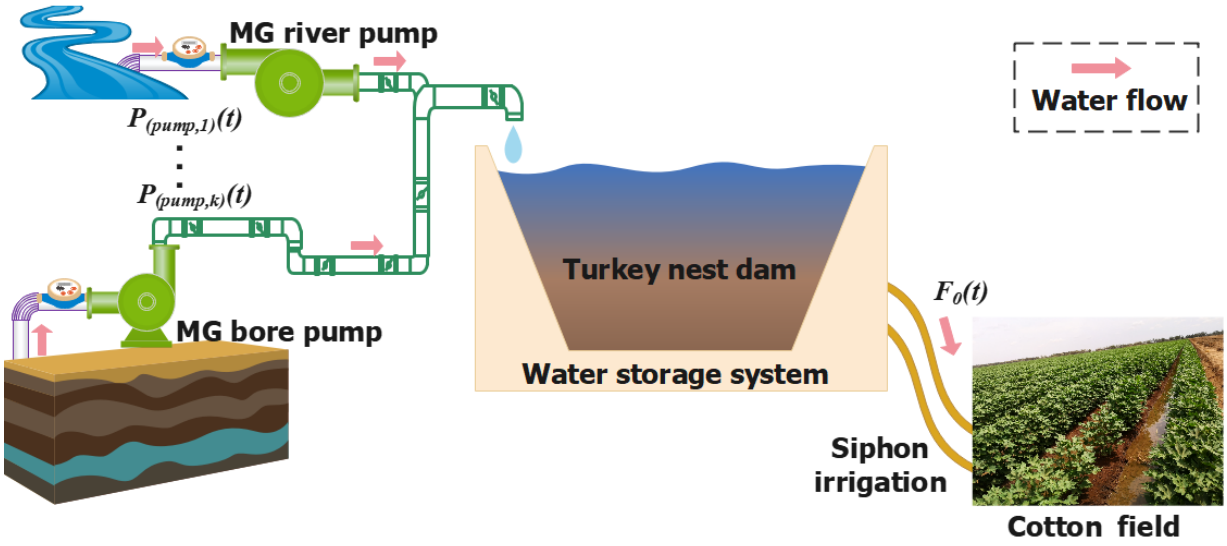

Figure 3.2: Cotton farm irrigation model

the power flowing from the PV and WT to the battery storage at time t, and $P_{m3}(t)$ denotes the excess power from the PV and WT to the grid. When water pumps are not switched on, the battery also can sell power (denoted by $P_{b2}(t)$) to the grid to make a profit. The power flows in this diagram are functions of time t. Hourly samples are taken in the models, and each year consists of 8760 hours. The water irrigation system of the cotton farm is illustrated in Figure 3.2. To meet the water irrigation demand, pumps lift water from the bore or river through ditches to turkey nest dams. Then the water will flow from the dams to cotton farms by gravity. In Figure 3.2, notation $P_{(pump,k)}(t)$ represents the nominal power of the k^{th} pump at time t; and $F_0(t)$ denotes the water flow rate from the dam to cotton field at time t.

3.2.1 Objective functions

From the system configuration in Figure 3.1, the following equations can express the MG design objective functions.

$$f_{op} = \sum_{t}^{T} \beta_1(\mathrm{t}) \cdot \mathrm{P_g(t)} - \sum_{t}^{T} \beta_2(\mathrm{t}) \cdot [\mathrm{P_{m3}(t)} + \mathrm{P_{b2}(t)}] + C_0 \tag{3.1}$$

$$f_{invest} = \sum_{p=1}^{L} k_{1p} \cdot m_{1p} \cdot x_{1p} \ + \sum_{q=1}^{M} k_{2q} \cdot m_{2q} \cdot x_{2q} \ + \sum_{r=1}^{N} k_{3r} \cdot m_{3r} \cdot x_{3r} \tag{3.2}$$

$$f_{payback} = \frac{f_{invest}}{C_{org} \ - \ f_{op}} \tag{3.3}$$

In (3.1), f_{op} represents the annual operational cost of the MG, $\beta_1(t)$ denotes the grid electricity price at time t, $T = 8760$ is the number of hours in a year, $\beta_2(t)$ is the FIT rate at time t (AU$/kWh), and C_0 represents the annual maintenance cost of the MG. Equation (3.2) calculates the capital investment cost of the MG, where there are L, M, and N different types of PV panels, WTs and battery storage, respectively. Notations k_{1p}, m_{1p}, and x_{1p} are the unit price (in AU$/kW), rated power (in kW), and the total number of installed panels of the p^{th} type of PV, respectively. Symbols k_{2q}, m_{2q}, and x_{2q} represent the unit price (in AU$/kW), rated power (in kW), and the number of installed units of the q^{th} type of WT, respectively. Similarly, k_{3r}, m_{3r}, and x_{3r} are the unit price (in AU$/kWh), single unit battery capacity (in kWh), and the total number of installed battery units

of the r^{th} type of battery storage unit. Since x_{1p}, x_{2q} and x_{3r} represent the MG equipment quantity, they need to satisfy integer constraints. Equation (3.3) gives the simple payback period ($f_{payback}$), in which C_{org} denotes the baseline annual operation cost before the installation of the MG. The multi-objective functions in (3.1-3.3) can be transformed into a single objective function in (3.4) by weighting factors λ_1, λ_2, and λ_3. However, these objective functions have different magnitudes, so it is convenient to normalize the objectives to obtain an optimal solution consistent with the weighting factor specified by the decision-maker. Therefore, a weighted summation normalization method is adopted to (3.8) - (3.10). These objectives are normalized by using the true variation intervals of the objective functions on the Pareto optimal set, and f_{op}^{norm}, f_{invest}^{norm} and $f_{payback}^{norm}$ represent the normalized f_{op}, f_{invest} and $f_{payback}$, respectively; f_{op}^{min}, f_{invest}^{min} and $f_{payback}^{min}$ are the Utopia points satisfying $f_{op}^{min} = f_{invest}^{min} = f_{payback}^{min} = 0$; and f_{op}^{max}, f_{invest}^{max} and $f_{payback}^{max}$ are the Nadir points of the individual objectives, in which f_{op}^{max} is based on the maximum energy to be purchased to satisfy the irrigation demand; f_{invest}^{max} and $f_{payback}^{max}$ are based on the farm owner maximum investment and payback willingness. Yalmip toolbox is used to solve this optimization problem. The weighting factors λ_1, λ_2, and λ_3 satisfy constraints in (3.8).

$$min(\lambda_1 \cdot f_{op}^{norm} + \lambda_2 \cdot f_{invest}^{norm} + \lambda_3 \cdot f_{payback}^{norm}) \tag{3.4}$$

$$f_{op}^{norm} = \frac{f_{op} - f_{op}^{min}}{f_{op}^{max} - f_{op}^{min}} \tag{3.5}$$

$$f_{invest}^{norm} = \frac{f_{invest} - f_{invest}^{min}}{f_{invest}^{max} - f_{invest}^{min}} \tag{3.6}$$

$$f_{payback}^{norm} = \frac{f_{payback} - f_{payback}^{min}}{f_{payback}^{max} - f_{payback}^{min}} \tag{3.7}$$

$$\lambda_1 + \lambda_2 + \lambda_3 = 1 \tag{3.8}$$

3.2.2 System constraints

According to the power flow in Figure 3.1, Equation (3.9) shows that the pump load is supplied by PV, battery storage and utility, while Equation (3.10) shows the power balance from PV and WT:

$$P_p(t) = P_{m1}(t) + P_{b1}(t) + P_g(t) \tag{3.9}$$

$$P_{m1}(t) + P_{m2}(t) + P_{m3}(t) = P_{PV}(t) + P_{WT}(t) \tag{3.10}$$

where:

- $P_p(t)$ is the total power of water pumps at time t;
- $P_{PV}(t)$ is the power from the PV at time t; and
- $P_{WT}(t)$ is power from the WT at time t.

3.2.3 Battery storage constraints

The state-of-charge (SoC) of the battery storage satisfies the following relation (3.11) derived from energy balance and is also subject to the boundary constraints in (3.12).

$$S_{SOC}(t) = S_{SOC}(t-1) + \frac{P_{m2}(t) - P_{b1}(t) - P_{b2}(t)}{\sum_{r=1}^{N} m_{3r} \cdot x_{3r}} \tag{3.11}$$

$$S_{soc}^{min} \leqslant S_{SoC}(t) \leqslant S_{soc}^{max} \tag{3.12}$$

where:

- S_{soc} (t) is the at time t;
- S_{soc}^{min} is the minimum bound of and is chosen as 20% in the case study; and
- S_{soc}^{max} is the maximum bound of SoC and is taken as 90% in the case study.

3.2.4 Grid feed-in constraints

When the MG is in grid-connected mode, the feed-in power satisfies the following constraints in (3.13)

$$P_{m3}(t) + P_{b2}(t) \leqslant Q_1, \forall t \tag{3.13}$$

where Q_1 denotes the allowed maximum power for grid feed-in.

3.2.5 PV constraints

The power generated from the PV satisfies the following constraints:

$$P_{PV}(t) = \sum_{p=1}^{L} x_{1p} \cdot P^0_{PV,p}(t) \tag{3.14}$$

$$P^0_{PV,p}(t) \leqslant m_{1p}\ (kW) \tag{3.15}$$

where $P^0_{PV,p}(t)$ denotes the PV power generation per panel at time t.

3.2.6 Wind generation constraints

Power generated by the WTs satisfies the following relations:

$$P_{WT}(t) = \sum_{q=1}^{M} x_{2q} \cdot P^0_{WT,q}(t) \tag{3.16}$$

$$P^0_{WT,q}(t) \leqslant m_{2q}\ (kW) \tag{3.17}$$

$$\sum_{q=1}^{M} m_{2q} \cdot x_{2q} \leqslant 10\ (kW) \tag{3.18}$$

where $P^0_{WT,q}(t)$ is the power from a type q WT at time t. Equation (3.18) represents that the total WT capacity installed should be less than 10 kW, which is the maximum power of any small-scale wind system allowed by the Australian government [109].

3.2.7 Water storage constraints

Assume that variable speed drives to control the water pumps, then the water storage reservoir satisfies the following constraints in (3.19) – (3.24):

$$S_{min} \leqslant S(t) \leqslant S_{max} \tag{3.19}$$

$$S(t) = S(t-1) + \sum_{k=1}^{n} P_{pump,k}(t) \cdot M_k - F_0(t) - V_L(t) + R_0(t) \tag{3.20}$$

$$V_L(t) = \frac{(1-\delta) \cdot D \cdot A}{T} \tag{3.21}$$

$$P_p(t) = \sum_{k=0}^{n} P_{pump,k}(t) \tag{3.22}$$

$$0 \leqslant P_{pump,k}(t) \leqslant P_{pump,k}^{rated} \tag{3.23}$$

$$F_0(t) = \frac{D \cdot A}{T_1} \tag{3.24}$$

where:

- S_{min} is the minimum amount of water in the reservoir (ML);
- S_{max} is the maximum allowed water volume of the reservoir (ML);
- $S(t)$ is the amount of water volume in the reservoir at the t^{th} hour (ML);
- $P_{pump,k}^{rated}$ is the rated power of the k^{th} pump (kW);

- M_k is the average amount of water that each kW of input power at the k^{th} pump can raise from the water source (e.g. river) to the reservoir (in ML/kW). That is, this $P_{pump,k}(t) \cdot M_k$ mega litre of water will be pumped from the water source to the reservoir once the k^{th} pump is run at its rated power, and this value depends on the water head from the water source to the reservoir;

- D is the annual water demand for cotton irrigation (ML/Ha);

- A is the size of the irrigated cotton farm (m^2);

- T_1 is the total irrigation hours in a year (Hours);

- $V_L(t)$ is the loss of water from evaporation and seepage at time t, and $V_L(t)$ is calculated by (3.21);

- δ is the on-farm water use efficiency during the irrigation period [110]; δ=80% in this study [111];

- n is the total number of pumps; and

- $R_0(t)$ is average rainfall at the t^{th} hour (ML). As a source of supplementary water, the ratio of annual rainfall to irrigation water can be obtained from CRDC publications. For example, the rainfall in 2016 was approximately

33% of total irrigation [3].

3.3 Case study

3.3.1 Basic information

Table 3.1: Pumps and water storage parameters used in the case study

Item	Value
Pump 1	75,812 kWh
Pump 2	63,551 kWh
Pump 3	12,865 kWh
Farm size	3×10^6 m^2
Average pumping head	25 m
Average energy consumption of lifting 1 ML water to 1-metre	4.55 kWh/(ML· m)
Average irrigation demand	6.5×10^{-4} ML/m^2
Maximum allowed water usage	1,500 ML/year
Reservoir size	1,200 ML
Rainfall	33.33%
Water-use efficiency	80%
Average wind speed at a height of 10-15m	3.42 m/s
Daily average solar irradiation in 2016	5.02 kWh/m^2
Operation cost @ TOU tariff	49,694 AU$/year

In Australia, the average amount of requested water of a cotton field is 6.8×10^{-4} megalitres (ML) per square meter, and the average area of a cotton farm is 3.05×10^6 square meters [84] in the last decades. The cotton farm considered in this case

Table 3.2: Cost breakdown of irrigation pumps and energy consumption with a flat-rate tariff (AU$ 0.29086/kWh)

Equipment	Energy use in 2016 (kWh)	Cost (AU$)
Pump 1	75,812.33	22,050.77
Pump 2	63,511.06	18,484.46
Pump 3	12,865.24	3,741.98
Annual cost	AU$ 44,277.21/year	

Table 3.3: Initial operation cost with TOU tariff (Peak Price: AU$ 0.405/kWh, Off-Peak Price: AU$ 0.223/kWh)

Equipment	Peak Cost	Off-Peak Cost	Total Cost
Pump 1	17,201.50	7,471.79	24,673.29
Pump 2	14,726.97	6,094.00	20,820.97
Pump 3	2,947.22	1,252.45	4,199.67
Annual cost	AU$ 49,693.93/year		

Table 3.4: FIT scheme

Name	Time	Price (AU$/kWh)
Peak	3 pm-7 pm	0.13730
Off-peak	Remaining hours	0.05796
Flat rate	Any time	0.07842

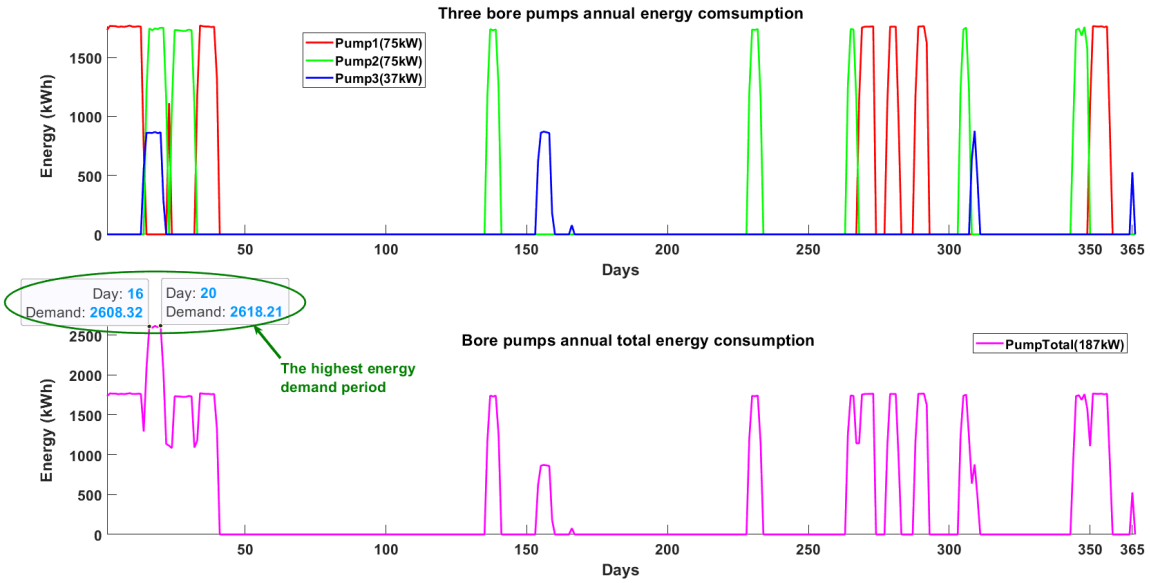

Figure 3.3: Load profile of the cotton farm bore pumps

study is in the southern part of Gunnedah, New South Wales, and its irrigation area in 2016 was 3×10^8 m^2 [10], [13]. There are three sub-bore pumps in this farm, which are powered by electricity, two with the rated power of 75 kW, and one with 37 kW [10]. The farm reservoir has a maximum water storage capacity of 1500 ML. The cotton farm parameters in this study are shown in Table 3.1. The water demand data are taken from the average water usage of cotton farms in the Murray-Darling Basin area in 2016, which includes the rainfall as a supplementary water source accounting for about 33% [3] of the total irrigation demand. The historical solar radiation data for the Gunnedah area in 2016 can be found in [112]. Currently, no MG is installed in the farm, and the corresponding baseline annual energy consumption and total cost of the three water pumps are shown in Table 3.2, where Ergon Energy small-business flat rate Tariff 20 is applied.

Table 3.3 calculates the corresponding operational costs under a different tariff, i.e., the Ergon Energy rural TOU Tariff 65. The FIT has two different schemes: a time-varying and a flat one[1], see Table 3.4. The energy consumption of three pumps in a year is shown in Figure 3.3.

3.3.2 Microgrid components and costs

Table 3.5: Specifications of PV panel

Smart Panel® 60-cell SPV310-60MMJ PV	
Panel power	0.253 kW
Performance ratio	0.75
Panel efficiency	18.9%
Panel dimensions	1650 × 992 × 40 mm
Maintenance cost	AU$ 5/year
Unit price	AU$ 250 (Including inverter)
Warranty	15 years

Table 3.5 shows the specifications of the PV panel considered in the case study. Table 3.6 lists information regarding three different sizes of WTs on the Australian market, and Figure 3.4 displays one WT average daily energy generation of each type in a year. Table 3.7 shows popular battery storage products from Tesla® and the corresponding data.

[1]https://www.esc.vic.gov.au/electricity-and-gas/electricity-and-gas-tariffs-and-benchmarks/minimum-feed-tariff#tabs-container1

Table 3.6: WT brand and price

Atlantis Solar® wind turbine	ASWT-2kW	ASWT-5kW	ASWT-10kW
Rated power (kW)	2	5	10
Cut-in speed (m/s)	3	2.5	3
Cut-out speed (m/s)	25	25	25
Rated wind speed (m/s)	9	10	10
Blade diameter (meter)	3.8	6.4	8
Generator efficiency	80%	80%	85%
Design life (years)	20	20	20
Minimum Tower height (meter)	8	10	12
Maintenance cost (AU$/Year)	800	1000	1500
Unit price (inlcuding installation cost)	AU$ 10 K/unit	AU$ 60 K/unit	AU$ 100 K/unit

Table 3.7: Battery storage brand and price

Tesla ® Powerwall 2 battery storage	
Usable capacity	13.5 kWh
Max charge and discharge	6.99 kW
Round trip efficiency	90%
Dimensions (L × W × H)	1150 × 755 × 155 mm
Maintenance cost	AU$ 300/year
Unit price	AU$ 10,600/unit
Warranty	10 years

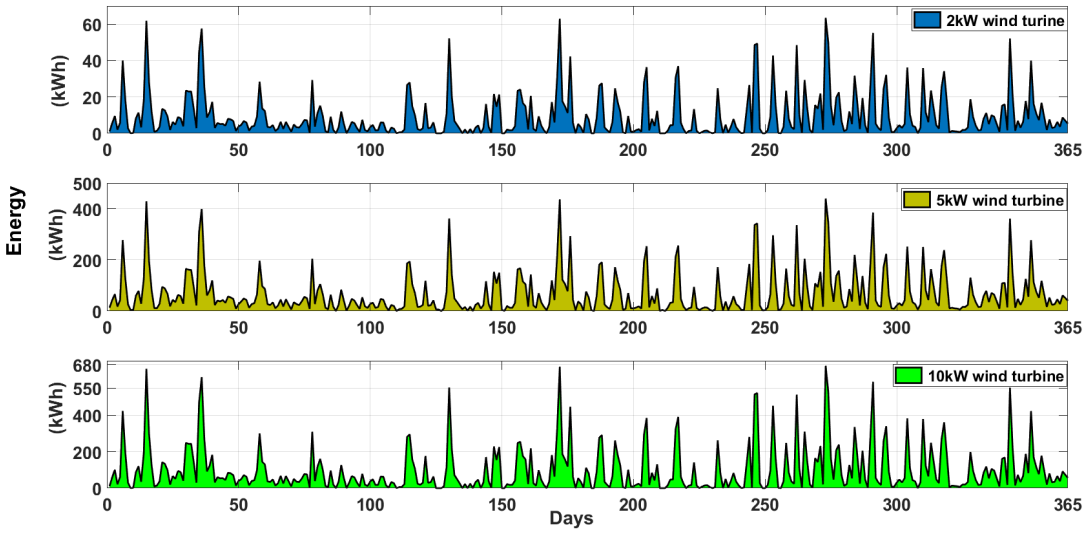

Figure 3.4: Daily energy generation of one WT from different types

3.4 Results and discussion

This case study is aimed at validating the proposed MG model. The results are discussed in the next three subsections below. The multi-objective optimization model is normalized, and the Yalmip optimization solver is applied together with the MATLAB fmincon toolbox to obtain the results. Table 3.8 provides the Baseline Case conditions based on the acceptable investment range for Australian cotton farmers. The historical data of the water pump energy consumption in 2016 is used in the case study as a baseline for comparison. The water demand data are taken from the average water usage of cotton farms in the Murray-Darling Basin area in 2016, which includes the rainfall as a supplementary water source accounting for about 33% [3] of the total irrigation demand. The historical solar radiation data for the Gunnedah area in 2016 can be found in [112]. Figure 3.5

show the annual power generation of 2 kW, 5 kW and 10 kW wind generators at the height of 10 - 15 meters, where the annual average wind speed is 3.4 m/s. Figure 3.6 shows the energy generated by a 1kW PV panel in the Gunnedah area in 2016.

Table 3.8: Baseline conditions of the case study

Items	Values
Minimum operation cost	0 AU$/year
Minimum investment cost	0 AU$
Minimum simple payback period	0 year
Maximum operation cost	50,000 AU$/year
Maximum investment cost	300,000 AU$
Maximum simple payback period	10 year
The total energy use of 3 pumps	152,228 kWh
Operation cost @ TOU tariff	49,694 AU$/year

3.4.1 Optimal microgrid design solution

Now consider the MG optimal design model in Section 3.3. The PV panel parameters are given in Table 3.5; the rated power of each PV panel is 253 W. The 2 kW, 5 kW and 10 kW WTs from Table 3.6 are available choices. The lithium-ion battery pack in Table 3.7 is used for the battery storage system, and each pack is rated as 13.5 kWh. Because the installation of the WT must comply with the Australian small renewable energy scheme, the total installed WT cannot be greater than 10 kW.

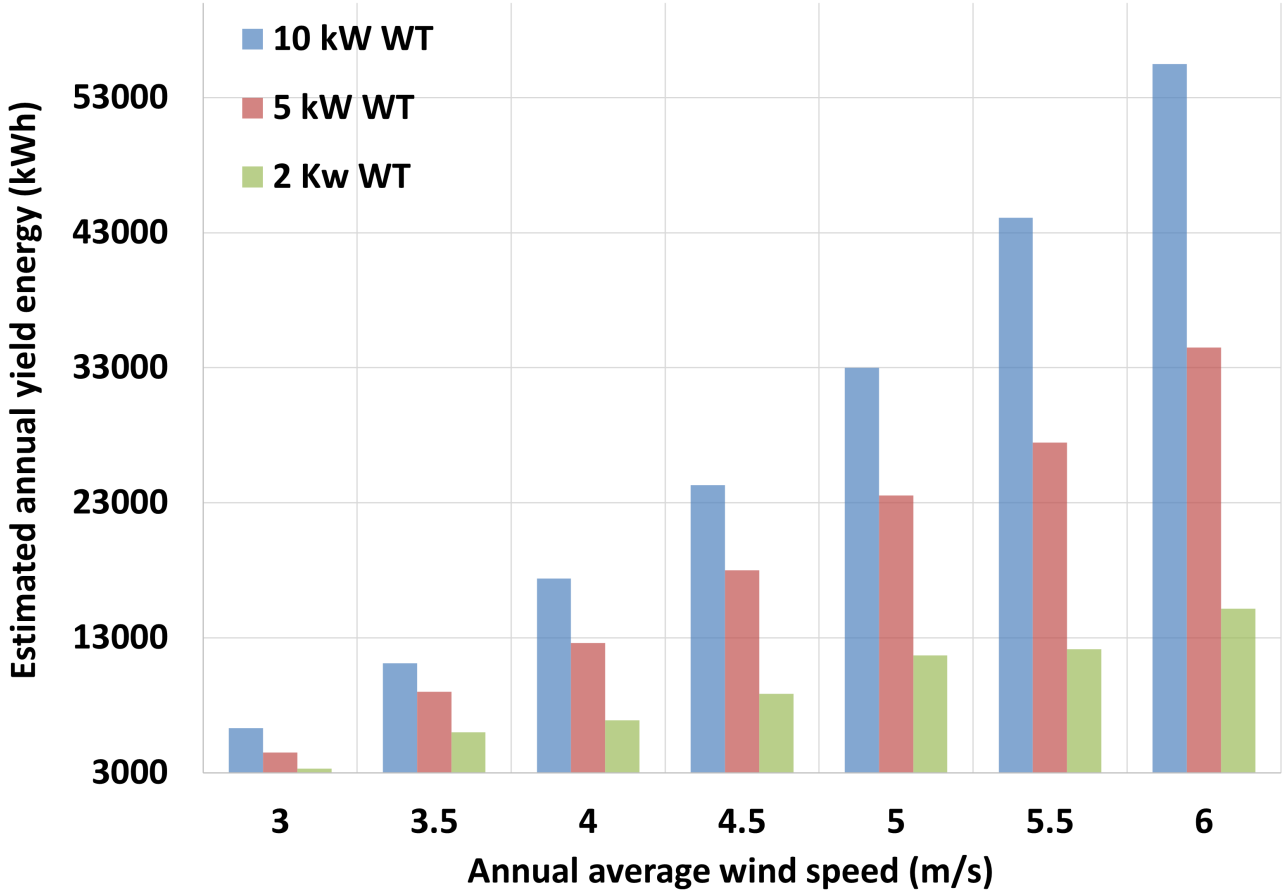

Figure 3.5: Annual energy yield of three types of WTs

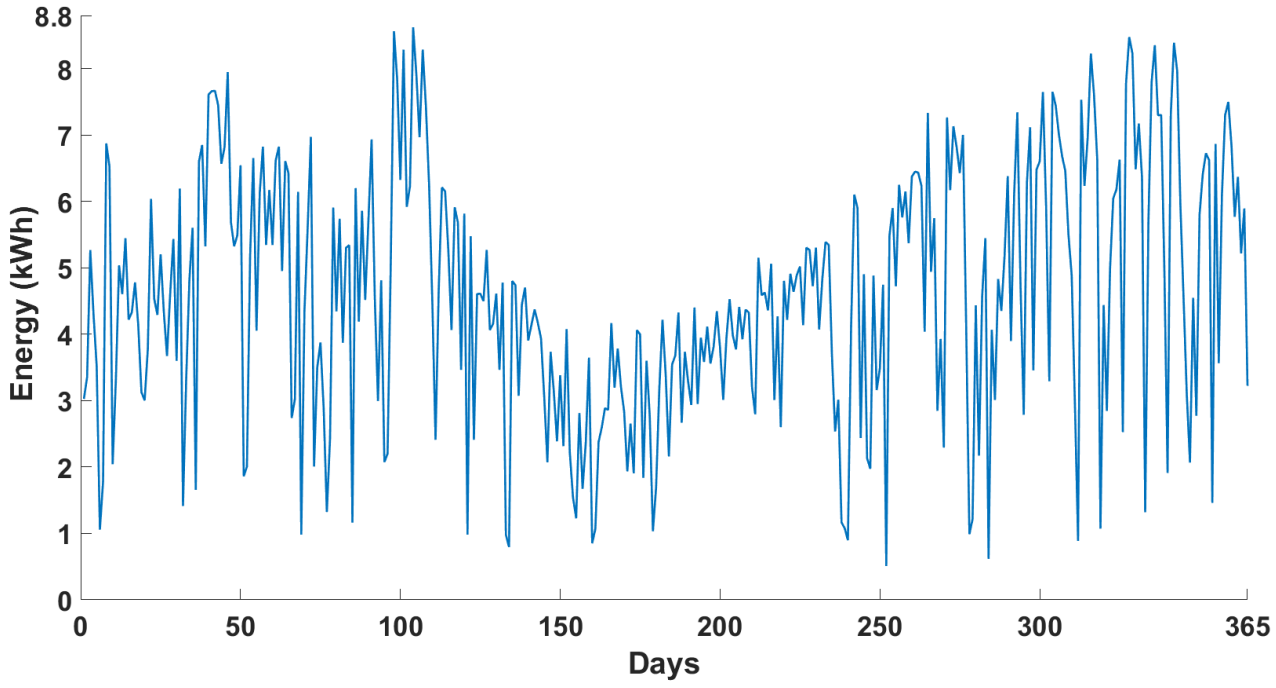

Figure 3.6: Daily generated energy of a 1kW PV panel at the farm location in 2016

Table 3.9: Baseline Case vs. Optimal Case results

Indicator	Baseline Case	Optimal Case
Energy purchased from grid in a year	152,228 kWh	98,937 kWh
TOU operation cost	AU$ 49,694	AU$ 21,612
Installed PV size	0	61.2 kW
Installed PV Qty.	0	242
Installed WT Qty.	0	10 kW × 1
Installed battery	0	135 kWh
Installed battery Qty.	0	10
Investment cost	0	AU$ 266,500
Feed-in energy in a year	0	89,613 kWh
Simple payback period	-	9.49 yrs

Figure 3.7 shows the changes of dam water volume. This curve is drawn based on the power consumption of pumps during the watering period in the cotton farm, rainfall and water loss. The total amount of water pumped, irrigation water usage, rainfall supplementary and water loss have to meet the maximum dam capacity and irrigation demand. It can be seen from Figure 3.7 that when the irrigation demand is 6.5×10^{-4}ML/m^2, the minimum water volume is 425.6 ML during the irrigation time, the maximum water volume of the dam reaches 532.7 ML, and the remaining water after irrigation is 518.4 ML. The amount of water in the dam increases after the start of the pumps and decreases during irrigation. The total amount of water pumped plus rainfall supplementation can satisfy the

total amount of water demand. Meanwhile, the total amount of pumped water is 1,338 ML, which is also within the limit of 1,500 ML for maximum water usage permission. Therefore, the irrigation and water pumping model can be verified to suit the irrigation system, and the total energy consumption of the pumps also satisfies the irrigation demand.

In this study, we define the Baseline Case as the current energy system at the cotton farm which does not have RESs, and the required energy is supplied by the power grid only. Table 3.9 gives the comparison result between the Baseline Case and Optimal Case in terms of the MG components, investment cost, operation cost, and simple payback period. Optimal Case ($\lambda_1 = 0.6$, $\lambda_2 = 0.2$ and $\lambda_3 = 0.2$) installed an MG and adopted TOU tariff and time-varying FIT in (3.4) to optimize the configuration. In addition, Optimal Case analyzes the importance of battery storage in the MG and how the battery systems store excess energy and sell it back to the grid to maximize the benefit. Figure 3.8 shows that RES generates electricity to supply the water pumps, but it does not have sufficient power to meet the pump load. Consequently, grid power is supplied to meet the shortage. Meanwhile, the MG system can sell excess power to the grid during off-peak irrigation periods. Since battery storage is an essential part of this study. Battery storage can support water pumping during the irrigation period and transfer the

energy back to the grid during the off-peak period of irrigation. Thus, Figure 3.9 shows the charging and discharging status of the battery over the year. The red bar is the excess energy charged to the battery storage from the MG. The magenta bars show that the battery storage provides energy to the pumps. During non-irrigation periods, the MG charges the battery storage and sells energy back to the grid when the PV stops generating power. Therefore, there are more benefits to choosing a time-varying FIT than using a flat-rate FIT. The brown bars in Figure 3.9 show the scale of the battery selling energy to the grid during the year.

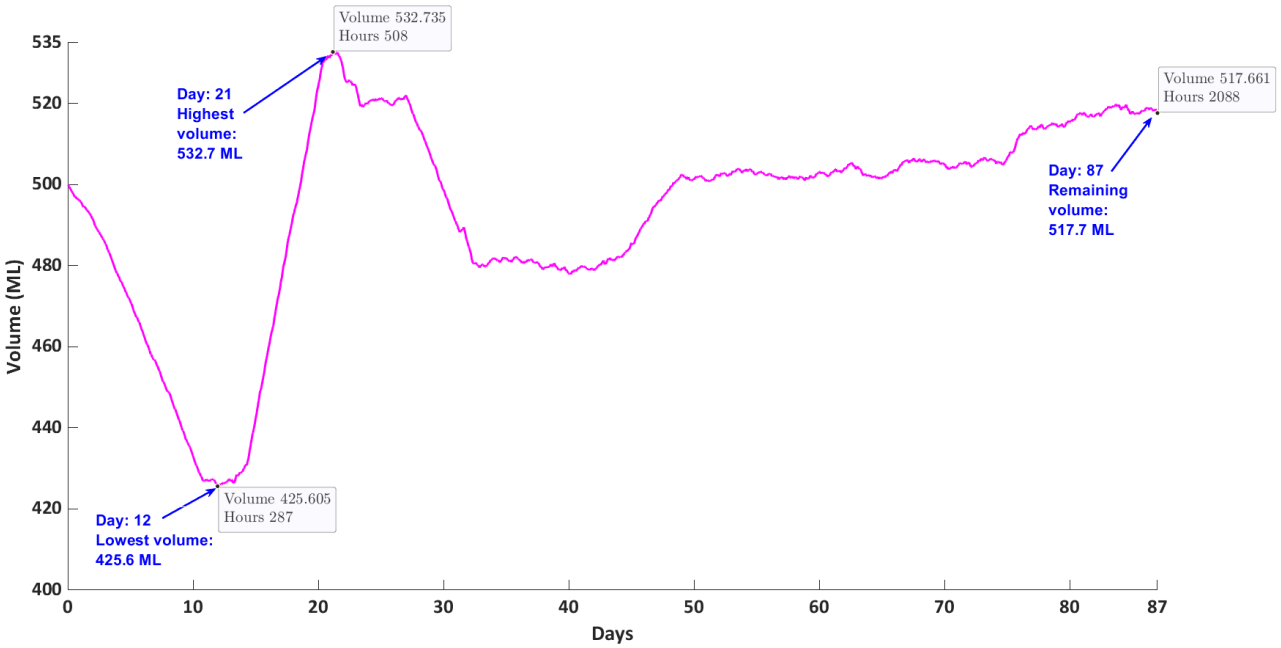

Figure 3.7: Water volume curve of the dam on the cotton farm

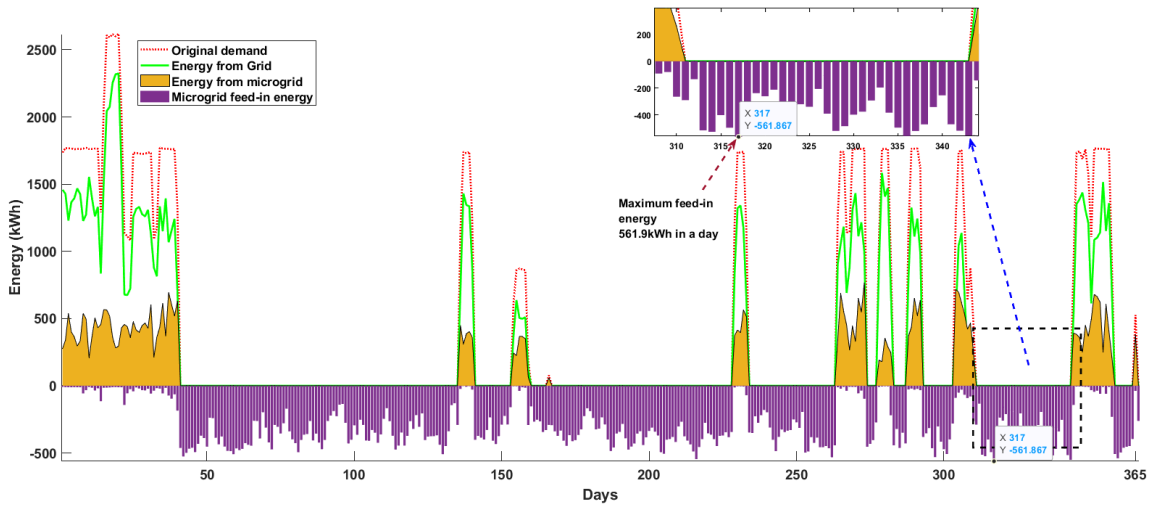

Figure 3.8: Microgrid energy distribution in Optimal case

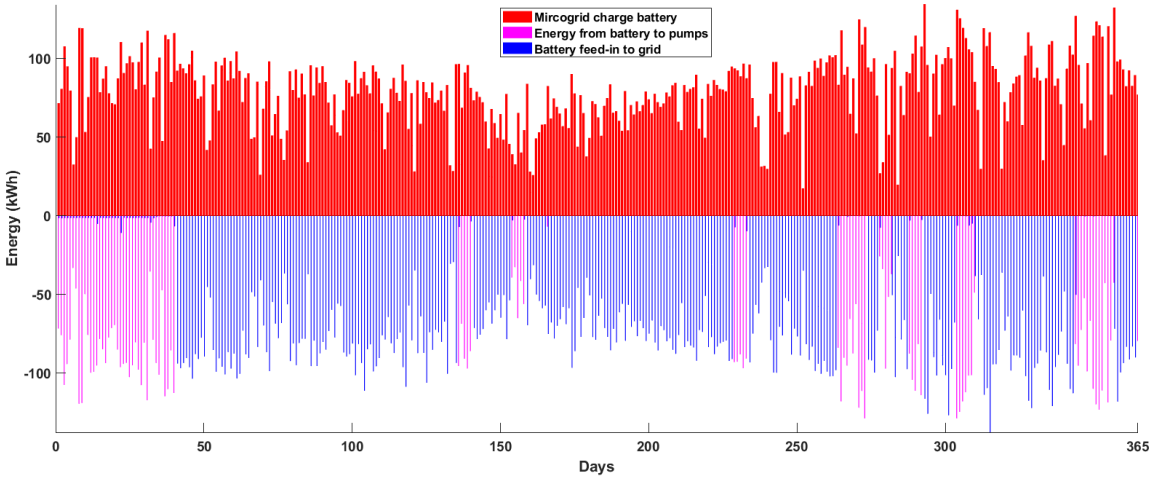

Figure 3.9: Battery storage charging/discharging status

3.4.2 Sensitivity analyses

In this section, we conduct a sensitivity analysis and discuss the impact of different factors on the designed MG system.

I. Impact of weighting coefficients

Table 3.10: Optimized microgrid design results of Optimal Case, Scenario 1 and Scenario 2

Item	Optimal Case	Scenario 1	Scenario 2
PV panel Qty.	242	210	206
WT 2kW Qty.	0	0	0
WT 5kW Qty.	0	0	0
WT 10kW Qty.	1	1	1
Battery pack Qty.	10	4	3
Total operational cost in the year (AU$)	21,611.8	24,284.8	27,751.4
Operation cost saving from Baseline Case	56.51%	51.13%	44.16%
Total investment (AU$)	266,500	194,900	183,300
Payback period (years)	9.49	7.7	8.35

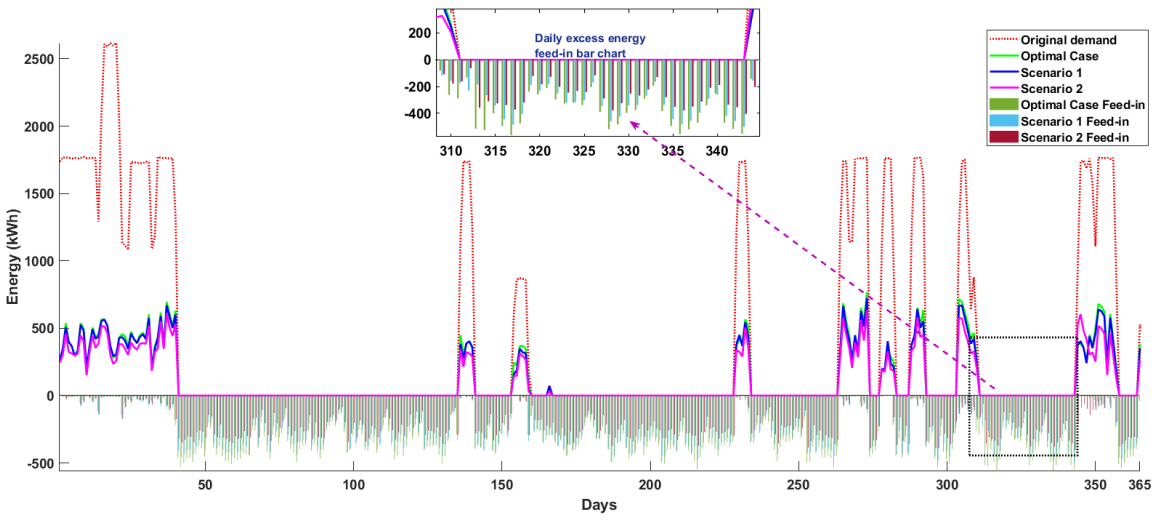

Figure 3.10: Microgrid power generation and the load demand

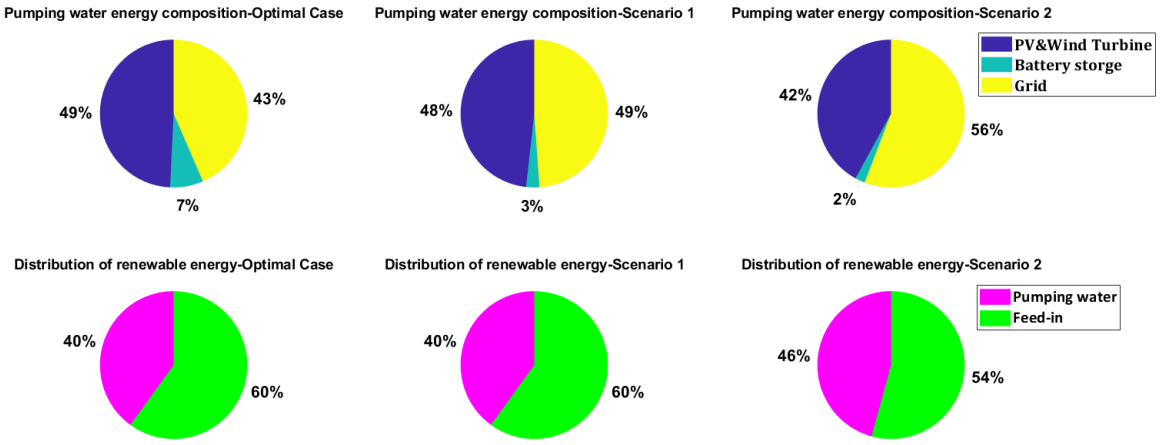

Figure 3.11: The energy contribution percentage of the microgrid components

Here two scenarios are considered; in the first scenario, i.e., Scenario 1, choose the weighting factors to be $\lambda_1 = 0.3$, $\lambda_2 = 0.1$ and $\lambda_3 = 0.6$. In Scenario 2, choose the weighting factors to be $\lambda_1 = 0.2$, $\lambda_2 = 0.6$ and $\lambda_3 = 0.2$. The other system parameters remain intact as the previous Optimal Case. The obtained results are shown in Table 3.10. By comparing the three results, $\lambda_1 = 0.6$ in the Optimal Case has the highest preference for operation cost minimization, and the MG supplies the majority of the required energy, implying the smallest operation cost. Scenario 1 has $\lambda_3 = 0.6$, i.e., the payback period has the highest weight, thus the obtained simple payback period is shorter than the Optimal Case. In Scenario 2, the weighting factor for investment is $\lambda_2 = 0.6$; therefore, the optimization results show that the investment cost is lower, but the operation cost is higher than the Baseline Case and Scenario 1. Also, the simple payback period of Scenario 2 is the

shortest in the three simulation cases. Figure 3.10 illustrates the comparison of Scenario 1 and Scenario 2 with the Optimal Case. Figure 3.11 shows the percentage of the MG components to meet the pumping load.

II. **Impact of different tariffs**

Tariff selection is also critical for operating costs and simple payback periods. In this case, two types of tariff and two types of FIT based on the tariffs shown in Table 3.2, Table 3.3 and Table 3.4 are adopted to see their effect on the MG configuration and simple payback period. Table 3.11 uses Baseline Case as a benchmark and lists the results of four tariff combinations. The operating cost of the case without MG is AU$ 49,694 under TOU tariff and AU$ 44,277 under the flat rate tariff. It can be found from Table 3.11 that the shortest simple payback period is 8.15 years, and the smallest investment is AU$ 183,300 among the four tariff options. Table 3.11 also illustrates that if the operating cost is higher, the investment cost will be higher, but the simple payback period is shorter. If the operating cost is lower, the investment cost is relatively minor, but the simple payback period will be longer.

Table 3.11: Optimization results for different tariff combinations

	Time-varying FIT based on TOU Tariff	Flat-rate FIT based on TOU Tariff	Time-varying FIT based on Flat-rate Tariff	Flat-rate FIT based on Flat-rate Tariff
Number of PV panels	242	238	234	206
WT (kW)	1×10 kW	1×10 kW	1×10 kW	1×10 kW
Battery storage numbers	10	6	7	3
Under MG operating cost (AU$/year)	21,612	22,319	20,532	24,422
Investment total (AU$)	266,500	223,100	232,700	183,300
Simple payback period (years)	9.49	8.15	9.80	9.23

III. Impact of wind speed and solar irradiation on the optimization MG system

Table 3.12: The results with increased average wind speed and daily solar global exposure

	Annual average wind speed increased to 5 m/s	Annual daily average global exposure increased to 6 kWh/m^2
PV panels number	348	245
WT configuration	1×10 kW	1×10 kW
Battery numbers	20	14
MG annual generation (kWh)	305,506.93	243,451.65
Operating cost under TOU tariff and time-varying FIT (AU$)	9,794	17,902.42
Operating cost reduction from Baseline case under TOU	80.29%	63.97%
Total investment (AU$)	399,000	309,650
Simple payback period (years)	10	9.74

WTs are one of the RESs mentioned in the previous section. The power generation of WTs changes significantly with wind speed. In the previous case study, the average wind speed of the case study cotton farm in 2016 was 3.42 m/s. The wind speed is scaled up to an average speed of 5 m/s to check the sensitivity of wind speed to the results, and all the parameters are kept the same as in the Optimal Case. The relevant results are listed in the first column of Table 3.12. Under the condition of higher wind speed, this system has higher power generation. As seen from Table3.12, the number of solar

panels is raised from 242 units to 348 units, and the number of battery storage is increased from 10 to 20 sets. This is because more operating cost reduction can be achieved with the increased wind speed, which in turn can offset some investment cost of PV and battery in the system. Now consider the impact of solar insulation, and it is assumed that the daily average global exposure is increased from 5.02 kWh/m^2 to 6.0 kWh/m^2 while the wind speed and all the other conditions remain the same as Optimal Case. The corresponding MG design results are listed in the second column of Table 3.12. Compared with Optimal Case, the number of solar panels is increased by 3, and the number of batter units is increased by 4. Therefore, the total investment is decreased by AU$ 43,150. The annual power generation is increased by 28,390.61 kWh; thus, the operating cost is reduced by AU$ 3,709.6, and the payback period is 3 months longer.

3.5 Summary

This chapter presents an MG optimal design model for Australian cotton farms. This method formulates the design as a multi-objective optimization problem, which is subject to various constraints on PV, WT, battery storage, and cotton irrigation demand. In the 3×10^6 m^2 cotton farm case study, a number of different MG scenarios are presented to illustrate the effectiveness of the proposed model.

Sensitivity analysis is also conducted to discuss the impact of weighting factors, battery storage and tariff options on the investment, operation cost and payback period. Compared with the existing energy consumption of this cotton farm, the designed MGs can reduce the operating costs by 44.16% to 56.51%, the simple payback periods are 8.35 years for Scenario 2 and 9.49 years for the Optimal Case, respectively. The grid-connected MG can also sell excess power to the grid to speed up the payback period. This case study provides a reference for cotton industry stakeholders to consider RES investment in cotton farms.

Chapter 4

A Model Predictive Control Approach to a Water Pumping System in an Australian Cotton Farm Microgrid

4.1 Introduction

Based on the results of Chapter 3 on cotton farm MG investment planning, we know that using rich renewable and clean energy sources can significantly save energy costs and reduce emissions of greenhouse gases during high pumping demand seasons for cotton farms equipped with renewable energy sources (RESs) based MGs [113]. In a typical rural MG system, the key components usually include a hybrid of traditional energy sources and RESs, for example, diesel gen-

erators, solar photovoltaic (PV), and wind turbines, which are further aided by energy storage systems [114], and economical operations [115]. The aforementioned hybrid energy MG can be optimally operated to efficiently use RES and save more operating costs. In literature, there are many MG optimal operation technologies that can optimally dispatch energy for cost-saving purposes; for example, an MG smart energy management system to optimize the operation with a matrix real-coded genetic algorithm is presented in [116]; Ref. [117] discusses hybrid RES's control and energy management tenets and introduces different optimization methodologies applied to hybrid energy systems; fuzzy logic control is proposed in [118] for the demand side management of residential electric water heater load, and an optimal pump operation schedule is given in [119] for minimizing electricity charges. However, these methods in [116], [118], [119] do not have any feedback to cater for real-time system changes. Indeed, these studies do not observe the output of the control process from the perspective of control theory [4]. Therefore, the robustness and stability of the obtained solutions need to be improved by closed-loop control techniques. Note that model predictive control (MPC) is a powerful closed-loop optimal control tool [120], and it has been successfully applied in many MG operation problems [121]. Generally, MPC is a control technique that optimizes the system under each moving prediction horizon [122]. After implementing the calculated control solution over a certain

time period, the controller iteratively solves the optimization problem over the next prediction horizon to cater for real-time system changes [123]. Therefore, any disturbances and uncertain system changes will be taken into account during the MPC optimization iteration process, and robustness can be achieved [124]. In addition, robust MPC and stochastic MPC on the relationship between stochastic uncertainty and cost function are also proposed in [125]. The implementation of robust MPC through numerical method is overviewed in [126]. Ref. [127] applies the stochastic MPC method to an urban drainage network and observes the effect of bias and uncertainty on the performance of MPC.

In this chapter, we are particularly interested in the application of MPC to the MG system at Australian cotton farms, where the MG consists of a diesel generator, renewable generation, and battery storage to supply the water pumping system at cotton farms. In literature, MPC has already been applied for pumping systems; for example, a water pumping station is operated using MPC after introducing the general convergence and robustness of the MPC algorithm in energy resource allocation in [61]; and open-loop and closed-loop optimization control methodologies are compared to validate MG economic impact and system robustness in [128]. However, these investigated water pumping systems are not powered by MGs, but by the external main grid only.

For a general MG, MPC has also been applied in its operational control. For

instance, Ref. [129] applies MPC in the energy management of an MG from the perspective of fault mitigation. MPC is used in [62] for the optimal operation of grid-connected wind farms which have hydrogen-based energy storage systems and local load. A supervised power management strategy system based on the MPC method is introduced in [130], which is designed for a stand-alone DC MG with distributed power generation, load and battery energy storage, in order to solve the optimization problem under operational constraints. In the agriculture sector, MPC has been successfully used to control water consumption during irrigation according to soil humidity [131]. Moreover, the key contribution of the control system of agricultural irrigation systems is irrigation management [132] and water use efficiency [133]. Meanwhile, the reduction of operating costs by configuring rural MGs and open-loop control is demonstrated in [134]. Ref. [135] proposes a method of load shifting to optimize the control of the water pumps to achieve operating cost reduction. However, there are quite limited studies and technical practices for the optimal operation of the Australian rural MG system to improve the operation efficiency of farm energy systems, especially for cotton cultivation. In particular, there is a lack of studies on the cotton farm MGs, which are very different to usual MGs as cotton farm MGs need to consider complicated water demand during the cotton growing period. For instance, water demand changes significantly during specific growing periods. Moreover, water irrigation, seepage

and evaporation at both the reservoir and cotton field, and precipitation also need to be considered. Therefore, this chapter aims to minimize the Australian cotton farm MG operating cost by proposing an MPC approach considering all the above-mentioned cotton-specific water demand constraints. Grid-connected and off-grid operations will be modelled within this MPC model. The benefits of this MPC approach will also be demonstrated when disturbances from rainfall and high water evaporation are present.

The main contributions of this study are briefed below.

- An MPC approach is developed to minimize cotton farm MG operating costs under both the grid-connected and islanded modes. The obtained MPC model can reduce operating costs by optimally controlling the power flow and the water pumps at the cotton farm.
- The proposed MPC approach is particularly effective in saving operating costs, given complicated disturbances from rainfall and evaporation that significantly affect the water demand load.
- Real-world data from an Australian cotton farm is applied in the case study, and the obtained results not only show the cost savings under grid-connected and islanded MG operational modes but also demonstrate maximized renewable energy utilization rates.

The following sections are laid out as follows. In Section 4.2, the MPC models of the cotton farm MG are presented for both the grid-connected and islanded modes. The closed-loop MPC algorithm is also explained. Section 4.3 and Section 4.4 give detailed case studies to validate the proposed MPC algorithm. Finally, conclusions are provided in Section 4.5.

4.2 A control model for cotton farm MG operation

The following assumptions are needed in the MG modelling. The objective is to minimize the operating cost of the water irrigation system at the cotton farm. The irrigation system includes several pumps which pump water to a reservoir, and water flows from the reservoir to the cotton field by gravity. Thus, we only need to control the water pumps properly to save energy costs. These pumps are powered by grid power under grid-connection mode and can also be powered by diesel generators and clean energy such as solar PVs. To minimize the irrigation cost of the cotton farm under various uncertainties and disturbances from water evaporation, precipitation and seepage, the MPC method is chosen. MPC is based on the principle of feedback control, and its iterative process can predict the disturbance factors. In actual cotton farms, weather can significantly impact irrigation activity. Therefore, the advantage of MPC against open-loop optimization is that it can respond to weather changes to achieve the purpose of energy

saving and cost reduction. The model's flow chart is presented in Figure 4.1.

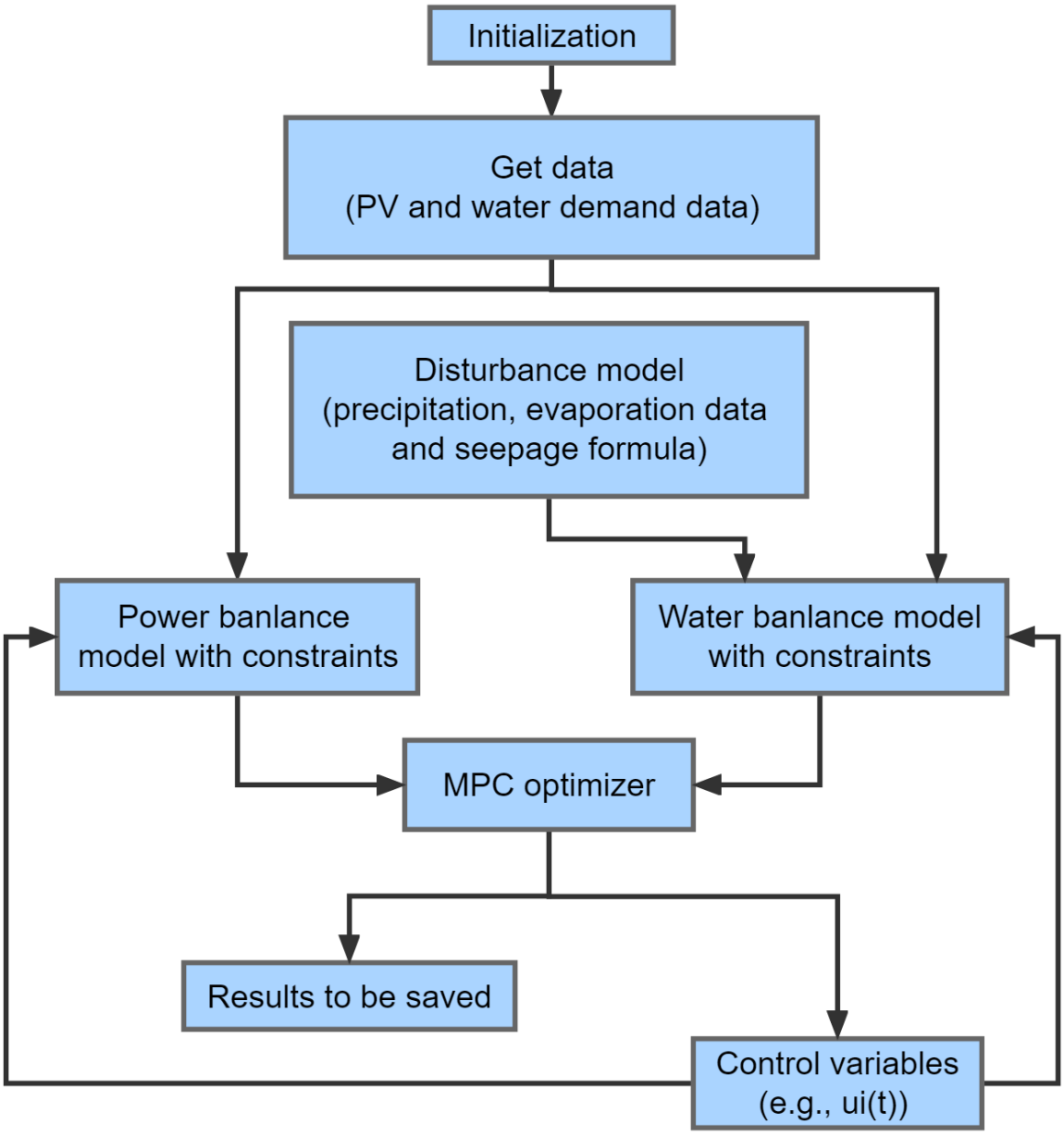

Figure 4.1: MPC concept block

4.2.1 MPC loops for the hybrid energy system

The basic MPC closed-loop method is shown in Figure 4.2. In the system of Figure 4.2, the optimal control model is solved over a moving time horizon, which is updated periodically to provide feedback and real-time system parameters changes,

such as renewable power generation changes and demand changes. The feedback mechanism can ensure timely correction of the optimal controller to achieve a stable solution against disturbances such as rainfalls and evaporation to be considered in this section. The following variables are defined for the Figure 4.2:

- Input: It is the control input of the hybrid system, which is obtained from the Optimizer, such as the on/off status of each water pump.

- Output: It is the output of the hybrid system, e.g., the water volume.

- Measured-output: It is the signal that is directly measured from the hybrid system. It is sent to the Prediction Model to predict the future output.

- Future output: It is the predicted response of the hybrid system over a future time horizon, which will be sent to the Optimizer.

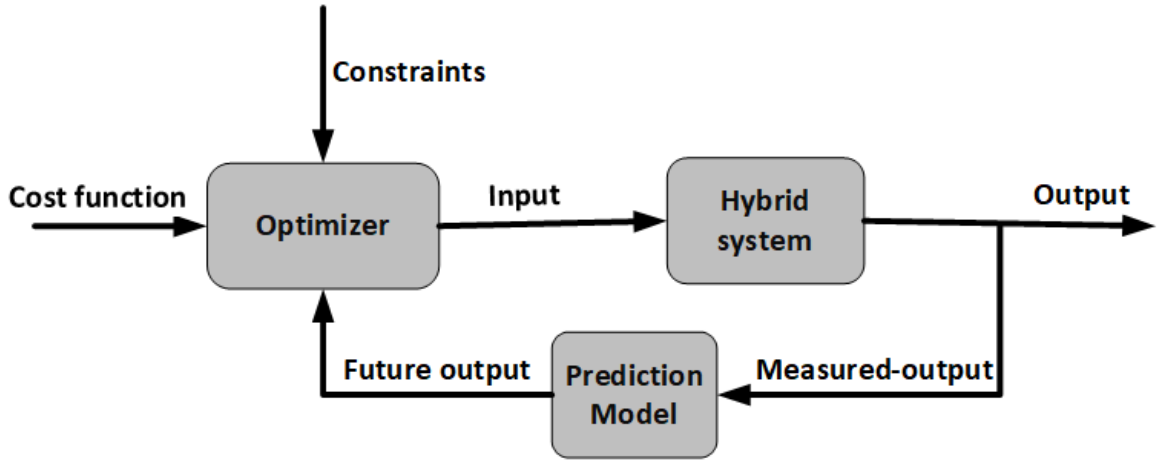

Figure 4.2: MPC closed-loop model

4.2.2 Water balance model

The water irrigation system is shown in Figure 4.3. Water inflow brought by pumps and precipitation needs to be balanced with the outflow caused by both irrigation needs and evaporation. The corresponding water balance model can be given below.

$$V(t+1) = V(t) + V_{inflow}(t) - V_{outflow}(t) \tag{4.1}$$

$$V_{inflow}(t) = \sum_{i=1}^{L} \frac{u_i(t) \cdot P_{rate,i} \cdot \Delta t}{E_{con,i} \cdot H_i} + \sum_{i=1}^{L^{ind}} \frac{u_i^{ind}(t) \cdot P_{rate,i}^{ind} \cdot \Delta t}{E_{con,i}^{ind} \cdot H_i^{ind}} + V_{R\_res}(t) \tag{4.2}$$

$$V_{outflow}(t) = V_{r2l}(t) + V_{L\_res}(t) \tag{4.3}$$

$$u_i(t) \ (or \ u_i^{ind}(t)) = \begin{cases} 0, \text{ when pump is off} \\ 1, \text{ when pump is on} \end{cases} \tag{4.4}$$

$$t = 1, \ldots, T$$

s.t.

$$V_{lower} \leq V(t) \leq V_{upper} \tag{4.5}$$

$$0 \leq \sum_{i=1}^{L} \frac{u_i(t) \cdot P_{rate,i} \cdot \Delta t}{E_{con,i} \cdot H_i} + \sum_{i=1}^{L^{ind}} \frac{u_i^{ind}(t) \cdot P_{rate,i}^{ind} \cdot \Delta t}{E_{con,i}^{ind} \cdot H_i^{ind}} \leq \frac{V_{max} \Delta t}{24} \tag{4.6}$$

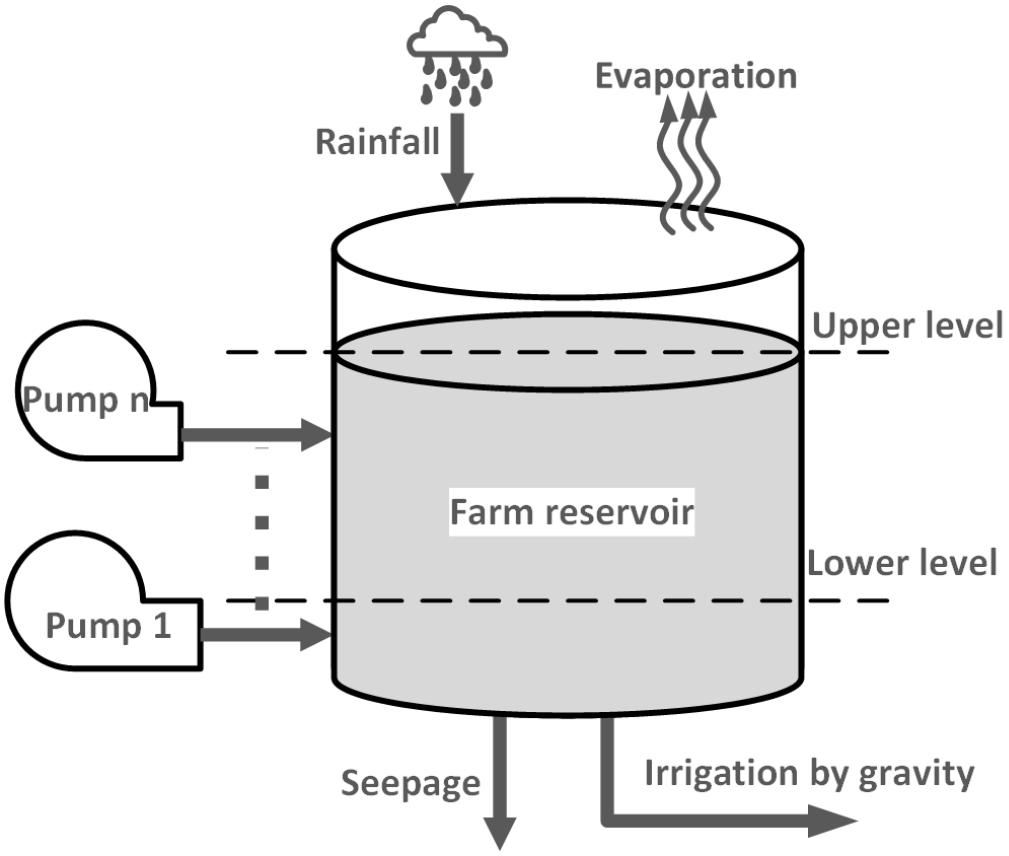

Figure 4.3: Farm water storage components and water balance model

where $\Delta t = 1$ h is the sampling time period, t is the time index, and T is the total length of the prediction horizon. Notation $V(t)$ represents the amount of water in the reservoir at the t^{th} hour, and V_{upper} (ML) and V_{lower} (ML) are the upper bound and lower bound of $V(t)$, respectively. Equation (4.1) gives the water balance relation, where $V_{inflow}(t)$ is the water inflow (in ML) and $V_{outflow}(t)$ is the water outflow (in ML). Equation (4.2) calculates $V_{inflow}(t)$ as the total amount of water pumped from all the pumps plus the amount of precipitation $V_{R\_res}(t)$; where the first two items on the right-hand side of (4.2) calculate the corresponding amount of water pumped by the MG pumps and the independent pumps beyond the MG, respectively. Here, it is assumed that the farm has two types of pumps; one is

supplied by the MG, and the other is called independent pumps, which are not supplied by the MG. In (4.2), $P_{rate,i}$ is the rated power of the i^{th} pump controlled by the MG; $P^{ind}_{rate,i}$ is the rated power of the i^{th} independent pump which is not supplied by the MG but by either the grid or diesel generators; $E_{con,i}$ and $E^{ind}_{con,i}$ are both equal to 4.55 kWh/m [136] which represent the energy needed to pump 1 ML of water for one meter of height for the two types of pumps; H_i and H^{ind}_i are the water heads (in meters) of the two types of pumps, and L and L^{ind} are the total numbers of pumps in these two types of pumps. Equation (4.3) calculates the outflow as the sum of water flow to the cotton field by gravity (i.e., $V_{r2l}(t)$ in ML) and the water loss $V_{L\_res}(t)$ (ML) due to evaporation and seepage. Notations $u_i(t)$ and $u^{ind}_i(t)$ in (4.4) are the binary on/off switching status control variables. In (4.5), V_{max} denotes the maximum water volume allowed per 24 hours to be collected from the water source (e.g., river or borehole) [137]. From the above equations, the following relation is derived.

$$V(t+1) = V(t) + \sum_{i=1}^{L} \frac{u_i(t) \cdot P_{rate,i} \cdot \Delta t}{E_{con,i} \cdot H_i} + \sum_{i=1}^{L^{ind}} \frac{u^{ind}_i(t) \cdot P^{ind}_{rate,i} \cdot \Delta t}{E^{ind}_{con,i} \cdot H^{ind}_i} + V_{R\_res}(t) - V_{r2l}(t) - V_{L\_res}(t) \quad (4.7)$$

4.2.3 Hybrid-power microgrid model

hybrid-power MG systems are one of the solutions for the electrification of remote cotton farm areas where grid expansion is difficult or not economical. Typically, the hybrid-power MG system integrates renewable energy sources such as solar and wind with conventional energy generators (e.g., utility grid or diesel generator) to provide electric power, and excess electricity can be either fed into the grid or stored in batteries for energy storage. Figure 4.4 shows a configuration of the grid-connected hybrid-power MG, and Figure 4.5 shows the islanded hybrid-power MG configuration.

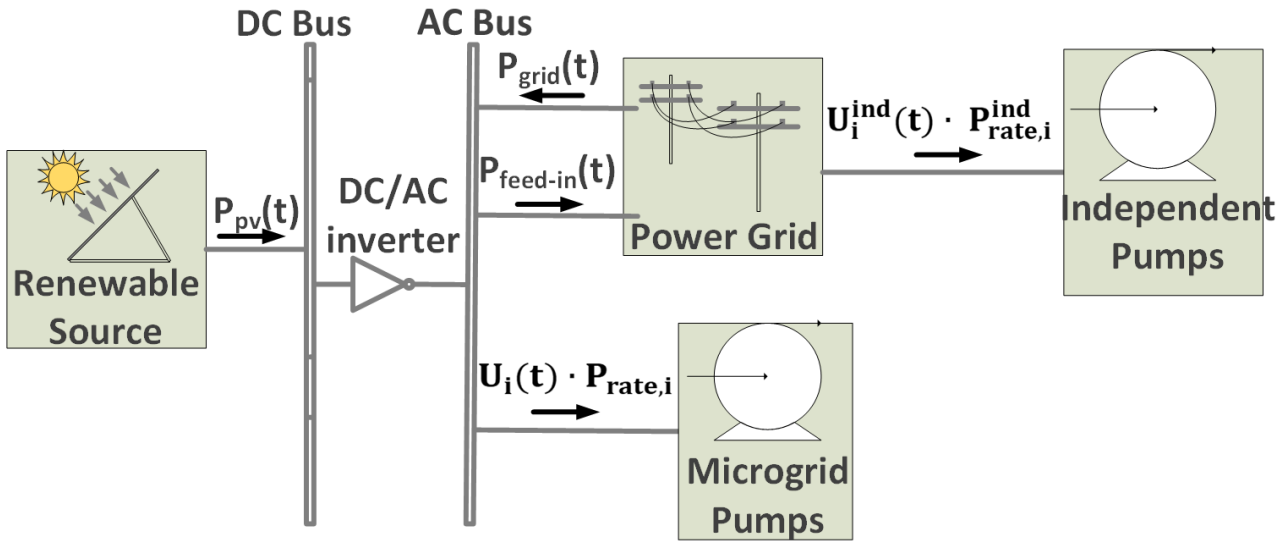

Figure 4.4: Grid-connected hybrid-power MG configuration

I. Grid-connected MG model

From Figure 4.4, a diesel generator should not be used in a grid-connected

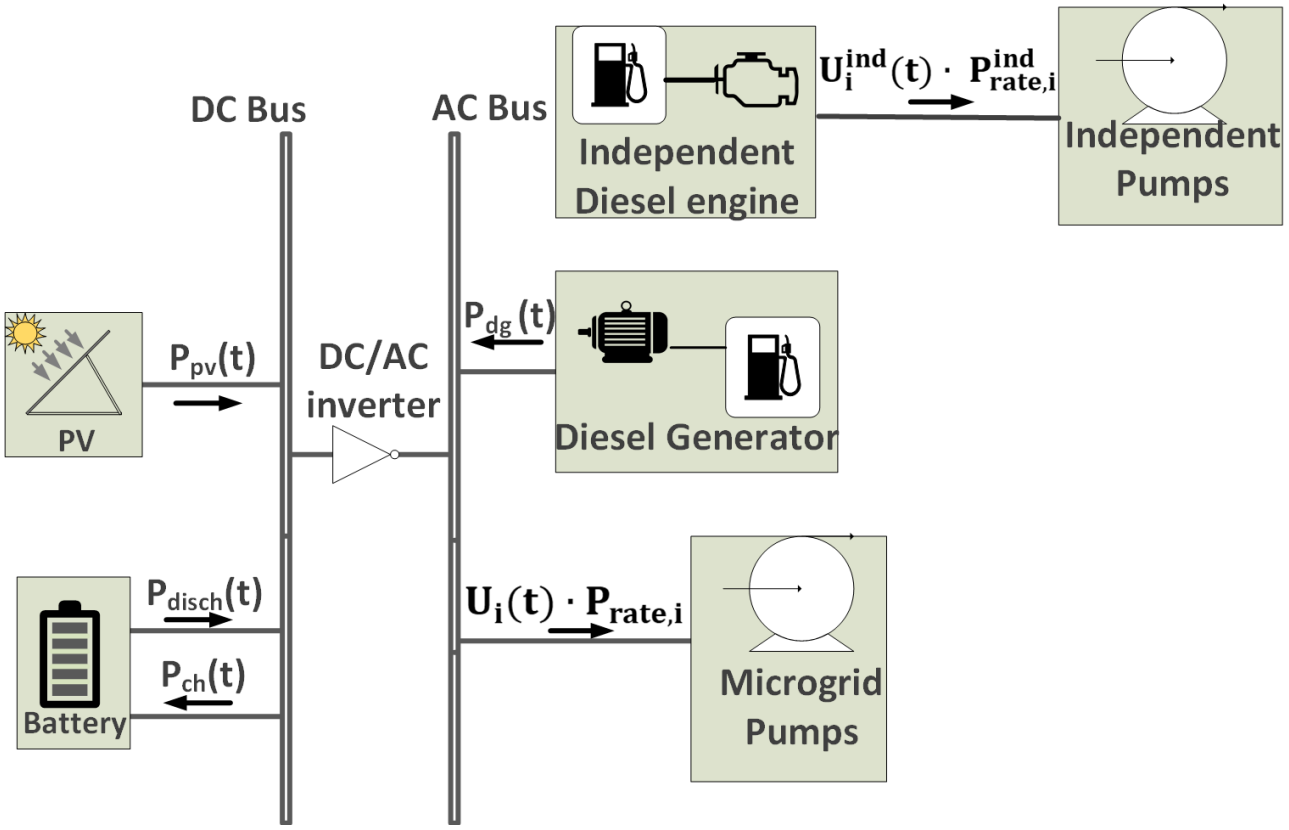

Figure 4.5: Islanded hybrid-power MG configuration

MG due to its high cost. Then the following relations hold.

$$P_{pv}(t) + P_{grid}(t) = \sum_{i=1}^{L} u_i(t) \cdot P_{rate,i} + P_{feed-in}(t) \tag{4.8}$$

$$P_{pv}(t) = \alpha \cdot P_{pv}^{0}(t) \tag{4.9}$$

$$0 \leq P_{grid}(t) \leq \eta_G(t) \cdot P_{pump}^{max} \tag{4.10}$$

$$0 \leq P_{feed-in}(t) \leq [1 - \eta_G(t)] \cdot P_{feed-in}^{max} \tag{4.11}$$

where $P_{pv}(t) \geq 0$ represents the PV power generation at the t^{th} hour; $P_{grid}(t) \geq 0$ is the power required from the grid at time t; $P_{feed-in}(t) \geq 0$

is the feed-in power flowing back to the grid; α is the number of the PV units installed; $P_{pv}^{0}(t)$ is the PV power output from a single unit; P_{pump}^{max} is the maximum power allowed for all the pumps; $\eta_G(t)$ is a binary variable which equals 1 when $P_{grid}(t) > 0$ and 0 otherwise; $P_{feed-in}^{max}$ is the maximum allowed feed-in power.

II. **Islanded microgrid model**

Equation (4.12) demonstrates the power balance model for the islanded MG which is based on Figure 4.5. The diesel generator can supply the power needed when the renewable energy generation is less than the required power.

$$P_{pv}(t) + P_{dg}(t) + P_{disch}(t) - P_{ch}(t) = \sum_{i=1}^{L} u_i(t) \cdot P_{rate,i} \tag{4.12}$$

s.t.

$$P_{pv}(t) + P_{disch}(t) - P_{ch}(t) \geq 0 \tag{4.13}$$

where $P_{dg}(t)$ is the power from the diesel generator, and $P_{ch}(t)$ and $P_{disch}(t)$ are the charging and discharging power of the battery storage at the t^{th} hour. As it is not economical to charge the battery from the diesel generator, the constraint in (4.13) ensures the unidirectional power flow from the DC to AC bus.

III. **Battery storage model**

Battery packs are chosen as the energy storage of the MG. The battery state-of-charge (SOC) can be expressed by (4.14), and the SOC constraint is expressed as (4.15). Eqs. (4.16-4.17) ensures the battery cannot charge and discharge simultaneously.

$$S^{SOC}(t+1) = S^{SOC}(t) + \frac{P_{ch}(t) \cdot \eta_{ch} - P_{disch}(t)/\eta_{disch}}{C_{max}} \tag{4.14}$$

s.t.

$$S^{SOC}_{min} \leq S^{SOC}(t) \leq S^{SOC}_{max} \tag{4.15}$$

$$0 \leq P_{ch}(t) \leq \alpha_B(t) \cdot P^{max}_{ch} \tag{4.16}$$

$$0 \leq P_{disch}(t) \leq [1 - \alpha_B(t)] \cdot P^{max}_{disch} \tag{4.17}$$

where

- $S^{SOC}(t)$ is the battery SOC at the t^{th} time;
- S^{SOC}_{min} is the minimum SOC, which is $S^{SOC}_{min} = 20\%$;
- S^{SOC}_{max} is the maximum SOC, which is $S^{SOC}_{max} = 80\%$;
- C_{max} is the maximum energy capacity of the battery storage;

- η_{ch} and η_{disch} are charging and discharging efficiencies, respectively;

- $\alpha_B(t)$ is the binary variable which denotes the battery charging status, and it equals 1 for charging and 0 otherwise.

- P_{ch}^{max} and P_{disch}^{max} are the maximum charging and discharging power, respectively.

4.2.4 Optimization model

The cost function $F(t)$ is defined as follows. For the grid-connected mode,

$$F(t) = \left[P_{grid}(t) + \sum_{i=1}^{L^{ind}} u_i^{ind}(t) \cdot P_{rate,i}^{ind}\right] \cdot \Delta t \cdot \mathcal{C}(t) - P_{feed-in}(t) \cdot \Delta t \cdot \mathcal{B}(t) \tag{4.18}$$

for the islanded mode,

$$F(t) = [P_{dg}(t) + \sum_{i=1}^{L^{ind}} u_i^{ind}(t) \cdot P_{rate,i}^{ind}] \cdot \Delta t \cdot \sigma \cdot \mathcal{M}(t) \tag{4.19}$$

where, $\mathcal{C}(t)$ is the grid energy price at the t^{th} time (e.g. TOU tariff (AU$/kWh)); $\mathcal{B}(t)$ is the feed-in tariff, σ is an energy conversion coefficient, (e.g. $\sigma = 0.2417$ L/kWh, which means that 0.2417 L diesel is consumed to generate 1 kWh [136]), and $\mathcal{M}(t)$ is the diesel price (AU$/L) at the t^{th} time.

I. **Open-loop optimal control model**

To minimize the operating cost over the prediction horizon (T) (e.g., 24

hours), the objective for open-loop optimization is given as (4.20),

$$\min_{u_i, u_i^{ind}} \sum_{t=1}^{T} F(t) \tag{4.20}$$

II. **Closed-loop optimal control model**

The objective function for the closed-loop MPC is obtained by updating the optimization period in (4.20) to a moving horizon as (4.21),

$$\min_{u_i, u_i^{ind}} \sum_{t=1+m}^{T+m} F(t) \tag{4.21}$$

where the period $[m+1, \cdots, T+m]$ is the moving prediction horizon, and the optimization model needs to be solved over each of these moving horizons subject to similar constraints like (4.8) - (4.17) over $[m+1, \cdots, T+m]$.

4.3 Case study 1 - MPC simulation on Kensal Green cotton farm

A case study is carried out to validate the proposed MPC approach.

4.3.1 Scenario 1. Grid-connected cotton farm (without battery storage)

A cotton farm in the southern part of Gunnedah, New South Wales, Australia, is studied here. The total irrigation area was 3×10^6 m^2 in 2016. This studied cotton farm has two sub-bore pumps with a rated power of 75 kW. The farm also has a 37 kW re-lift pump to lift water from the Mooki river. One of the 75 kW pumps is directly connected to the grid, and the MG only supplies the other 75 kW bore pump and the 37 kW re-lift pump. The MG also has a 50.6 kW solar system [138]. In 2016, the pumping system pumped 1,004 ML water from the bore and 247 ML water from the river, while the maximum allowed water intake is 30 ML/day in the irrigation season [139]. Table 4.1 lists the cotton farm's pumps [140] and water storage parameters [141] used in the case study. The studied cotton farm's grid-connected MG system includes a RES and an energy storage system (ESS). The load includes an MG-supported pump system and an independent grid-connected pump. Water is pumped into the reservoir from a borehole or the Mooki river and irrigates the cotton farm by gravity (see Figure 4.6). The high irrigation water demand period considered here is about 87 days from November 2016 to January 2017. As shown in Figure 4.6, the pump control solution needs to optimally identify the switching status of pumps #1, #2 and

#3 for cost minimization purposes. Rainfall, seepage and evaporation are used as external disturbances to verify the robustness of this closed-loop MPC strategy, which will be discussed in the simulation result part.

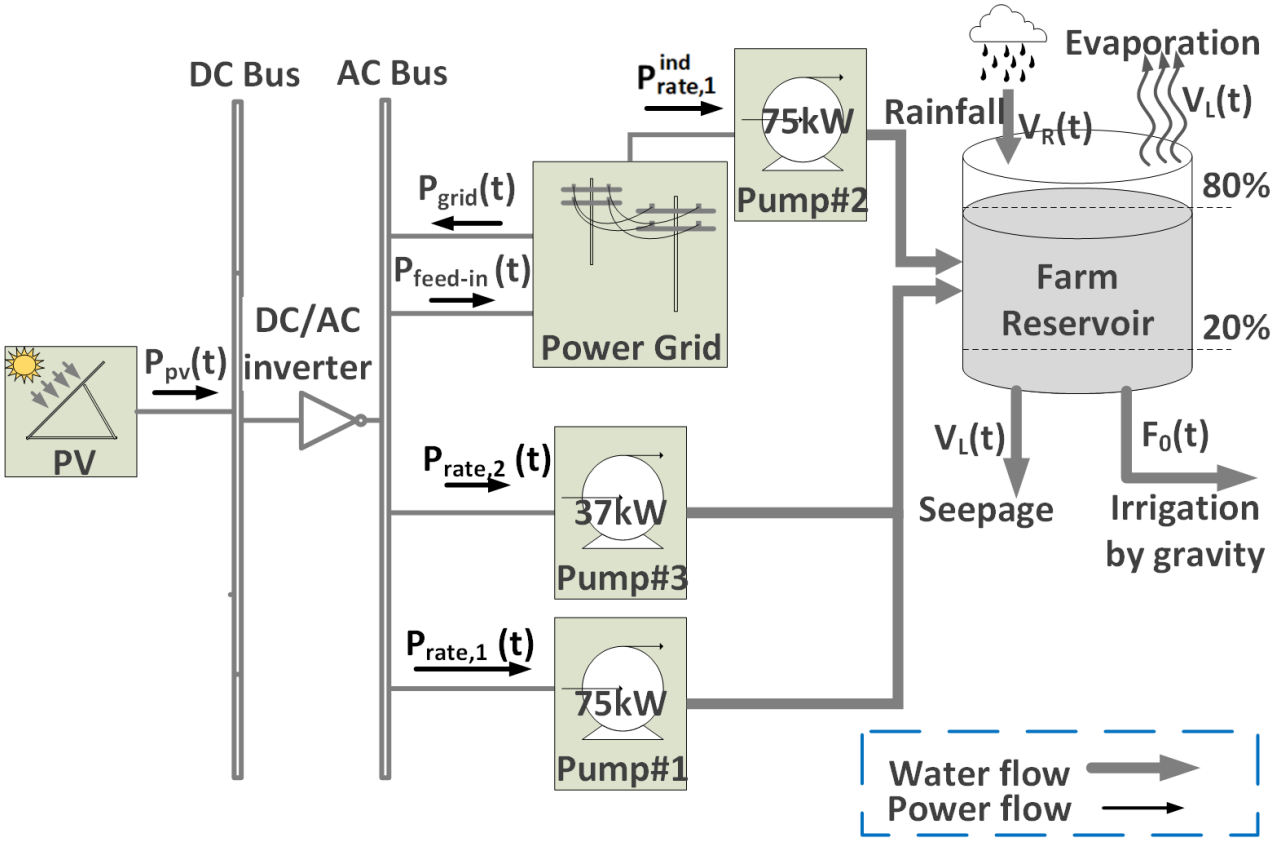

Figure 4.6: Grid-connected microgrid simulation model

I. Baseline Electricity Operating Costs

Table 4.2 presents the electricity cost of the cotton farm irrigation system over the considered 2016 irrigation period (i.e., 11/2016—01/2017). The owner of the farm controls the pumps by personal experience only.

II. Assumptions of closed-loop control model

Table 4.1: Key parameters of the studied cotton farm

Items	Values
Bore Pump #1	
(MG connected pump)	75 kW
Bore Pump #2	
(Independent pump)	75 kW
River Pump #3	
(MG connected pump)	37 kW
Cotton farm size	300 $\times 10^4$ m^2
Bore pumping head	31 m
River pumping head	12 m
Average energy consumption of	
lifting 1ML water per meter	4.55 kWh/(ML $\cdot$ m)
Average irrigation demand	6.5 $\times 10^{-4}$ ML/ m^2
Maximum allowed water usage	1800 ML/year
Reservoir size	800 ML
Daily average solar irradiation	
in 2016	5.02 kWh/m^2
Solar PV system installed	50.6 kW
Flat rate tariff in 2016	0.26 AU$/kWh
Feed-in tariff in 2016	0.06 AU$/kWh

Table 4.2: Energy costs breakdown in 2016

Items	Pumps	Values
Operation time	#1	1,034 h
	#2	882 h
	#3	360 h
Consumption	#1	75,812.33 kWh
	#2	63,551.06 kWh
	#3	12,865.24 kWh
Electricity cost	#1	19,711.2 AU$
	#2	16,523.3 AU$
	#3	3,345.0 AU$
Water pumped	#1	537.5 ML
	#2	450.5 ML
	#3	235.6 ML

In order to use the closed-loop MPC method to control the pumping system of the cotton farm, the following information will be applied in the simulation.

a. There are two pumps supplied by the MG and an independent pump #2 (75 kW) not supplied by the MG.

b. The pumps need to pump river water or bore water to the reservoir, and then the water flows from the reservoir to the cotton field by gravity.

c. The load factor is assumed to be one, i.e., reactive power is ignored.

d. Historical irrigation and pump power consumption data of the cotton farm in the 2016 irrigation period (i.e., 11/2016 - 01/2017) are taken, and the total irrigation period is 87 days.

e. In the baseline case, $V_{R\_res}(t) = V_{L\_res}(t) = 0$ ML, which means that in the baseline case, rainfall, evaporation and seepage losses are ignored.

III. **Robustness validation in the cotton farm**

The robustness of the closed-loop MPC is evaluated in this case study. The closed-loop MPC model can compensate for the disturbance within a range to ensure the stable operation of the system. In order to demonstrate the

robustness of the system under different conditions, two disturbance cases are designed to meet the requirements of the case study.

a. The first disturbance is the received rainfall. Rainfall data can be found in the Australian Government Bureau of Metrology (BOM). The 30-year average daily rainfall in mm/m^2 at the area of this cotton farm [142]. The total surface area of this reservoir is about 10^5 m^2. The 2016 rainfall data from the BOM are added as a disturbance to the MPC model. Then the water level at the reservoir is increased after the rainfall, and the irrigation demand at the cotton planting area is also decreased. Then $V_{R\_res}(t)$ can be calculated by (4.22), and (4.23) gives the rainwater received by the cotton planting area.

$$V_{R\_res}(t) = R_{data}(t) \cdot Z_{res} \cdot 10^{-6} \tag{4.22}$$

$$V_{R\_land}(t) = R_{data}(t) \cdot Z_{land} \cdot 10^{-6} \tag{4.23}$$

where $R_{data}(t)$ (mm/hour) represents hourly precipitation data from BOM; $Z_{res} = 10^5$ (m^2) is the surface area of the reservoir, the constant 10^{-6} is to convert the precipitation unit from mm/m^2 to ML/m^2. The notation $V_{R\_land}(t)$ (mm/h) represents the amount of rainwater received in the cotton farm at the t^{th} hour, and $Z_{land} = 3 \times 10^6$ (m^2) is the farmland area.

b. The second type of disturbance is the water loss caused by crop evapotranspiration, reservoir evaporation and seepage. During extended periods of hot weather, water loss will increase due to evapotranspiration and evaporation. Therefore, based on the relationship between radiation and evapotranspiration [143], the disturbance of additional water loss in the farmland caused by radiation, V_{eva_land}, can be expressed by (4.24). In addition, the evaporative loss from a farm reservoir can be defined as in (4.25) [144]. The water loss from reservoir $V_{L\_res}(t)$ is defined as (4.27) . Precipitation and high evapotranspiration/evaporation are both likely to occur during the cotton growing cycle.

$$V_{eva\_land}(t) = 0.408 \cdot (R^{rad}(t) - R^{rad}_{avg}) \cdot Z_{land} \cdot 10^{-6} \tag{4.24}$$

$$V_{eva\_res}(t) = \frac{0.67 \cdot E_{pan} \cdot Z_{res} \cdot 10^{-6}}{T_{hr}} \tag{4.25}$$

$$V_{se\_res}(t) = \frac{V_{upper} \cdot 10\%}{8760} \tag{4.26}$$

$$V_{L\_res}(t) = V_{eva\_res}(t) + V_{se\_res}(t) \tag{4.27}$$

where 0.408 is the conversion factor of evaporation volume [143]; $R^{rad}(t)$ is the hourly radiation value (MJ/m^2/h), and R^{rad}_{avg} is the monthly average value of radiation, and both values are obtained from BOM. In (4.25), $V_{eva\_res}(t)$ is the hourly water loss of the reservoir due to evaporation, 0.67 is the evaporation conversion factor [144]; E_{pan} (mm) represents evaporation from a class A open pan for the period; in this case, E_{pan} is 673.9 mm which represents the summation of the mean monthly pan evaporation of November, December in 2019 and January in 2020 [145]; and T_{hr} is the total hours in these three months which is used to convert the total pan evaporation to hourly data (e,g., $T_{hr} = 2,088$ h in this study); in (4.26), V_{se_res} is the hourly seepage loss of the reservoir, where it is assumed that the annual farm reservoir seepage loss is 10% of the reservoir upper bound volume [146]. Considering both the rainy season and hot weather, the water flowing from the reservoir to cotton farmland, V_{r2l} (t), is defined as (4.28)

$$V_{r2l}(t) = \begin{cases} 0, & \text{if } V_{R\_land}(t) - V_{eva\_land}(t) \geq V_{d0}(t) \\ V_{d0}(t) - V_{R\_land}(t) + V_{eva\_land}(t), & \text{else} \end{cases} \tag{4.28}$$

where $V_{d0}(t)$ is the irrigation water demand.

4.3.2 Scenario 2. Islanded MG with battery storage

The studied cotton farm has not yet installed battery storage. Nevertheless, the farm owner wants to go off-grid with a battery storage system in the future [147].

Table 4.3: Parameters of islanded MG case study

Items	Values
Energy coefficient (σ)	0.2417 $L(Diesel)/kWh$
Average diesel consumption of lifting 1 ML water per meter	1.1 $L/(ML \cdot m)$
Average diesel price in 2016	1.15 $AU\$/L$
Battery storage capacity	20 kWh
Rated power of the battery (charge/discharge)	10 kW

I. **Baseline of the islanded microgrid system**

In this baseline case, we use the parameters in Table 1 and replace the grid power supply with diesel generators without battery storage, and the owner manually controls all three pumps. Operating cost is the cost of diesel fuel consumption.

II. **Islanded microgrid with battery storage via MPC**

It is assumed that a 20 kWh battery storage is added to this islanded MG

system, and the impact on operating cost is analyzed. Figure 4.7 shows the islanded MG system of the cotton farm composed of PV, battery storage, and diesel generator. Electric pump #1 (75 kW) and electric pump #3 (37 kW) are the loads to be driven by this system. Pump #2 (75 kW) is driven by a diesel engine directly, and the diesel consumption of the 75 kW pump motor is 18.13 L/h. The pumping system operating costs are only diesel consumption. System operating cost can be optimized by controlling the on-off state of the three pumps. The parameters used are shown in Table 4.3.

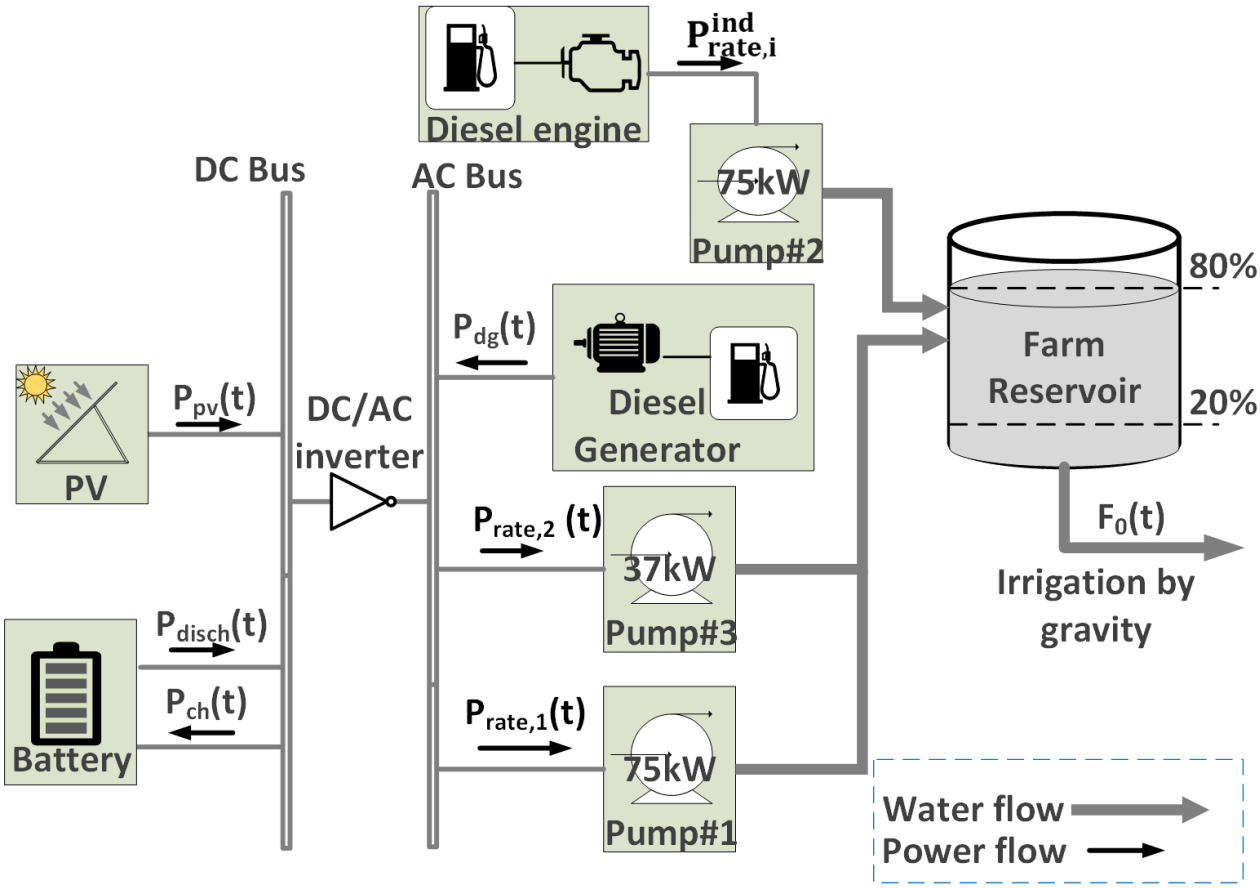

Figure 4.7: Islanded microgrid simulation model

4.3.3 Results and discussions

To validate the proposed MPC approach, grid-connected and islanded MG operational modes are considered here. The whole irrigation season is 87 days only; therefore, the MPC approach is compared with the baseline case over this whole irrigation period. The above 87 days are sampled each hour, and the total control period is 2088 hours. The baseline data are found from the 2016 historical irrigation data from a cotton farm at Gunnedah, New South Wales, Australia

I. **Comparison of simulation results of MPC with Baseline**

This section compares manual control (baseline) with the open-loop and closed-loop MPC solutions under grid-connected and islanded conditions, where we assume the same water irrigation demand for these different cases. The open-loop solution is derived from (4.20) over the first 24 hours. The MPC solution is also derived for the same 24 hours, but its component is derived by iteratively solving the optimization problem over the moving 24 hours horizons. Figure 4.8 shows the changes of the reservoir water volume under baseline and MPC within the prediction horizon (24 hours); the baseline curve shows that the water level is decreasing, while the MPC curves keep the water level around 500 ML. Table 4.4 shows the operating cost

and the volume of water pumped for manual control, grid-connected and islanded open-loop optimization and MPC approach to control water pumps within 24 hours. The baseline case has the cheapest operating cost, i.e., AU$ 399.5. And because the baseline case has only pump #1 working in the first 24 hours, the reservoir water is dropped to 495.8 ML. The operating costs of grid-connected and islanded MPCs are AU$ 411.61 and AU$ 408.37, respectively, because MPC has predicted the water demand after the first 24 hours and can provide better control. The open-loop solution of grid-connected and islanded MGs has a higher operational cost than the corresponding MPC solutions, and their remaining reservoir water volume is also lower than MPC.

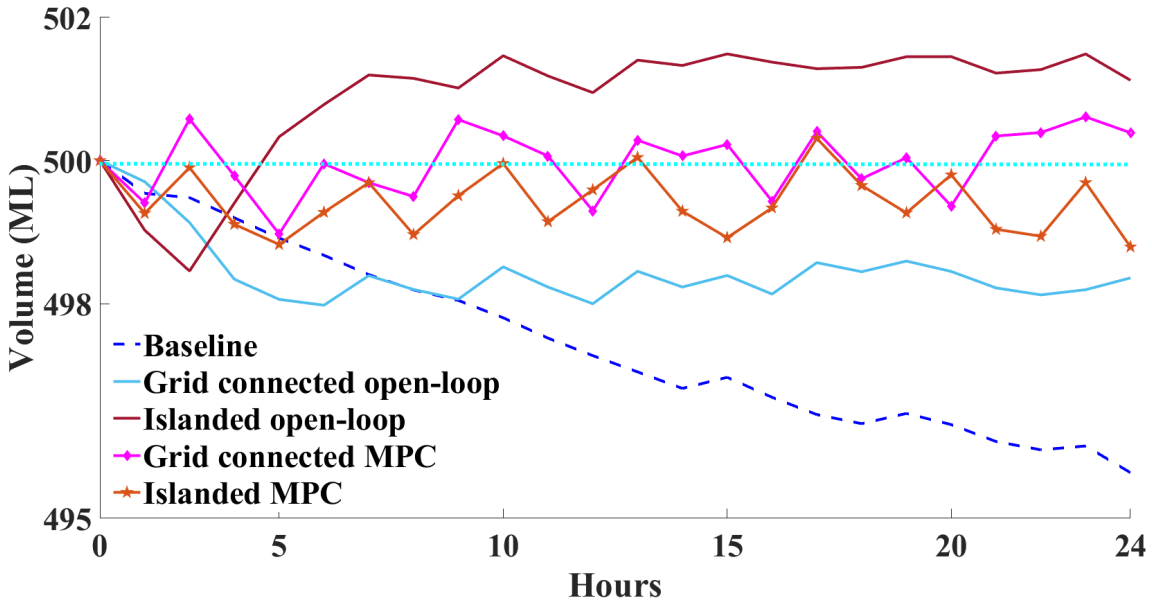

Figure 4.8: Reservoir water volume changes in the baseline, grid-connected and islanded cases

II. Comparison of results in different scenarios of grid-connected MG

Table 4.4: Comparison of each pumping control mode in 24 hours

	Total operating cost (AU$)	Pumped water (ML)
Baseline	399.5	12.30
Grid-connected open-loop	429.61	14.7
Grid-connected MPC	411.61	18.38
Islanded open-loop	429.78	16.10
Islanded MPC	408.378	17.46

This section compares the MPC and its robustness in the different scenarios defined in Section 4.3. The comparison includes the pumping volume and operating costs for the following scenarios in the 87-day irrigation period:

a The manual control models.

b The MPC model without disturbance.

c The MPC model with rainy season disturbance.

d The MPC model with both the rainfall and high evaporation season disturbance.

- **Case i. Baseline case**: The baseline case is the existing manual control result, which is calculated from the historical water pump power

consumption data, water head, and the volume of pumped water. The manual operation is controlled based on the farmer's personal experience. The total baseline operating cost is AU$ 39,580 over the whole irrigation period, and 1,180.7 ML water is pumped within this period.

- **Case ii. MPC – without disturbance**: Now consider the case of the MPC approach where disturbances from rain and evaporation are ignored. The MPC optimization horizon is $[m, m + 24]$, and the solution is recalculated for each $m = 1, \cdots, 2088$. The real-time measured reservoir water level is fed back to the MPC controller as the initial reservoir water level for each optimization period. Figure 4.9 shows the obtained reservoir water volume under this closed-loop MPC solution. By this MPC approach, the operating cost can be reduced while maintaining properly the reservoir water level within an acceptable range. The results are shown in Table 4.6, where the total operating cost under MPC is AU$ 27,556 for the whole irrigation period, which is AU$ 12,023.5 lower than the baseline.

- **Case iii. MPC – with rain season disturbance**: Now consider the disturbance caused by rain and precipitation data from November 2016 to January 2017 is considered. During the considered period, there were

three occurrences of heavy rainfalls which brought significant changes to the water level of the reservoir. For example, from December 23 to December 24, 2016 (i.e., 1300^{th} to 1315^{th} hours in Figure 4.9, 41 mm/m^2 precipitation was received which brought 39.28 ML water to the reservoir. Then the MPC solution stops the water pumps during the 1274^{th} hour to the 1399^{th} hour due to the received rainwater, and the pumps remain to be switched off until the reservoir water level drops to 500 ML. Due to the additional water contributed by the rainy season, the operating cost during the whole irrigation period is A$16,019.5 (e.g., 40.47%) lower than the baseline period which is calculated from Table 4.6.

- **Case iv. MPC – with rainy and high-evaporation days**: In hot weather, the hourly evapotranspiration and evaporation are higher than the monthly average, and it is added together with precipitation data to the case study to calculate the MPC solution. The evapotranspiration and evaporation data can be calculated based on the hourly radiation data from Bureau of Meteorology (BOM). Figure 4.9 shows that after high evaporation and precipitation disturbances are added to the system, the highest water volume in the reservoir reaches 552.8 ML, and

the lowest volume reaches 488.2 ML. However, when the disturbance is removed, the water level still returns to around 500 ML.

Table 4.5 compares the working hours and operating cost for all three pumps under open-loop and MPC solutions; Table 4.6 presents the pump operating hours and costs, along with the amount of water pumped during the entire irrigation period; and Figure 4.9 illustrates the reservoir water level under different control scenarios.

Table 4.5: Open-loop optimization and MPC before disturbance 24 hours (1268^{th} -1291^{st} hour) results comparison

Test cases	Pump #1 75 kW		Pump #2 75 kW		Pump #3 37 kW		Total operational cost (AU$)
	Work hours	Water lift (ML)	Work hours	Water lift (ML)	Work hours	Water lift (ML)	
Case ii (open-loop)	4	2.13	9	4.79	4	2.71	261.37
Case ii (MPC)	8	4.25	10	5.32	5	3.89	279.39
Case iii (open-loop)	4	2.13	9	4.79	4	2.71	261.37
Case iii (MPC)	5	2.66	2	1.06	1	0.68	103.92
Case iv (open-loop)	8	4.25	13	6.91	10	6.77	429.4
Case iv (MPC)	5	2.66	3	1.6	3	2.03	198.31

This MPC algorithm is implemented using MATLAB 2021b with IBM CPLEX 12.10.0 on a laptop with Intel (R) Core (TM) i7-8650U CPU @ 2.11GHz and 16G RAM. Now we can compare the open-loop and MPC results under the disturbance situations in Table 4.5. One of the rainfall disturbances occurred

Table 4.6: Results over the entire irrigation period

	Case i	Case ii	Case iii	Case iv
Pump #1				
Energy consumption (kWh)	71,386	36,450	32,700	50,250
Water lift (ML)	506	258.42	231.82	356.26
Pump #2				
Energy consumption (kWh)	63,527	62,775	50,250	35,625
Water lift (ML)	450.4	445.05	365.26	252.57
Pump #3				
Energy consumption (kWh)	12,242	26,048	21,349	23,310
Water lift (ML)	224.21	477.07	391.00	426.92
Total operational cost (AU$)	39,580	27,556	23,560	26,278

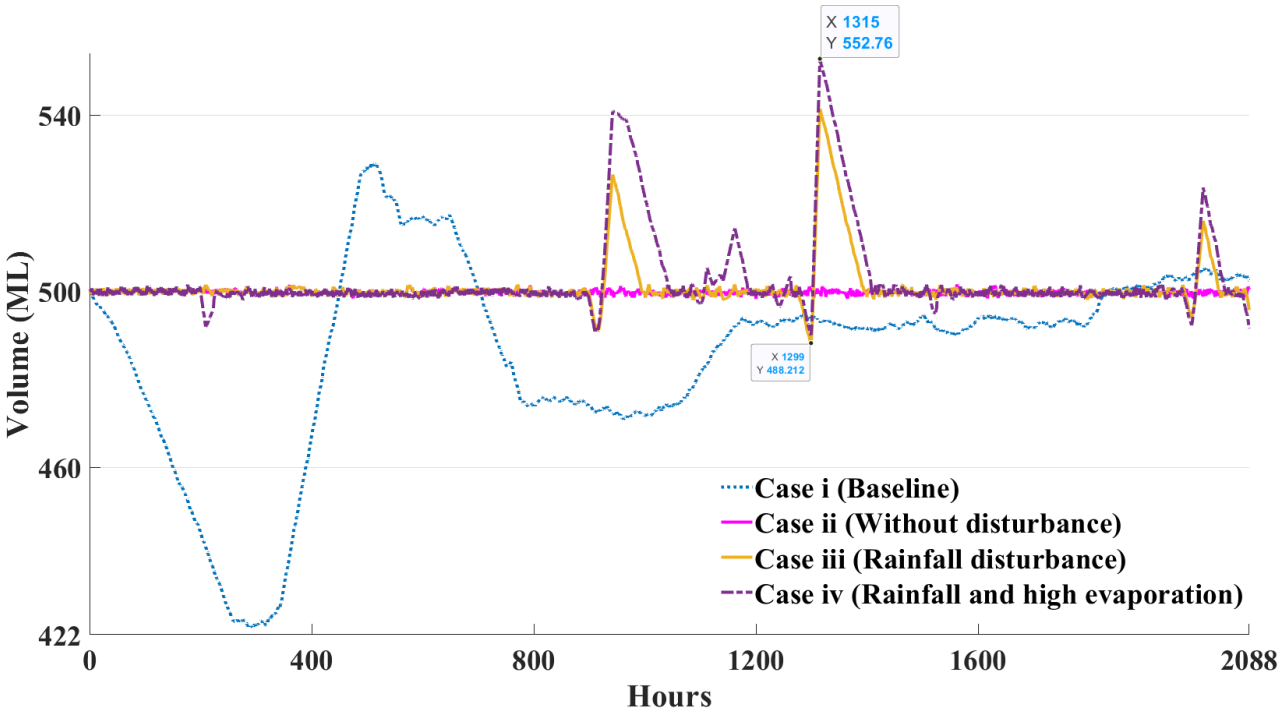

Figure 4.9: Reservoir water volume changes in the baseline and grid-connected cases under different scenarios

during $1300^{th} - 1315^{th}$ hour, and one of the high evaporation disturbances occurred during $1281^{st} - 1288^{th}$ hour, we use starting time 1268^{th} hour and ending time 1291^{st} hour for the simulation. In Case ii, the MPC method has a higher operational cost than the open-loop solution because the MPC solution can predict the next 24 hours, which will have high water demand, and consequently, 3.83 ML more water is pumped than the open-loop solution during the same period. In Case iii, open-loop optimization is not affected during the $1268^{th} - 1291^{st}$ hour, which has no rainfall. Thus, we can find its optimization results are the same as those of Case ii; however, the MPC method uses predicted information up to 1315^{th} hour, which covers one of the rainfall disturbance periods. Therefore, the MPC solution in Case iii has AU$ 157.45 lower in operational cost than the open-loop solution. In Case iv, high evaporation disturbance can affect both MPC and open-loop, but the operating cost of MPC is AU$ 231.09 lower than open-loop operation. From Table 4.6, the operating cost of Case ii is AU$ 12,024 lower than Case i; and in Case iv, 33.6% of annual irrigation operating costs can be saved from Case i, which implies 20.7% less energy purchased from the grid. The operating cost of Case iv is higher than that of Case iii, but AU$ 1,278 is lower than that of Case ii. The operating costs of all the MPC solutions are less than that of the baseline.

III. Comparison of results in different scales of islanded microgrid with battery storage

In the case of islanded MG, MPC is designed to reduce the operating cost of the islanded MG. In order to show the impact of different scales of MGs on the cotton farm, it is assumed that the current solar and battery systems (denoted as small MG) are increased to four times (denoted as large MG); see also Table 4.7. Figure 4.10 shows the comparison results of baseline and MPC with 2 different MG scales (small MG and large MG). From Figure 4.10, the utilization rate of the MG pumps (Pump #1 and Pump #3) in the baseline is not as high as that of the MPC method; this is because the water volume pumped by the independent pump #2 in the baseline is obviously greater than the amount of water pumped by the small MG or large MG. Furthermore, Figure 4.10 shows the percentage of energy utilization. During the 87-day irrigation period of the baseline, solar energy contributed 9% (13,820 kWh) of the total energy. However, the use of diesel fuel provided 91% (133,335.5 kWh) of the total energy. In the MPC-based small MG case, the contribution of solar and diesel energy is 16% and 84%, respectively. In the MPC-based large MG case, solar energy contributes 64%, and diesel energy contributes 36% of the total energy.

Table 4.7: Islanded microgrid parameters

	Islanded small MG	Islanded large MG
PV size	50.6 kW	202.4 kW
Battery capacity	20 kWh	80 kWh

Table 4.8: Computation details of the case study

	Number of variables per iteration	Number of constraints per iteration	Total calculation time (s)
Grid-connected MPC without disturbance	288	161	5,420
Grid-connected MPC with rain disturbance	288	167	5,711
Grid-connected MPC with rain and evaporation disturbance	288	184	6,460
Islanded MPC	264	230	12,380

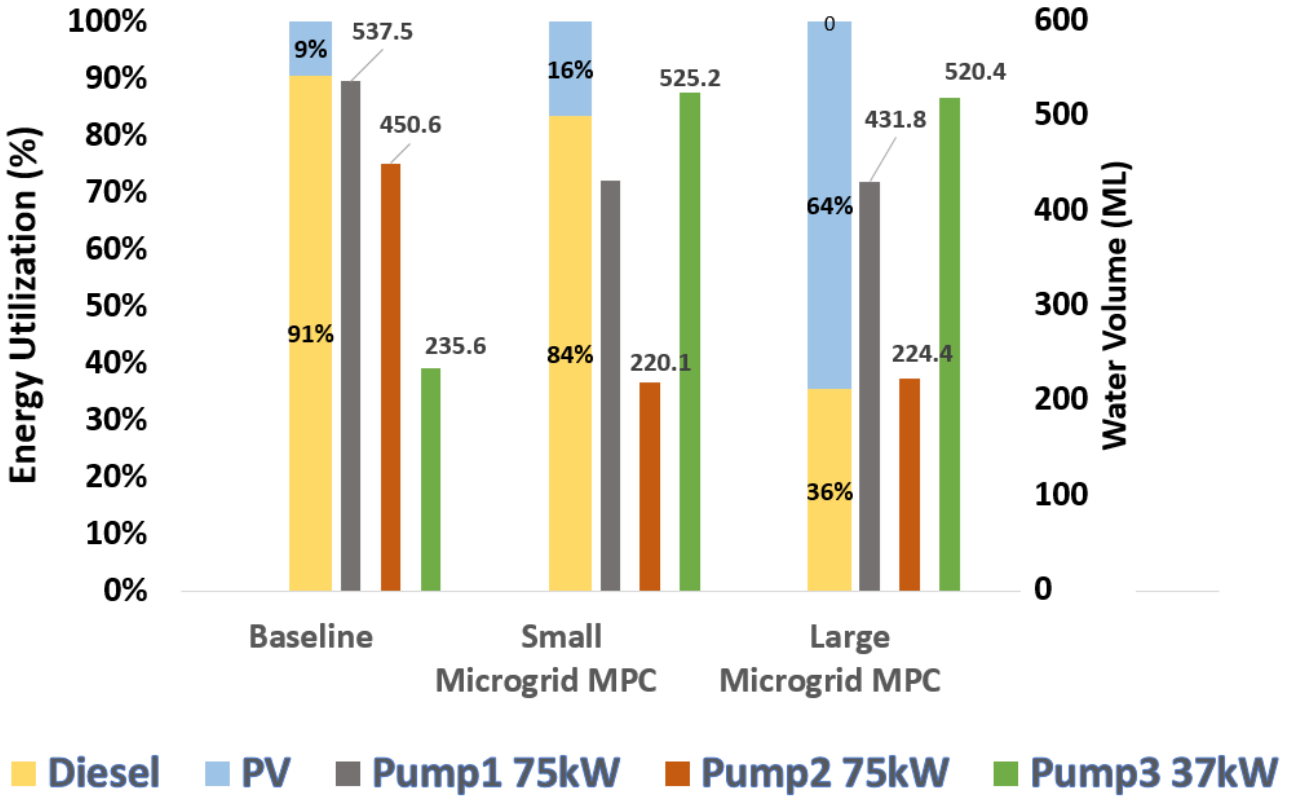

Figure 4.10: Islanded MPC and baseline comparison

Figure 4.11a shows the daily energy production from the small MG component to meet the pump load. The main energy for pumping water is diesel, and the 20 kWh battery discharged energy around 0.1% $\sim$ 0.2% of the required energy. In Figure 4.11b, the PV size and battery capacity are increased to 4 times; thus, the energy from diesel power generation decreases significantly, and the PV energy production is significantly increased. Furthermore, the battery discharges 3.1% $\sim$ 3.2% energy to the pumping system, and the daily data of battery output energy for one week are shown in Figure 4.12, where the positive value means discharge and negative one means charge. It can be seen that the battery output of the large MG is notably

higher than that of the small MG case. With the MPC approach, the utilization rate of renewable energy in the small MG case is 7% higher than the baseline under the same PV and battery storage conditions. In Figure 4.12 only the first 7 days of the irrigation period are shown. This particular phase is characterized by high demand for water, and in order to meet this demand, energy from the PV system of the small MG is utilized to power the pumps with no excess power to charge the battery. As a result, there is no need for power charging or discharging of the battery on days 1, 5, 6, and 7. On the other hand, the large MG has the capability to optimize its operations by utilizing excess energy for charging and discharging the battery more frequently during the same period. This means that the large MG can take advantage of surplus energy to store it in the battery for later use or to discharge it when there is a higher demand for power. The diesel utilization rate for the small MG is 91% of the Baseline case during the entire irrigation period. However, increasing the MG scale to 4 times in the large MG case can make the renewable energy utilization rate reach 64%. Therefore, diesel usage is reduced to 36%. The operational cost of the baseline can be obtained through total energy from case i, and then times diesel coefficient and price from Table 4.3. Table 4.9 shows that the operation cost of the small MG under MPC is AU$ 9,738 lower than the baseline, but the water volume

pumped by the small MG under MPC is 4.1 ML lower than the baseline, and the reduced volume is compensated by the water stored in the reservoir to satisfy the irrigation requirement. In the large MG case, the amount of water pumped is 1 ML lower than that of the small MG, but the operating cost is AU$ 4,503 lower than the small MG. The large MG under MPC has the lowest operating cost of AU$ 26,661, while the baseline has the highest cost. To solve the considered optimization problems, Table 4.8 presents the detail of the computation size and the calculation time for each simulation.

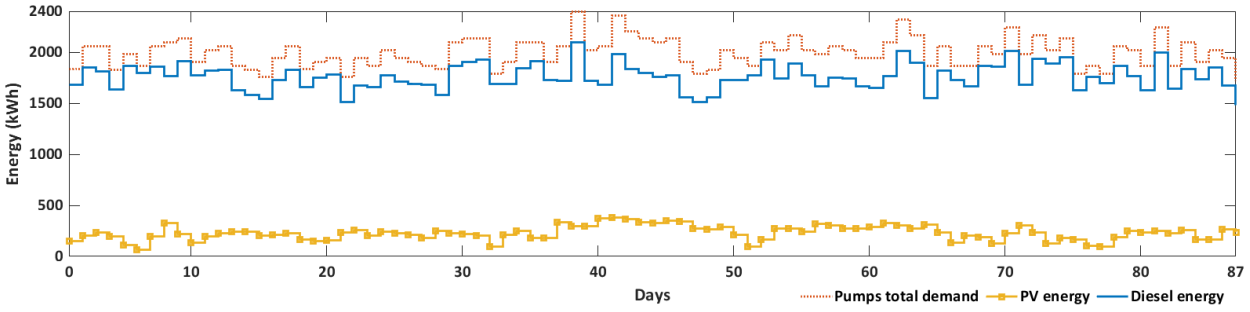

(a) Small Microgrid

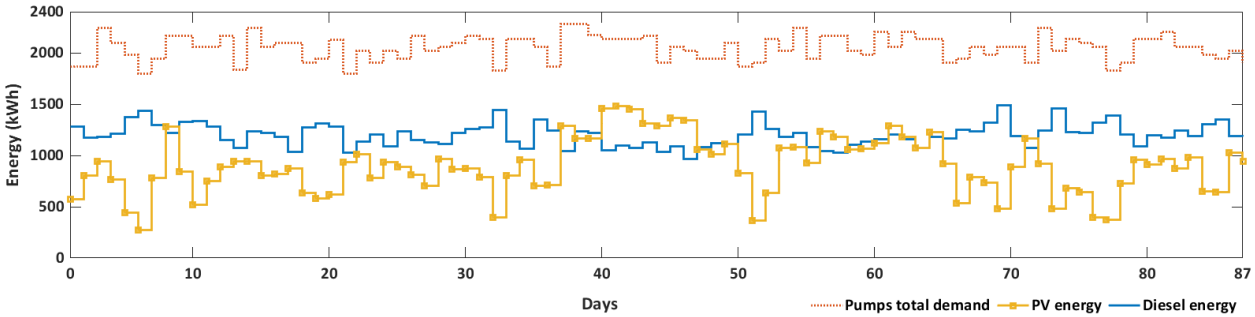

(b) Large Microgrid

Figure 4.11: MPC results comparison of small and large microgrids

Table 4.9: Operating cost comparison of islanded microgrids

	Baseline	Islanded small MG with MPC	Islanded large MG with MPC
Total operating cost (AU$)	40,902	31,164	26,661
Pumped water (ML)	1,180.7	1,177.6	1176.6

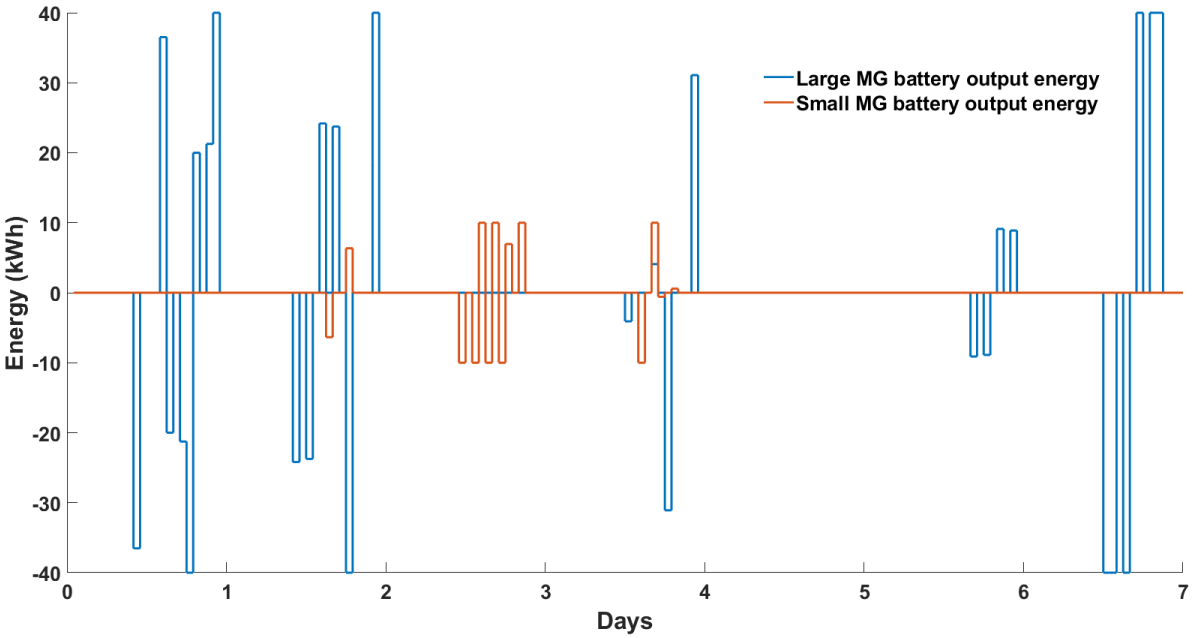

Figure 4.12: Small and large MG battery output energy comparison

4.4 Case study 2 - MPC simulation on Waverleigh cotton farm

The Waverleigh cotton farm is located 25 minutes away from Narromine, New South Wales. This cotton farm installed Australia's largest solar-diesel MG bore pumping water pump system in September 2018.

4.4.1 Waverleigh cotton farm background

Since the farm is far away from the utility grid, diesel-driven water pumps are the main energy consumption of cotton farms. In September 2018, the REAQUA^{TM} company installed a 500 kW off-grid MG system for the cotton farm and used a 250 kW electric motor to replace the diesel-driven motor for one of the water pumps. Therefore, diesel generators and solar energy are seamlessly blended through VSD and inverters. In the water flow, all the pumps pump water into the Turkey Nest Dam, and the water from the dam is used to irrigate crops by gravity which is the same method as the aforementioned case study. The pumping system block is shown in Figure 4.13. Table 4.10 shows the Waverleigh cotton farm's information used for the simulation, which is taken from [148]–[150].

In this case study, an existing MG system with the designed MPC operation approach is simulated, which is based on the 2018-2019 pumped water historical

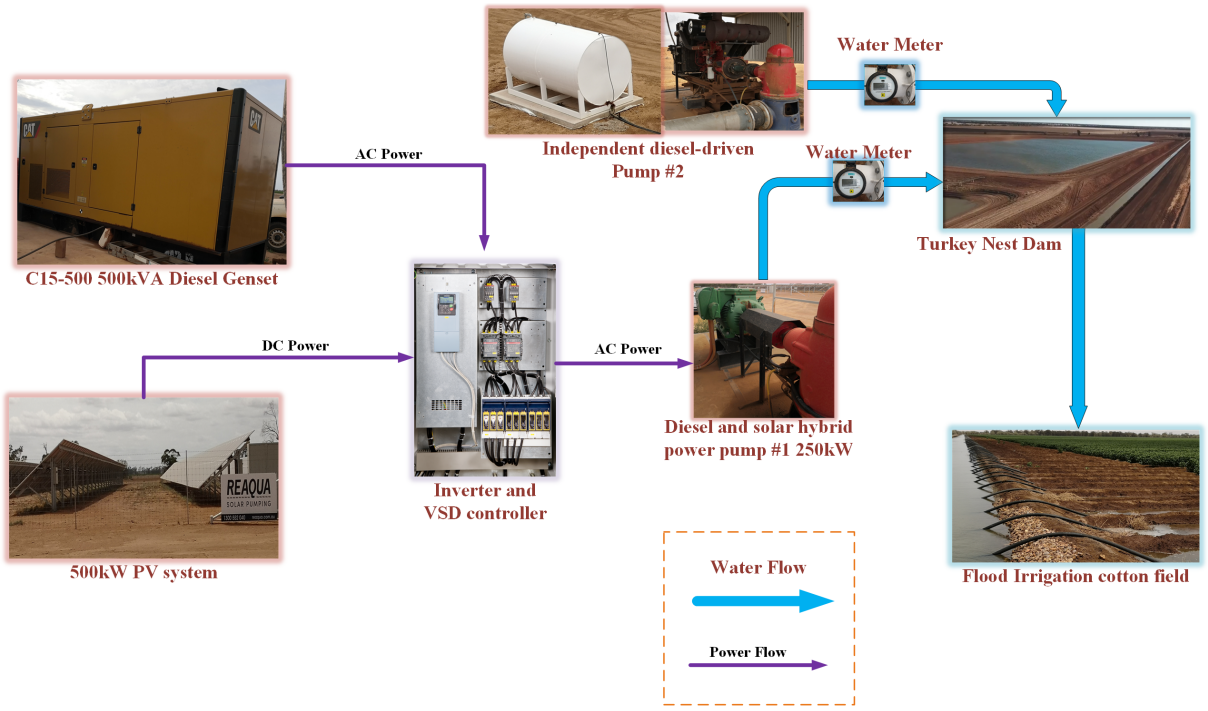

Figure 4.13: Pumping system block of the Waverleigh cotton farm

Table 4.10: Waverleigh cotton farm's parameters

Items	Values
MG bore Pump #1 rated power ($P_{rate,1}$)	250 kW
Independent bore Pump #2 rated power ($P^{ind}_{rate,1}$)	250 kW
Farm area	5 $\times 10^6$ m^2
Bore pump #1 head	90 mTDH
Independent bore pump #2 head	90 mTDH
Average energy for lifting 1 ML/mTDH	4.55 kWh/ML/mTDH
Average water demand (W_{irr})	6.5 $\times 10^{-4}$ ML/m^2
Maximum allowed water usage	3500 ML/year
Reservoir capacity	1300 ML
Installed solar PV capacity	500 kW
Diesel price in 2019 (after subsidy)	1.45 AU$/L

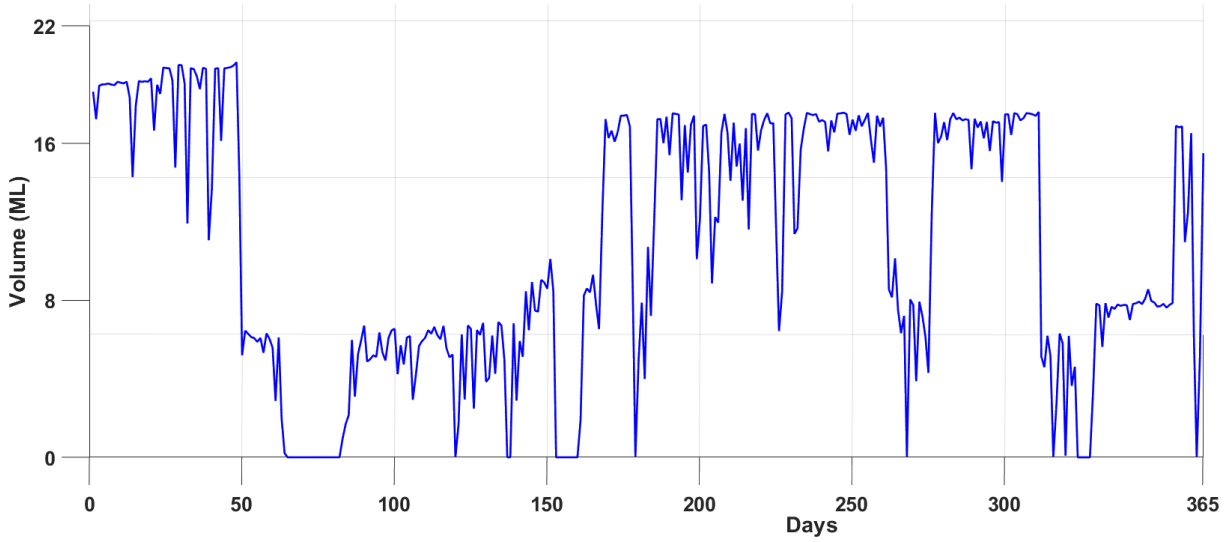

(a) Daily pumped water volume

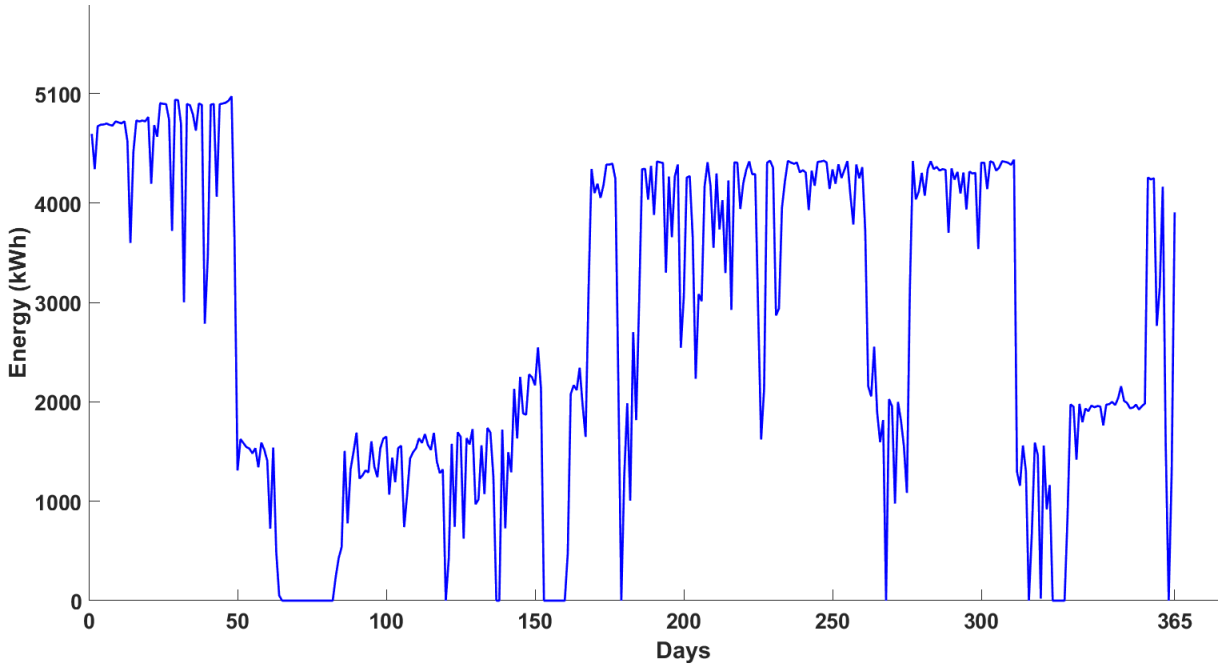

(b) Daily energy consumption

Figure 4.14: Pumped water and energy usage of MG pump #1

data of the hybrid energy-based pumping system. Based on the historical analysis of the MG bore pumps, combined with the irrigation water demand of 5×10^6 m^2 cotton fields, Figure 4.14 shows the energy consumption and pumped water volume of the MG bore pump in a year. Based on [151], we obtained the energy consumption information of the Waverleigh cotton farm under the current operation mode, which is shown in Table 4.11. Therefore, the manual control mode for the existing MG energy consumption is used as the benchmark. The MG bore pump pumped 76.8% of the total annual water demand, which is about 2,688 ML. The usage of hybrid-power bore pumps saved 43% of the diesel used for pumping water throughout the year, which is 165,000 litres of diesel, compared with the non-MG case. The average price of diesel in 2019 is AU$ 1.45/L, so the diesel cost saving is AU$ 239,250. Therefore, the total operational cost of the benchmark is AU$ 317,145 in 2018-2019.

Table 4.11: Waverleigh cotton farm's energy usage benchmark

Items	Values
Total water demand	3,500 ML
Total diesel consumption	383,721 L
Total operational cost of pumping water	AU$ 317,145

I. **Scenario 1. MPC simulation for an islanded microgrid without battery storage in Waverleigh cotton farm**

As all of the pumps in this studied cotton farm use VSD technology, the input energy of the motor can be changed based on demand. Therefore, in the simulation related to VSD pumps, the continuous real value of power is adopted for the MG pump #1 input power. The water flow rate in this case study can be expressed in the following equation:

$$Q_{flow} = \frac{1000 \times \eta_{pump} \times \eta_{motor} \times P_{inpwr}}{g \times \rho \times H} \times 3.6 \tag{4.29}$$

where Q_{flow} is the pump flow rate (ML/h); P_{inpwr} is the pump input power (kW); g is the gravitational constant (9.81 m/s^2); ρ is the density of water (1000 kg/m^3); H is the head developed by the pump (m); η_{pump} is the pump efficiency (75%); η_{motor} is the motor efficiency (90%) [152], and the value 3.6 is the constant for converting water flow from m^3/s to ML/h. In this simulation model, Equation (4.6) can be specified for this cotton farm as:

$$0 \leq \frac{u_1(t) \times P_{rate,1} \times 1}{4.55 \times 90} + \frac{u_1^{ind}(t) \times P_{rate,1}^{ind} \times 1}{4.55 \times 90} \leq \frac{V_{max} \times 1}{24} \tag{4.30}$$

$$0 \leq u_1(t) \leq 1 \tag{4.31}$$

$$0 \leq u_1^{ind}(t) \leq 1 \tag{4.32}$$

$$Q_{flow,1}^{MG}(t) = u_1(t) \times P_{rate,1} \tag{4.33}$$

$$Q_{flow,1}^{ind}(t) = u_1^{ind}(t) \times P_{rate,1}^{ind} \tag{4.34}$$

where $u_1(t)$ and $u_1^{ind}(t)$ are the continuous control variable for the MG pump and independent pump, respectively. $Q_{flow,1}(t)$ and $Q_{flow,1}^{ind}(t)$ are the water flow rate of the MG pump and independent pump, respectively. Consequently, Equations (4.33) and (4.34) can calculate the pumped water volume from the MG pump and independent pump. Figure 4.15 shows the hourly water changes of the dam under the MPC for an islanded MG, which is based on the historical irrigation water demand from 2018 to 2019.

II. **Scenario 2. MPC simulation for an islanded microgrid with battery storage in Waverleigh cotton farm**

Based on the situation of the Waverleigh cotton farm that the current MG cannot use the excess energy, we consider using a battery ESS to store the

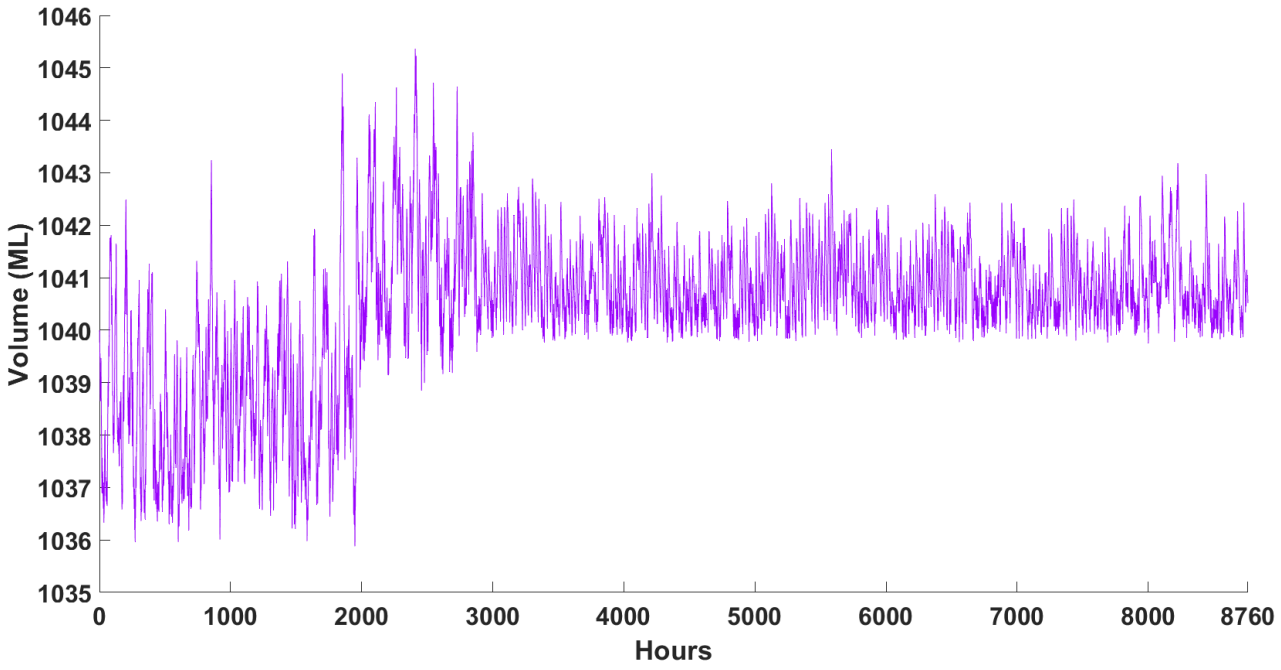

Figure 4.15: Dam water level changes under the MPC for an islanded microgrid

excess energy of the solar system and supply energy to the hybrid-power bore pump at other times. Due to the wide variety of battery storage, we assume that the TESLA^{TM} Powerall + series[1] is used in this case, and we perform a simulation based on the characteristics of Powerwall +.

Table 4.12: Tesla^{TM} Powerwall+ specifications

Items	Values
Energy capacity	13.5 kWh
Continuous power output (No sun)	7 kW
Farm area	5 $\times 10^6$ m^2
Inverter efficiency	97.5 %
Stack maximum number	10 unit

[1]https://www.tesla.com/sites/default/files/pdfs/powerwall/Powerwall%202_AC_Datasheet_en_AU.pdf

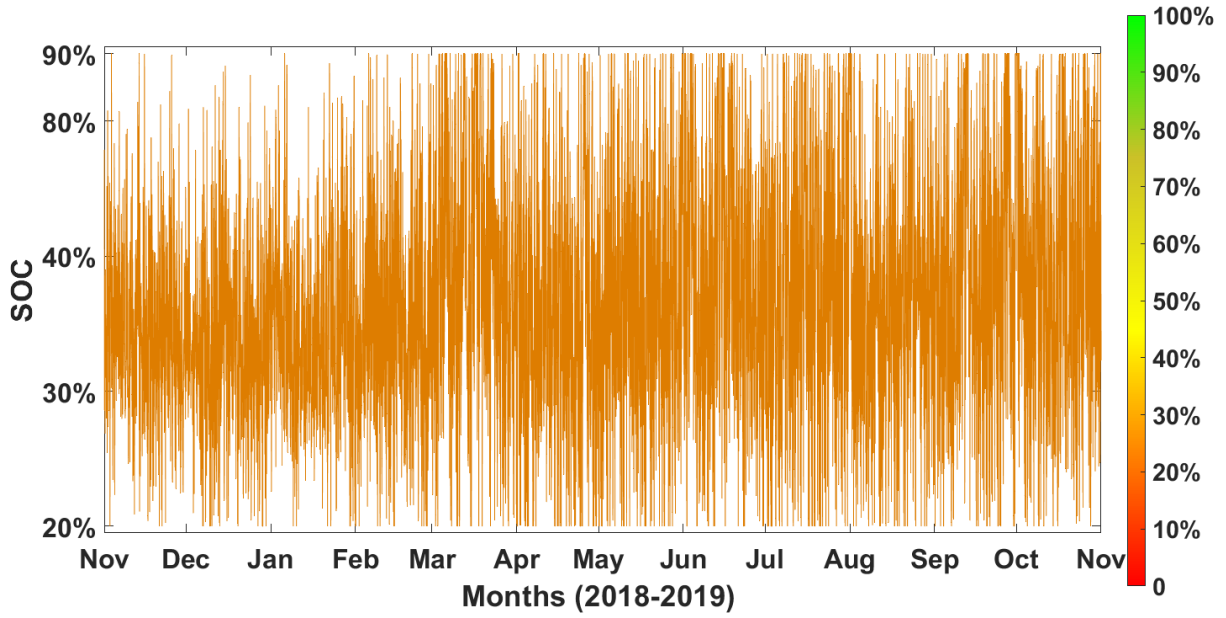

Figure 4.16: Hourly SoC curve of the 135 kWh battery during the year

Therefore, we assume that the largest capacity battery storage system is installed in the farm. Thus $C_{max} = 135$ kWh; P_{ch}^{max} and P_{disch}^{max} can be defined as in the following.

$$P_{ch}^{max} = P_{disch}^{max} = 7 \times 97.5\% \times 10 = 68.25kW \tag{4.35}$$

Then we add the battery storage system to the scenario 1 simulation model, execute the MPC optimization algorithm, and compare the savings in operating costs. Figure 4.16 depicts the battery SoC curves for the proposed case study.

4.4.2 Results and analysis of case study 2

Based on the historical data of Waverleigh cotton farm's annual water pump operation and PV-based MG operation, this case study simulates two different scenarios, which are the islanded MG without battery ESS and islanded MG with a 135 kWh battery ESS. The simulation of this case study runs for 8760 hours (365 days) of the calculation horizon, the time interval is 1 hour, and the prediction horizon is 24 hours.

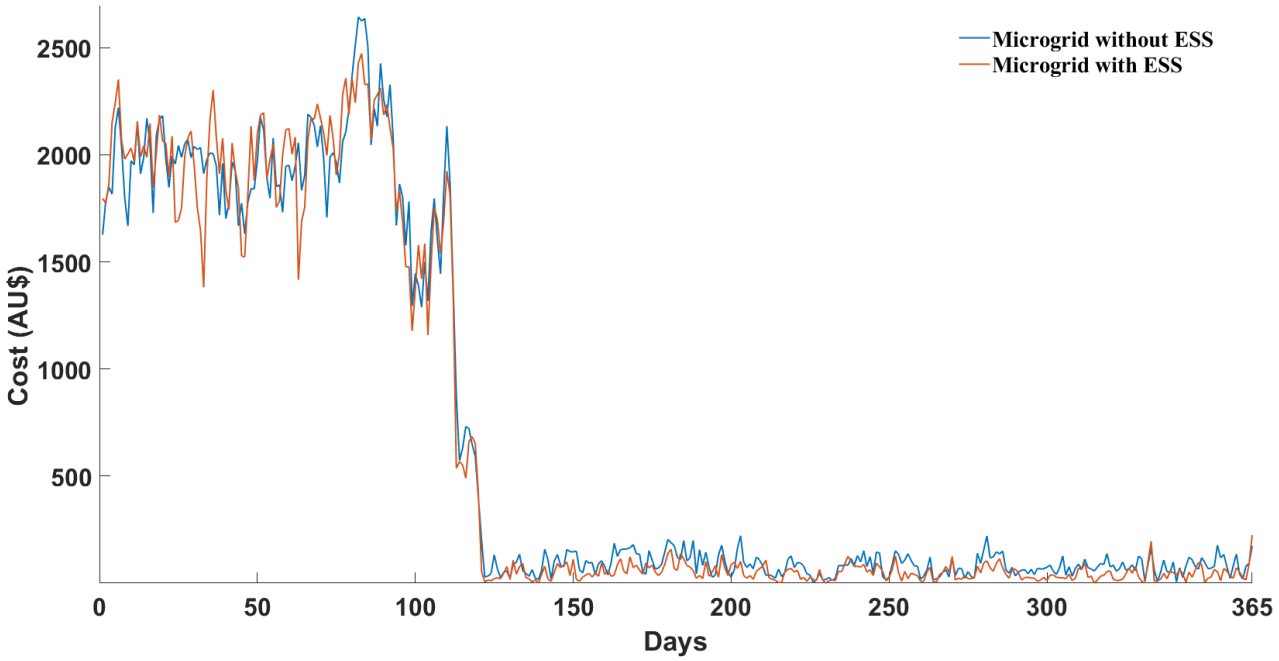

Figure 4.17: Operational cost curves of Scenario 1 and Scenario 2

Now, we compare the simulation results of MPC with the benchmark. The benchmark describes the manual control method currently used at Waverleigh cotton farm. Figure 4.17 shows the average daily operating cost curve comparing scenario 1 and scenario 2.

As shown in Figure 4.17, the daily operating cost of an MG with a battery ESS is lower than that of an MG without a battery ESS most of the time. In the first 4 months, due to the peak irrigation period, the average daily operating cost was around AU$ 2,000. On non-irrigated cotton field days, the operating cost was reduced, and the average daily operating cost was around AU$ 200. Based on the MG bore pump 1's historical data at this cotton farm, Figure 4.18 shows the daily energy consumption curves of MG pump 1 in the benchmark, scenario 1 and scenario 2 during the whole year.

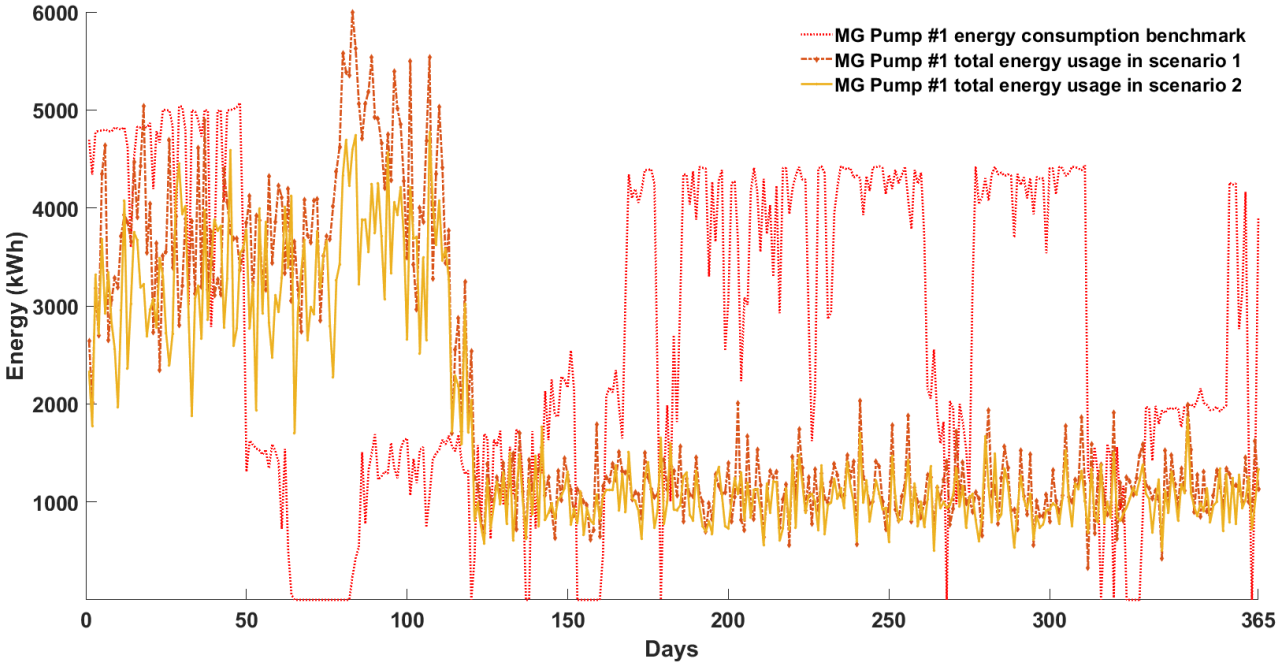

Figure 4.18: Energy consumption curves of MG pump #1 in 365 days

To evaluate the impact of MPC approach on operating costs, Table 4.13 compares the operating costs of the three scenarios.

In Table 4.13, the operational cost of the MG without ESS under MPC is AU$

Table 4.13: Waverleigh cotton farm operating cost comparison (Nov 2018- Oct 2019)

	Total operational cost (AU$)	Total pumped water (ML)
Benchmark	317,145	3,488
Scenario 1 (Without ESS)	242,970	3,453
Scenario 2 (With ESS)	234,260	3,296

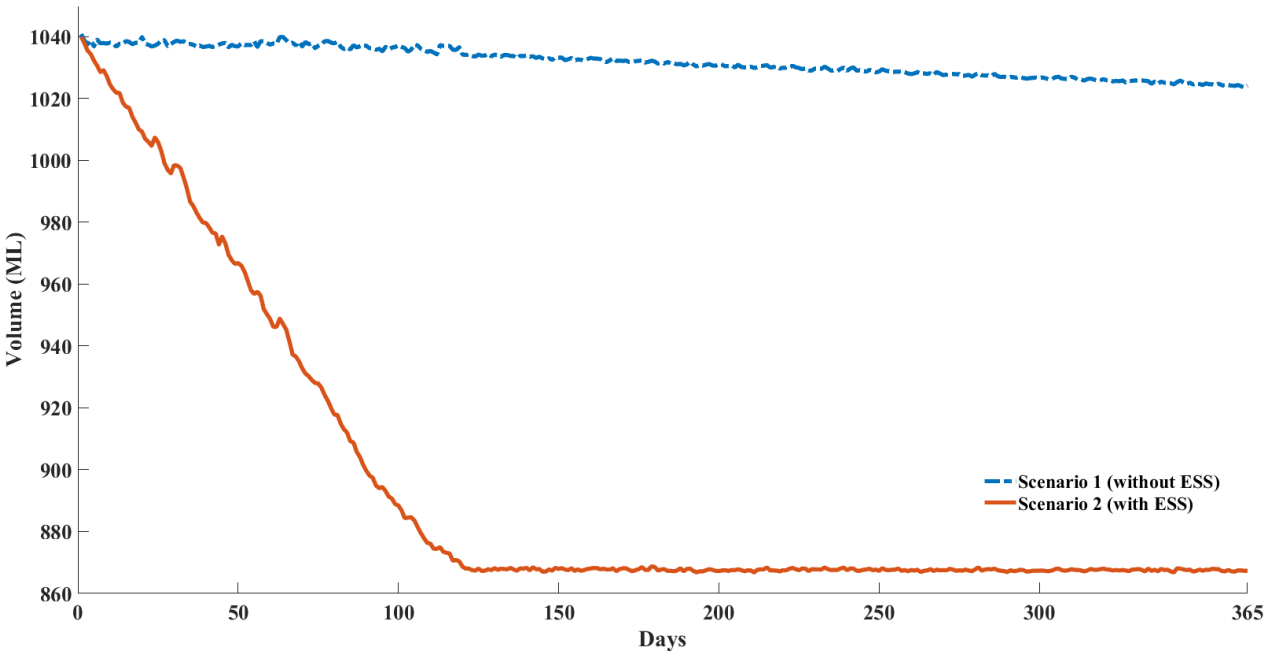

Figure 4.19: Dam water volume changes of Scenario 1 and Scenario 2 in 365 days

74,175 lower than the benchmark, and the operational cost of the MG with ESS is the lowest of the three scenarios which have AU$ 82,885 savings per year when compared with the benchmark. In this case, the amount of water pumped is similar between the benchmark and Scenario 1, but the average operating cost of all the scenarios is consistent with the benchmark, which is between 70 to 71 AU$/ML. Figure 4.19 shows the daily dam water volume changes of scenario 1 and scenario 2. The blue dotted curve shows the dam water volume changes of scenario 1 which has no ESS. The water volume slightly decreases in scenario 1 because there is no ESS to store the excess energy, and the dam needs to store more water as there will be less energy available for pumping water, but without exceeding the maximum water usage (e.g., 3500 ML/year). For scenario 2 with ESS, the battery storage can store the excess energy. Thus, only a smaller amount of water is needed in the dam, and if needed, more water can be pumped by using ESS.

4.5 Summary

This chapter introduces an MPC approach to minimize the operating cost for the MG of an Australian cotton farm. Disturbance from evaporation, seepage and rain is studied to illustrate the robustness of the MPC approach. Case study 1

shows that in this MPC solution, the grid-connected cotton farm MG under the underlying disturbance can reduce its annual irrigation operating costs by AU$ 13,302, or 33.6%, compared to the Baseline; it consumes the energy of 51,161.5 kWh, i.e., 20.7% less energy purchased from the grid, which is under climate-impacted conditions in the same year. Meanwhile, in the small islanded MG case, the proposed MPC scheme improves the clean energy utilization rate of 7%. It reduces the diesel consumption of 8,467 L, equivalent to saving the operating cost of AU$ 9,738, compared with the Baseline of the islanded case. In the case of the large-scale islanded MG, the utilization rate of clean energy is achieved at 64%, and the operating cost compared with the Baseline is also reduced by AU$ 14,241, i.e., 34.8%. Case study 2 uses another cotton farm's scenarios to validate the MPC approach that can help farm owners reduce their operational costs under the existing MG. Compared with the benchmark of case study 2, the MG without ESS can save AU$ 74,175 of the operational costs under MPC which is 23% of the benchmark, and the MG with ESS can achieve 26% operational cost saving under MPC operation.

Chapter 5

A Scenario-based Stochastic Model Predictive Control Approach for Microgrid Operation at an Australian Cotton Farm Under Uncertainties

5.1 Introduction

In the previous chapter, we introduced the classical MPC approach for MG operation to reduce the operational cost of the water pumping system in the cotton farm by utilizing RES efficiently. However, different to conventional power generation, renewable energy (such as solar) is always intermittent, which brings significant uncertainties to power generation and scheduling [153]. In recent years, more

and more literature has combined small-scale agricultural RES with traditional generator sets to establish the MG system, which is considered an emerging way to absorb RES on the demand side. Therefore, the operational cost can be reduced by improving the utilization rate of renewable. MPC has advantageous features to operate MG owing to its capability to handle uncertainties [154]. Accordingly, MPC methods have been widely applied to MG operations. In [155], an MPC method using mixed integer linear programming is adopted to solve the MG operation problem while satisfying time-varying operational constraints. In addition, Ref. [156] proposes an online optimal operation method for combined cooling, heating, and power MG systems based on MPC, which compensates for prediction errors through two hierarchies of feedback correction. The above studies emphasize the robustness of MPC and note that uncertainty will affect the results; however, the uncertainties are not modelled. Many studies have discussed methods of generating appropriate scenarios to model uncertainty [157]. A nonlinear programming method based on scenario trees is proposed in [158], in order to generate a large number of scenarios and then reduce them to a limited number of discrete matrices as the typical scenario results. Ref. [159] presents a stochastic programming method using scenario generation to deal with stochastic load and wind power uncertainty. In [160], the energy storage system operation scheduling problem is formulated as a two-stage stochastic programming model

based on the scenario-based method. In addition, there are several studies using scenario-based approaches to build stochastic models in MG operation studies. In [161], the uncertainty of RES output power and load demand forecast errors are modelled by scenario-based techniques for optimal energy management of MGs. A RES stochastic model is adopted in [162], which uses the scenario reduction process to convert the stochastic problem into many deterministic problems with different probabilities and then optimizes each deterministic problem. The above-mentioned literature focuses on mathematical algorithms, but the description of the uncertain phenomena and effects in the actual applications is limited.

On the other hand, scenario-based stochastic MPC has been applied to smart grid operation area [163]. Ref. [164] introduces different classifications of the available methods based on the dynamic characteristics of the system, management of the probabilistic constraints, feasibility, and the properties of convergence. Additionally, Ref. [165] provides an overview of the core concepts related to MPC and stochastic optimal control under uncertainties and discusses the disturbance estimation and the impact of the estimation quality on MPC performance. In [166], a scenario-based MPC approach is proposed through a data-driven machine learning method. Ref. [167] implements a scenario-based MPC controller for heating, ventilation, and air conditioning systems in buildings. Furthermore, a scenario-

based model predictive operation control of rural area islanded MG is proposed in [168]. Nevertheless, the methods mentioned above do not accurately model the uncertainties from different sources and do not compare the impact of different uncertainty models on the optimization results for grid-connected MG and islanded MG. Chapter 4 takes advantage of the MPC strategy to minimize the operational cost of the cotton farm MG system in Australia. This chapter extends the study in Chapter 4 and proposes two uncertainty models (i.e., static scenario-based and dynamic scenario-based uncertainty models) to assist the optimal operation of cotton farm MG under uncertainty during an irrigation period. Here, the static scenario-based uncertainty model refers to the case that the uncertainty dataset for scenario generation and reduction is fixed for the entire irrigation period, and the resultant typical scenarios are used for all the MPC iterations. On the other hand, in the dynamic scenario-based uncertainty model, the uncertainty dataset will be dynamically updated for scenario generation and reduction along with the moving time horizon within MPC; consequently, the corresponding typical scenarios are dynamically updated within each MPC iteration. After deciding the uncertainty scenarios using either the static or dynamic scenario-based methods, a stochastic MPC strategy is proposed for the above two uncertainty models. The demand and weather uncertainties on both grid-connected MG and islanded MG are also considered. This study uses the SCENARD toolbox [169] based on

the Kantorovich distance [170] method to deal with uncertainties. CPLEX 12.10 with MATLAB is used to solve the underlying optimization problems. Therefore, the novelties are to consider both static and dynamic scenario-based uncertainty models and their impact on both cotton farm grid-connected MG and islanded MG. The remaining part of this chapter is organized as follows. Section 5.2 describes the cotton farm MG and scenario-based uncertainty models. Section 5.3 presents a case study to simulate the proposed methodology based on the actual data from a cotton farm in New South Wales. Section 5.4 discusses the simulation results for each case, and Section 5.5 summarizes the chapter by highlighting the significant meaning of the main results.

5.2 MPC of cotton farm microgrids and scenario-based uncertainty modelling

Based on the current situation of using hybrid RESs and the geographical location of general Australian cotton farms, the MG system in Australian cotton farms can be divided into grid-connected MG and islanded MG. Therefore, the following assumptions are used to model the studied cotton farm MG. Cotton farms have their own water storage system for irrigation and tailwater recovery. The pumps will pump water from the bore or river into the reservoir, and the siphon pipes are

used for the water to flow from the reservoir to irrigate cotton farms by gravity. Note that this study does not discuss tailwater recovery. Therefore, the volume of irrigation water is the cotton planting water demand, and the water balance model in Section 5.2.2 is built based on these assumptions. The most popular RES in Australian cotton farms is solar PV. Consequently, this study uses PV to build the grid-connected MG which allows excess energy to be fed back to the utility network. Figure 5.1 shows the working architecture of the grid-connected MG in a cotton farm, where the MG river pump or MG bore pump means these pumps all connected to MG, and the independent pump is the pump that cannot be connected to the MG, but connected to the grid directly. The islanded MG can be built by PV, battery storage, diesel generator, and a dummy load, where the dummy loads refer to loads that can consume excess energy to balance the generation-load relation. The excess energy can be stored by battery storage or absorbed by the dummy load. Figure 5.2 illustrates the working structure of the islanded MG in a cotton farm, where the load is made of the dummy load, MG pumps powered by the MG, and the independent pumps driven by a diesel motor directly. The MPC methodology has an excellent performance in predictive control and handling uncertainties, which is suitable for cotton farms challenged with climate change and operational cost reduction and therefore adopted in this study. As for uncertainty modelling, we take advantage of the scenario-based

approach to generate and reduce scenarios based on historical data to build the stochastic model.

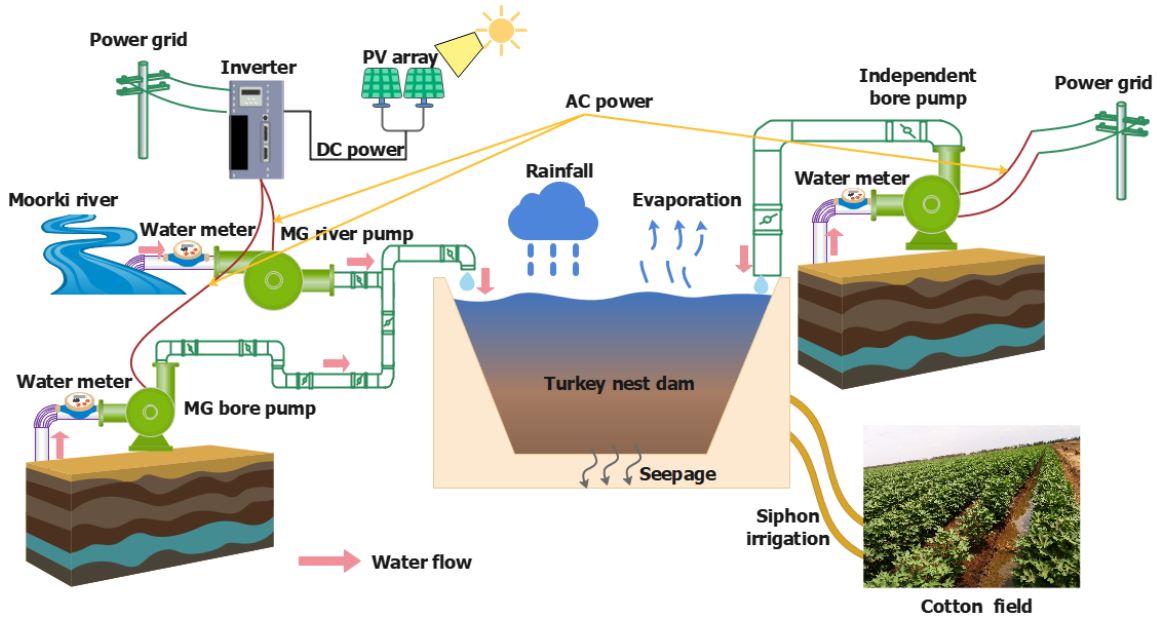

Figure 5.1: Grid-connected cotton farm microgrid and pumping water system

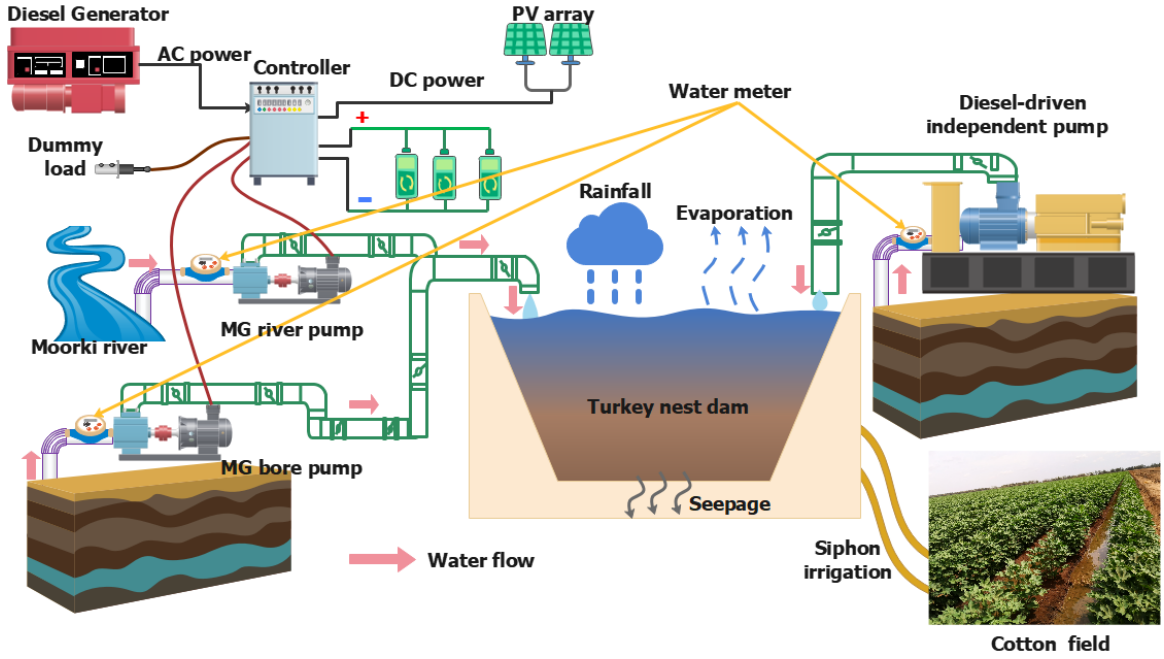

Figure 5.2: Islanded cotton farm microgrid and pumping water system

5.2.1 Power balance model of grid-connected microgrid

In this section, we consider the grid-connected MG which consists of only PV. The power balance can be represented as (5.1), and Equation (5.2) represents the total PV power based on installed PV panel numbers; see also Section 4.3.1.

$$P_{solar}(t,s) + P_{grid}(t,s) = \sum_{i=1}^{K} x_i(t,s) \times P_{pump,i}^{MG} + P_{fi}(t,s) \tag{5.1}$$

$$P_{solar}(t,s) = \sigma \times P_{solar}^{panel}(t,s) \tag{5.2}$$

s.t.

$$0 \leq P_{grid}(t,s) \leq \xi(t,s) \times P_{pump}^{total} \tag{5.3}$$

$$0 \leq P_{fi}(t,s) \leq [1 - \xi(t,s)] \times P_{fi}^{max} \tag{5.4}$$

where i is the index of pumps; K denotes the number of MG pumps; x_i is the binary control variable for the pump's on/off state in grid-connected MG; s represents the index of typical scenarios; P_{solar} is the PV power generation (kW); P_{grid} is the power purchased from the utility grid (kW); $P_{pump,i}^{MG}$ indicates the rated power of i^{th} pump connected to MG (kW); P_{fi} expresses the feed-in power to the grid (kW); P_{pump}^{total} is the sum of all the pump's maximum rated power (kW); σ denotes the number of installed PV panel units; P_{solar}^{panel} represents the power output of a single PV panel (kW); ξ is a binary variable indicating the grid energy

import or export, with $\xi(t,s) = 1$ meaning that MG purchases energy from the grid (import) at time t in scenario s, and $\xi(t,s) = 0$ meaning the MG sells energy to the grid (export) at time t and scenario s, and P_{fi}^{max} indicates the maximum power allowed to be fed into the grid (kW). Equations (5.3) and (5.4) represent the constraints that power purchase from the grid and feed-in to the grid cannot happen at the same time.

5.2.2 Power balance model of islanded microgrid

An islanded MG consists of PV, diesel generators, and battery storage. Due to the remote location of cotton farms, the cost of connecting to the grid is too high. Therefore, a common solution is using diesel generators as a backup energy source to build an islanded MG with renewable energy. The battery storage can help save diesel fuel during the irrigation period by storing excess energy, while the dummy load is used to consume the excess energy if the battery is full. Therefore, the power balance can be established as in (5.5).

$$\sum_{i=1}^{K} x_i(t,s) \times P_{pump,i}^{MG} + P_{charge}(t,s) + P_{dum}(t,s) = P_{solar}(t,s) + P_{diesel}(t,s) + P_{discharge}(t,s) \quad (5.5)$$

where, P_{charge} and $P_{discharge}$ represent the charge and discharge power of the battery storage, respectively; $P_{dum}(t, s)$ is a dummy load at time t and scenario s used to consume the excess energy when the battery is fully charged; and P_{diesel} is the power generated by diesel generator (kW).

5.2.3 Battery model for islanded microgrid

In the islanded MG system, storing and utilizing excess renewable energy can save operational costs. In this study, we consider the low-cost lead-acid battery for energy storage systems and compare the degradation cost with its energy cost saving. Battery charging and discharging can be decided by several parameters, e.g., battery capacity B_{cap} (kWh), charging and discharging efficiency η_c and η_d. Equation (5.6) illustrates the SoC model, and Equations (5.7) - (5.9) list the SoC limits and the constraint that charging cannot happen at the same time as discharging. On the other hand, a battery can store energy, but charging and discharging also cause battery degradation. Equations (5.10) - (5.11) show the Lead-acid battery storage degradation cost, f_{deg}, based on the Lead-acid battery degradation coefficient κ_d [171].

$$S^{SOC}(t+1, s) = S^{SOC}(t, s) + \frac{P_{charge}(t, s) \times \eta_c \times \Delta t}{B_{cap}} - \frac{P_{discharge}(t, s) \times \Delta t}{B_{cap} \times \eta_d} \tag{5.6}$$

s.t.

$$S_{min}^{SOC} \leq S^{SOC}(t,s) \leq S_{max}^{SOC} \tag{5.7}$$

$$0 \leq P_{charge}(t,s) \leq \xi_B(t,s) \times P_{charge}^{max} \tag{5.8}$$

$$0 \leq P_{discharge}(t,s) \leq [1-\xi_B(t,s)] \times P_{discharge}^{max} \tag{5.9}$$

$$\kappa_d = \frac{C_{Bat}}{B_{cap} \times \eta_d \times K_c \times \alpha} \tag{5.10}$$

$$f_{deg}(t,s) = P_{charge}(t,s) \times \Delta t \times \kappa_d + P_{discharge}(t,s) \times \Delta t \times \kappa_d \tag{5.11}$$

where Δt is the time interval, $\Delta t = 1$ h in this study; S^{SOC} indicates the state of charge of battery storage (%); S_{max}^{SOC} and S_{min}^{SOC} denote the maximum and minimum SoC, respectively; here we take $S_{min}^{SOC} = 10\%$ and $S_{max}^{SOC} = 100\%$. P_{charge}^{max} and $P_{discharge}^{max}$ are the charge and discharge limit of the battery storage, respectively; ξ_B is a binary variable of battery charge or discharge, with $\xi_B(t,s) = 1$ indicating that battery is charged at time t in scenario s and $\xi_B(t,s) = 0$ indicating the battery is discharged at time t and scenario s; C_{Bat} is the battery storage cost (AU$); K_c is the number of the life cycle at the rated depth of discharge (DoD), and α (%) is DoD of the battery system.

5.2.4 Water balance model during the irrigation period

The pumps pump water from the bore/river into the reservoir during the cotton irrigation period and the form of energy changes from electrical to potential energy. Farmers irrigate cotton fields with water from the reservoir by gravity. Therefore, the water balance is established by the volume of water inflow and outflow of the reservoir in (5.12).

$$W(t+1,s) = W(t,s) + W_{inflow}(t,s) - W_{outflow}(t,s) \tag{5.12}$$

$$W_{outflow}(t,s) = W_{irr}(t,s) + W_{eva}(t,s) + \frac{W_{see}}{24 \times 365} \tag{5.13}$$

where W (ML) is the total water volume of the reservoir; W_{inflow} (ML) and $W_{outflow}$ (ML) represent the water inflow from and outflow volume to the reservoir; W_{irr} and W_{eva} are the hourly cotton farm irrigation water volume (ML) and hourly evaporation volume from reservoir (ML), respectively; W_{see} (ML) is the value of average annual seepage from the reservoir, which is 10% of the reservoir capacity [146]. In the grid-connected MG, all the pumps (including MG pumps and independent pumps) are electric. In the islanded MG, the MG pumps are electric, while the independent pumps are all diesel pumps. The water inflow W_{inflow} for grid-connected MG and islanded MG are expressed as (5.14), respectively. Also, the daily water usage limit W_{max}^{daily} (ML) [137] for grid-connected MG and islanded MG are expressed by (5.16).

$$\begin{cases} W_{inflow}(t,s) = \sum_{i=1}^{K} \frac{x_i(t,s)\times P_{pump,i}^{MG}\times\Delta t}{\varepsilon_{con,i}\times h_i} + \sum_{i=1}^{K^{in}} \frac{x_i^{in}(t,s)\times P_{pump,i}^{in}\times\Delta t}{\varepsilon_{con,i}^{in}\times h_i^{in}} + W_{R\_res}(t,s), \\ \text{(grid-connected MG water inflow)} \\ \\ W_{inflow}(t,s) = \sum_{i=1}^{K} \frac{x_i(t,s)\times P_{pump,i}^{MG}\times\Delta t}{\varepsilon_{con,i}\times h_i} + \sum_{i=1}^{K^{in}} \frac{x_i^{in}(t,s)\times V_{diesel,i}^{in}\times\Delta t}{\delta_{diesel,i}^{in}\times h_i^{in}} + W_{R\_res}(t,s), \\ \text{(islanded MG water inflow)} \end{cases} \tag{5.14}$$

$$x_i(t,s)\ (or\ x_i^{in}(t,s)) = \begin{cases} 1, \text{ when the } i^{th} \text{ pump is on} \\ 0, \text{ when the } i^{th} \text{ pump is off} \end{cases} \tag{5.15}$$

s.t.

$$\begin{cases} \sum_{t=1}^{T} \left(\sum_{i=1}^{K} \frac{x_i(t,s)\times P_{pump,i}^{MG}\times\Delta t}{\varepsilon_{con,i}\times h_i} + \sum_{i=1}^{K^{in}} \frac{x_i^{in}(t,s)\times P_{pump,i}^{in}\times\Delta t}{\varepsilon_{con,i}^{in}\times h_i^{in}} \right) \le W_{max}^{daily}, \\ \text{(grid-connected MG water daily limit for all pumps)} \\ \\ \sum_{t=1}^{T} \left(\sum_{i=1}^{K} \frac{x_i(t,s)\times P_{pump,i}^{MG}\times\Delta t}{\varepsilon_{con,i}\times h_i} + \sum_{i=1}^{K^{in}} \frac{x_i^{in}(t,s)\times V_{diesel,i}^{in}\times\Delta t}{\delta_{diesel,i}^{in}\times h_i^{in}} \right) \le W_{max}^{daily}, \\ \text{(islanded MG water daily limit for all pumps)} \end{cases} \tag{5.16}$$

$$\sum_{t=1}^{T} \left(\frac{x_i(t,s) \times P_{pump,i}^{MG} \times \Delta t}{\varepsilon_{con,i} \times h_i} \right) \le B_{i,max}^{MG,daily} \tag{5.17}$$

$$\begin{cases} \sum_{t=1}^{T} \left(\frac{x_i^{in}(t,s) \times P_{pump,i}^{in} \times \Delta t}{\varepsilon_{con,i}^{in} \times h_i^{in}} \right) \leq B_{i,max}^{in,daily}, \\ \text{(grid-connected MG water daily limit for each independent pump)} \\ \sum_{t=1}^{T} \left(\frac{x_i^{in}(t,s) \times V_{diesel,i}^{in} \times \Delta t}{\delta_{diesel,i}^{in} \times h_i^{in}} \right) \leq B_{i,max}^{in,daily}, \\ \text{(islanded MG water daily limit for each independent pump)} \end{cases} \tag{5.18}$$

where x_i^{in} is the binary control variable for the independent pump's on/off state in islanded MG; K^{in} expresses the number of independent pumps; $P_{pump,i}^{in}$ indicates the rated power of i^{th} independent pump in GMG (kW); W_{R_res} is the hourly precipitation amount into the reservoir (ML); T is the prediction horizon (e.g., 24 hours); $\varepsilon_{con,i} = \varepsilon_{con,i}^{in} = 4.55$ kWh/ML/mTDH is the electricity consumed for lifting 1 ML water to 1-metre TDH [136], [172]; $\delta_{diesel,i}^{in}$ denotes the diesel consumption of the i^{th} independent pump in IMG for lifting 1 ML water to 1 mTHD (L/ML/mTHD); h_i and h_i^{in} (mTDH) are the THD of the i^{th} MG pump and independent pump, respectively. When $T = 24$ h, W_{max}^{daily} is the maximum amount of water that can be pumped in a day by all the pumps; $V_{diesel,i}^{in}$ denotes the hourly fuel consumption of i^{th} independent diesel-driven pump in islanded MG (L/h). $B_{i,max}^{MG,daily}$ and $B_{i,max}^{in,daily}$ (ML) denote the maximum amount of water that can be pumped by the i^{th} MG pump and independent pump in a day, respectively.

5.2.5 Objective functions

The objective is to reduce the operational cost of the MG. The operational cost of grid-connected MG and islanded MG are defined in (5.19) and (5.20), respectively.

$$\begin{aligned} Y(t,s) = &\left[P_{grid}(t,s) + \sum_{i=1}^{K} x_i^{in}(t,s) \times P_{pump,i}^{in}\right] \\ &\times \Delta t \times \beta_{buy}(t) - P_{fi}(t,s) \times \Delta t \times \beta_{sell}(t), \\ &\text{for grid-connected MG} \end{aligned} \tag{5.19}$$

$$\begin{aligned} Y(t,s) = &\left[P_{diesel}(t,s) \times \psi + \sum_{i=1}^{K^{in}} x_i^{in}(t,s) \times V_{diesel,i}^{in}\right] \\ &\times \Delta t \times \beta_{diesel}(t) + f_{deg}(t,s), \\ &\text{for islanded MG} \end{aligned} \tag{5.20}$$

where $Y(t,s)$ is the operational cost of the MG; $\beta_{buy}(t)$ and $\beta_{sell}(t)$ (AU$/kWh) represent the tariff of purchasing energy from the grid and the feed-in tariff of selling energy to the grid at the t^{th} time, respectively; $\beta_{diesel}(t)$ indicates the diesel price at the t^{th} time, and ψ is the electricity to diesel conversion coefficient.

5.2.6 MPC methodology

In order to obtain the result of minimizing the operational cost, the first step is to optimize the operational cost in a prediction horizon (T) (e.g., 24 hours) with

the open-loop optimization model (5.21) by considering all the typical scenarios.

$$\begin{aligned} \min_{x_i, x_i^{ind}} & \sum_{s=1}^{Z} \sum_{t=1}^{T} \lambda_s \times Y(t,s) \\ & t = 1, \ldots, T \\ & s = 1, \ldots, Z \end{aligned} \tag{5.21}$$

where, λ_s represents the probability of the scenario set s after scenario reduction; and Z is the number of the typical scenarios. In addition, the closed-loop MPC model (5.22) is based on (5.21) and moving the prediction horizon to the next interval with periodically updated system information to provide feedback to the controller. Figure 5.3 illustrates the closed-loop MPC concept. In this study, the disturbances encompass RES uncertainty and reservoir volume uncertainty arising from weather changes. The control variables include each pump's on/off states, the battery charge/discharge power, and the power generated by the diesel generator. The "State/output feedback" is used as an input to the next iteration to update the system dynamics. The "Control result feedback" reflects the value of the control variable after each moving horizon, which is optimized in the latest iteration. The "Predictor" block combines the "State/output feedback" with the "Control result feedback" to predict the "Future output". Subsequently, the "Future output" is inputted to the Optimizer block for the next iteration.

$$\min_{x_i, x_i^{ind}} \sum_{s=1}^{Z} \sum_{t=1+m}^{T+m} \lambda_s \times Y(t,s) \tag{5.22}$$

where the period $[1+m, \cdots, T+m]$ is the window of moving prediction horizon.

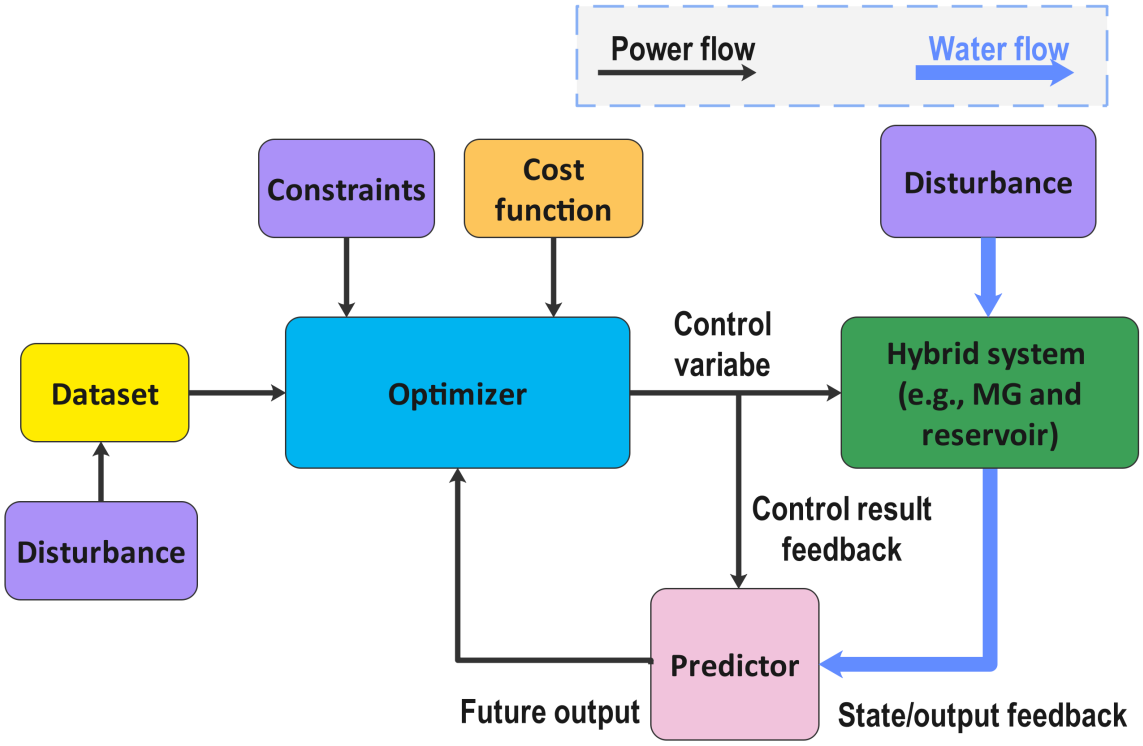

Figure 5.3: Closed-loop MPC model

5.2.7 Scenario-based model

This study proposes scenario-based techniques to deal with uncertainty datasets for the MG system. Firstly, we need to determine the uncertainties affecting the operational costs of pumping water on the cotton farm, e.g., RES in the power balance model, precipitation, evaporation, and irrigation demand in the water balance model. We propose two scenario-based uncertainty models to process the

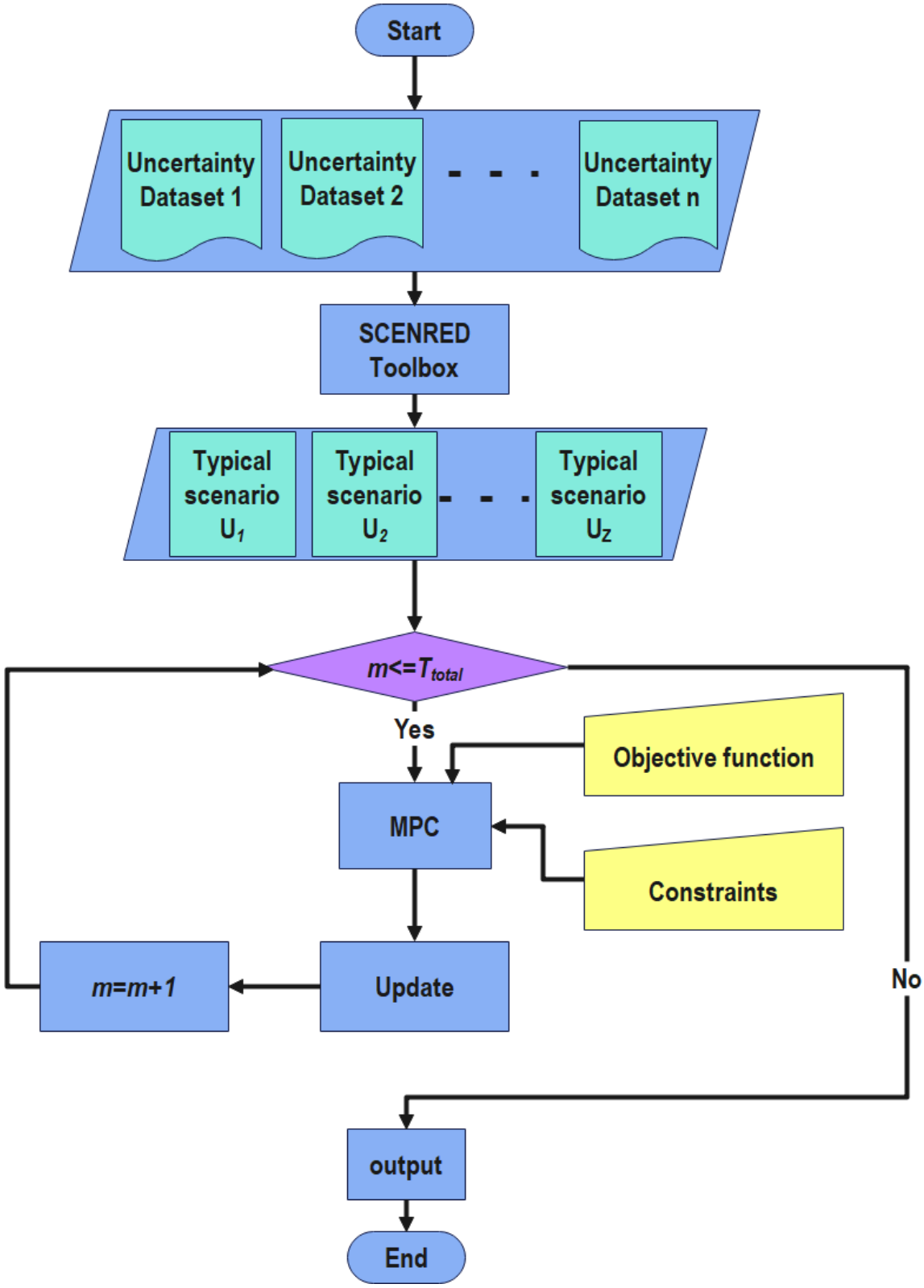

Figure 5.4: Static scenario-based MPC model

above-mentioned uncertainties, which are the static scenario-based uncertainty model and the dynamic scenario-based uncertainty model. In the static uncertainty model, the whole uncertainty datasets during the entire irrigation period are used only once for scenario generation and reduction, and the resultant typical scenarios are fixed for all the MPC iterations. The computation time of this uncertainty model is less as the scenario generation and reduction only needs to be conducted once in the whole MPC time horizon, while the uncertainty representation accuracy is sacrificed. Figure 5.4 shows the static scenario-based MPC optimization flowchart. In Figure 5.4, all the uncertain datasets are formed by matrices and inputted to SCENRED toolbox, where scenario generation and reduction process are completed. Then the typical scenarios with their corresponding probability are sent to the MPC stage to obtain the optimal operational cost results.

In the dynamic scenario-based uncertainty model, within each moving time horizon, the future period in close proximity T^{scen} (e.g., ten days or fortnight into the future) can be chosen with the available historical data. Therefore, the corresponding typical scenarios after scenario generation and reduction are dynamically updated within each MPC iteration. The dynamic scenario-based model is more accurate as it uses the data in close proximity to generate the typical scenarios;

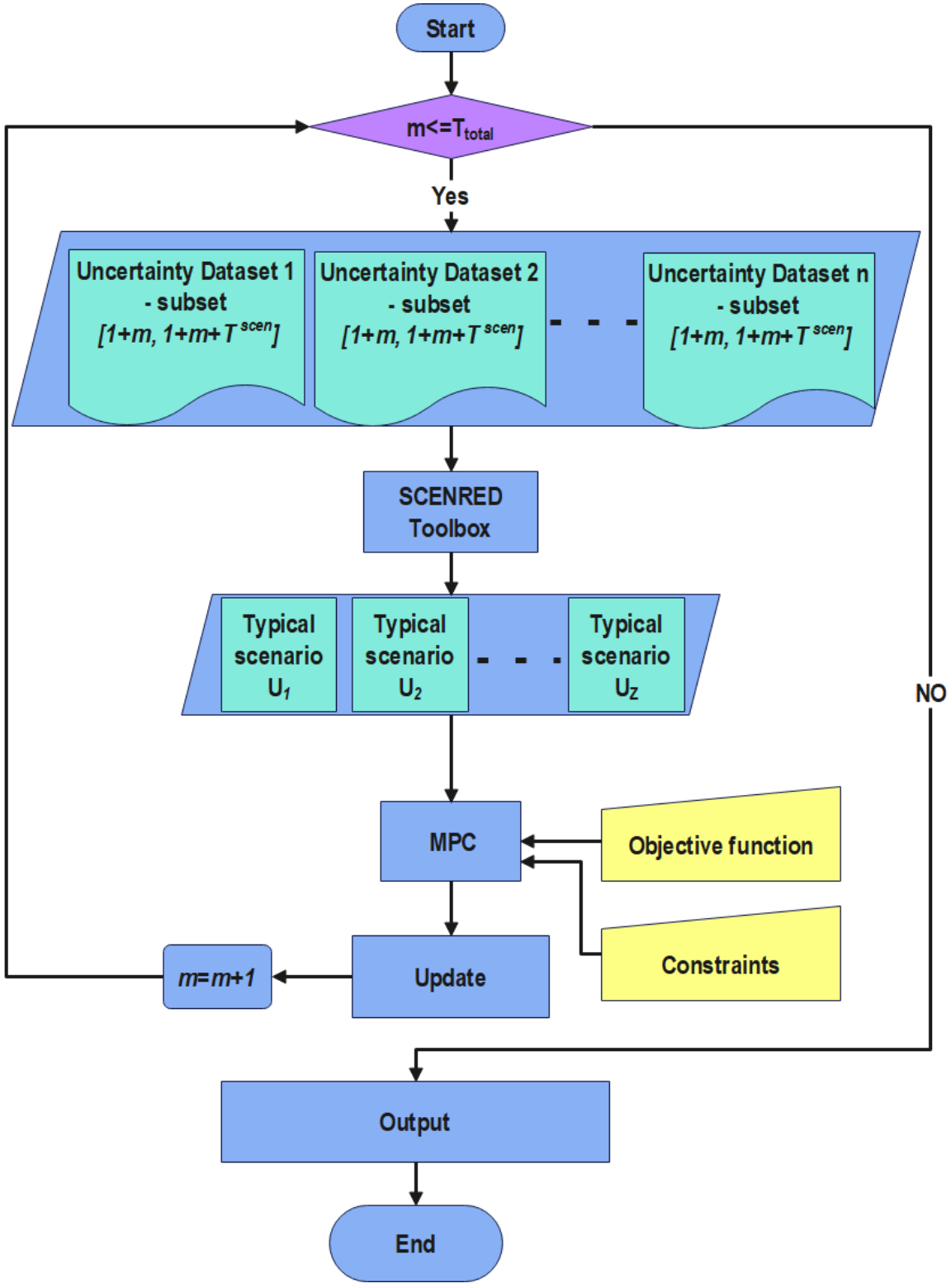

Figure 5.5: Dynamic scenario-based MPC model

however, the computation time may be an issue due to the necessity of scenario generation and reduction within each moving time horizon. Figure 5.5 illustrates the dynamic scenario-based MPC optimization process. The scenario generation and reduction are updated within each MPC iteration, and the typical scenarios are continuously updated.

In summary, the difference between the static and the dynamic scenario-based uncertainty models is that the static one obtains the scenarios once for all; while the dynamic case needs to update the typical scenarios for the entire process continuously.

5.3 Case study

5.3.1 Case study overview

In order to simulate the proposed scenario-based stochastic MPC approach for the cotton farm MG, we use the cotton farm information based on Section 4.3 from a real cotton farm located in Gunnedah, New South Wales, Australia. The corresponding historical data are used for the irrigation period of 87 days (early November 2016 to the end of February 2017) in this study. Five different cases are adopted to compare the results and demonstrate the applicability of the approach, which include Baseline case and standard MPC, static scenario-based MPC for grid-connected MG, dynamic scenario-based MPC for grid-connected

MG, static scenario-based MPC for islanded MG, and dynamic scenario-based MPC for islanded MG.

Table 5.1: System parameters of the grid-connected MG in the cotton farm

Items	Values
MG bore Pump #1 ($P^{MG}_{pump,1}$)	75 kW
MG river Pump #2 ($P^{MG}_{pump,2}$)	37 kW
Independent bore Pump #1 ($P^{in}_{pump,1}$)	75 kW
Farm area	3 $\times 10^6$ m^2
Bore pump head (h_1 or h^{in}_1)	31 mTDH
River pump head (h_2)	12 mTDH
Average energy for lifting 1 ML/mTDH (ε_{con})	4.55 kWh/ML/mTDH
Average water demand (W_{irr})	6.5 $\times 10^{-4}$ ML/m^2
Maximum allowed water usage	1800 ML/year
Reservoir capacity	800 ML
Average hourly seepage ($W_{see}/(24 \times 365)$)	4.56 m^3/h
Installed solar PV capacity ($\sigma \times P^{panel}_{solar}$)	50.6 kW
Fixed-rate tariff in 2016 (β_{buy})	0.26 AU$/kWh
FIT in 2016 (β_{sell})	0.06 AU$/kWh

5.3.2 Case 1: Baseline case and standard MPC.

The Baseline case is that farmers manually control all pumping systems based on their irrigation experience, and they can also obtain future weather information from the Bureau of Meteorology (BOM) or local weather stations. Figure 5.1 demonstrates the equipment layout and irrigation mode of the grid-connected MG in the study cotton farm. Table 5.1 lists the corresponding system parameters

in Figure 5.1 [138]. Based on Section 4.3, the breakdown energy cost of the Baseline case is listed in Table 5.2. While for the standard MPC of this study, the operational cost of the studied cotton farm is discussed in Section 4.3. For a comparison of the current study, the Baseline and standard MPC results from Section 4.3 are shown in Table 5.3.

Table 5.2: The details of the pump operation in the Baseline case in 2016

	Values
MG bore Pump #1 work hours	1,034 h
MG river Pump #2 work hours	882 h
Independent bore Pump #1 work hours	360 h
MG bore Pump #1 usage	75,812.33 kWh
MG river Pump #2 usage	63,551.06 kWh
Independent bore Pump #1 usage	12,865.24 kWh
Total operational cost	AU$ 39,580
Total pumped water	1,223.6 ML

Table 5.3: Operational results of Baseline case and standard MPC

MG items	Operational cost (AU$)	Total pumped water (ML)
grid-connected MG Baseline	39,580	1,224
grid-connected MG MPC	27,556	1,181
islanded MG Baseline	40,902	1,181
islanded MG MPC	31,164	1,178

5.3.3 Case 2: Static scenario-based MPC for grid-connected MG

In this case, we take advantage of the static scenario generation and reduction from Section 5.2.7 to obtain ten sets of typical scenarios and the corresponding probability of each scenario using the 87-day historical data. For the operational cost optimization, ten typical scenarios are substituted into (5.21). At last, the closed-loop MPC of (5.22) with a prediction horizon of 24 hours is used to obtain each pump's operation status and the operational cost of the entire irrigation period.

5.3.4 Case 3: Dynamic scenario-based MPC for grid-connected MG

The simulation is based on the dynamic scenario-based uncertainty model in Section 5.2.7, which uses the historical data of 14 days ahead of the current time instant. For this study, we compare both the static and dynamic scenario-based MPC approaches. Thus, the same historical data are used for this approach. The differences between the static and dynamic scenario-based approaches are that in the dynamic one, we obtain 10 typical scenarios based on the moving 14-day datasets, and the obtained 10 typical scenarios will be updated at each MPC iteration whenever the optimization horizon changes.

5.3.5 Case 4: Static scenario-based MPC for islanded MG

Many cotton farm pumping sites in Australia are far from the grid [173]. islanded MGs using diesel generators, solar energy, and lead-acid battery storage are widely built on cotton farms. Based on the previous MPC study for islanded MG in Section 4.3.2, the islanded MG of the studied cotton farm is shown in Figure 5.2, with the system parameters in Table 5.4. Then, we substitute the historical data of the studied cotton farm in 2016 and adopt the algorithm proposed in Section 5.2.7. The pump operation during the entire irrigation period can be optimized for the islanded MG system. Also, the operation cost under uncertainties can be obtained.

5.3.6 Case 5: Dynamic scenario-based MPC for islanded MG

Dynamic scenario generation and reduction are applied for islanded MG using the model in Section 5.2.7, and then the operational cost and each pump's action can be obtained by the underlying stochastic MPC methodology. In order to compare both the static and dynamic scenario-based MPC, the same cotton farm's historical data are used.

Table 5.4: System parameters of the islanded MG in the studied cotton farm [174]

Items	Values
Diesel conversion	
coefficient (ψ)	0.2695 L/kWh
Diesel consumption	
for lifting 1ML/m water (δ_{diesel})	1.1 L/ML/mTDH
Unit price of diesel in 2016	
(after subsidy) (β_{diesel})	AU$ 1.15 /L
Lead-acid battery	
capacity (C_{Bat})	25 kWh
Lead-acid battery	
cost (B_{cap})	AU$ 2,750
Charge/discharge	
efficiencies (η_c or η_d)	90%
Charge/discharge limit	
($P^{max}_{charge}/P^{max}_{discharge}$)	15 kWh
Lead-acid battery life cycle	
($K_c \times \alpha$)	2000 @ 60% DoD

5.4 Results and discussions

This section discusses the key results of MPC for cotton farm MG under uncertainties. Scenario generation and reduction methodology are employed to simulate four different cases (cases 2 - 5), and the results from each case are analyzed and compared to the Baseline case.

I. **Static scenario generation and reduction**

In this study, the cotton farm data during the irrigation period of 2016-2017 include historical solar generation data, rainfall data [142], hourly evaporation data of the cotton farm area [175] and the cotton life-cycle water demand data. For the entire irrigation period, scenario generation and reduction can be illustrated in Figure 5.6a and Figure 5.6b, respectively. From Figure 5.6a, it can be seen that all historical data of uncertainty are arranged in groups of 24 hours each, spanning a total of 87 days. The four different types of uncertain historical data include hourly PV power generation, hourly rainfall, hourly evaporation volume, and hourly water demand. On the other hand, Figure 5.6b indicates that the historical data of the aforementioned four types of uncertainties have undergone static scenario generation and reduction, resulting in 10 sets of typical scenarios, as seen in Figure 5.6b.

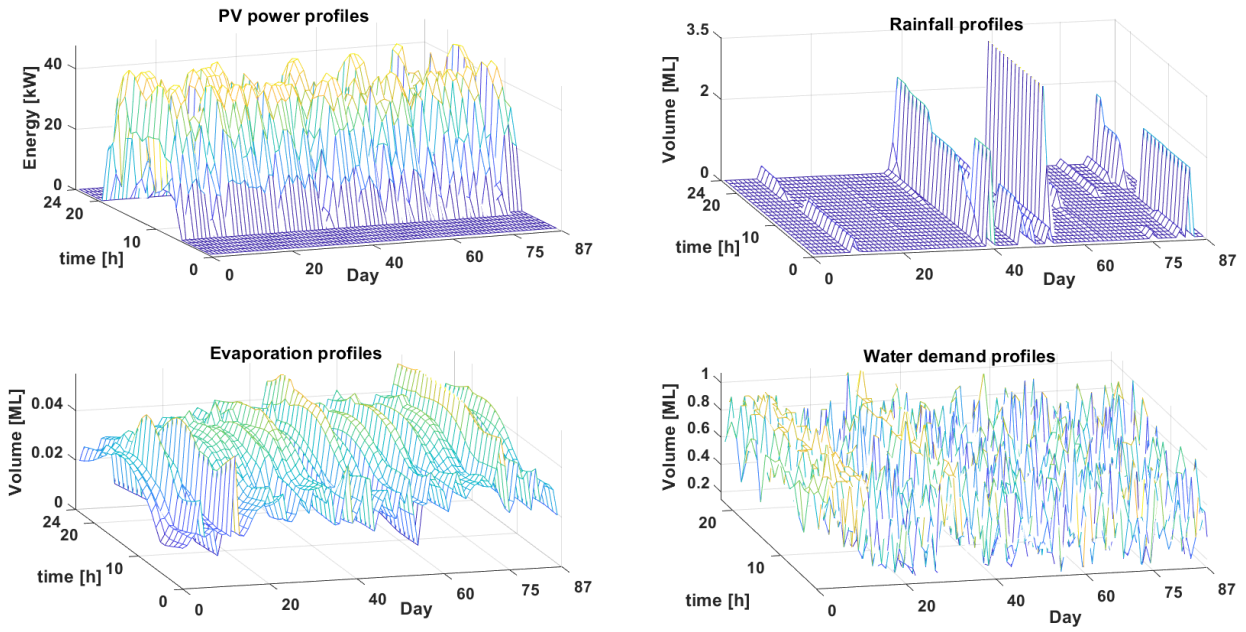

(a) Uncertainty data for the entire irrigation period

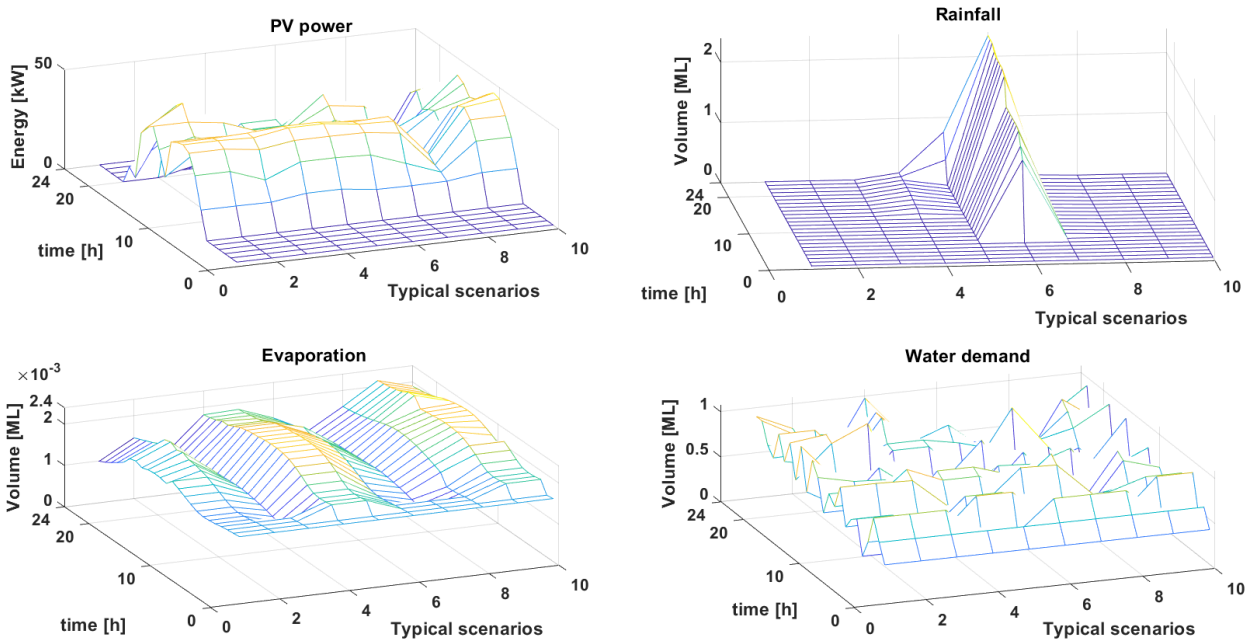

(b) Ten typical scenarios after reduction

Figure 5.6: Static scenario generation and reduction for the studied cotton farm

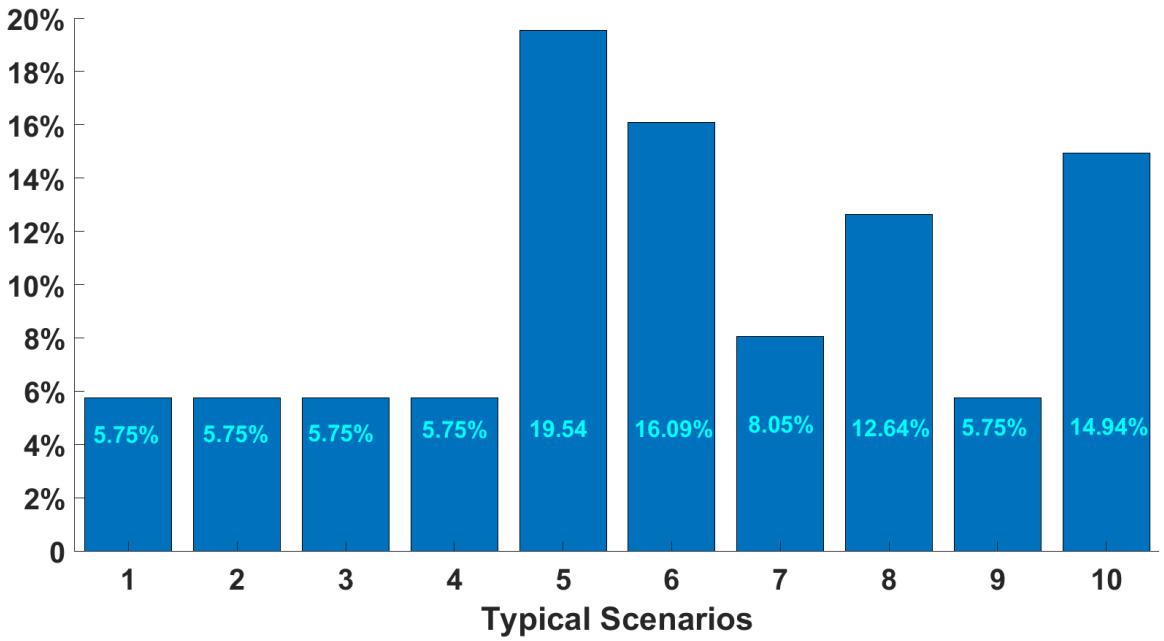

Figure 5.7: Probability of static typical scenarios

Note that the scenario generation and reduction is only conducted once during the entire irrigation period. Each typical scenario has its corresponding probability, as shown in Figure 5.7.

II. Dynamic scenario generation and reduction

In the dynamic scenario generation and reduction method, we take the two-week data ahead of the current time instant to produce 10 typical scenarios. For instance, Figure 5.8a and Figure 5.8b show the evaporation curves before and after scenario generation and reduction methodology in 4 consecutive MPC iterations. Note that the scenario generation and reduction on a small variation of data is conducted in each MPC iteration to obtain the dynamically updated typical scenarios, as seen in Figure 5.8.

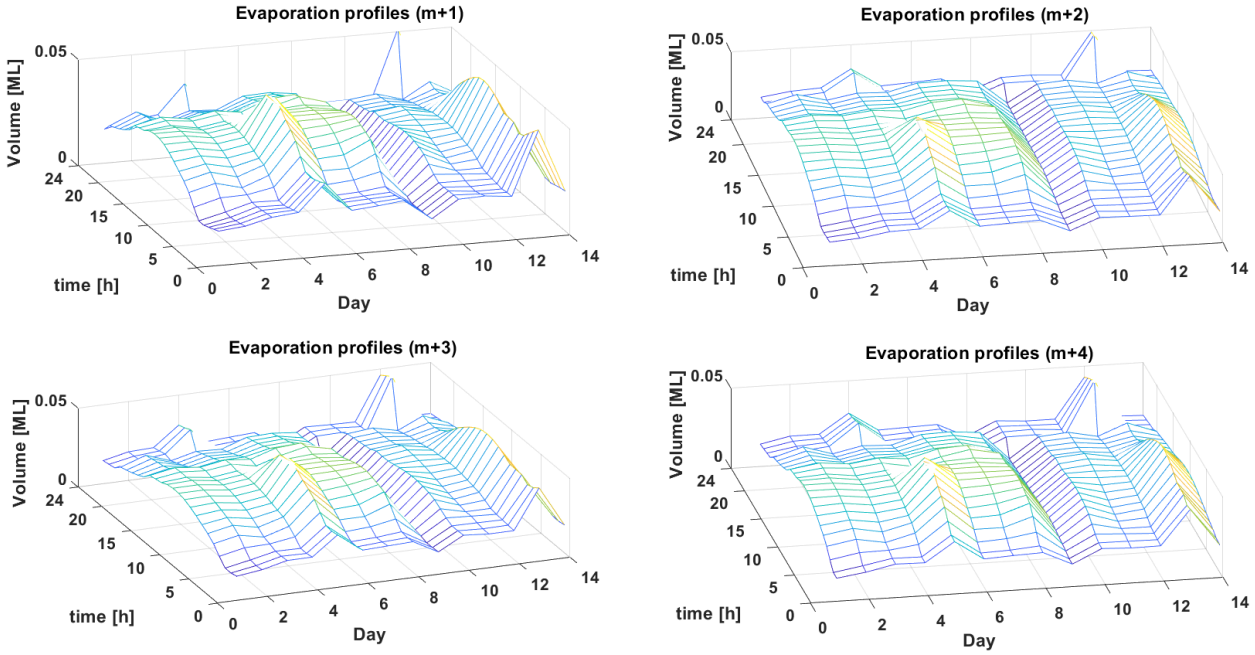

(a) 14-day evaporation data

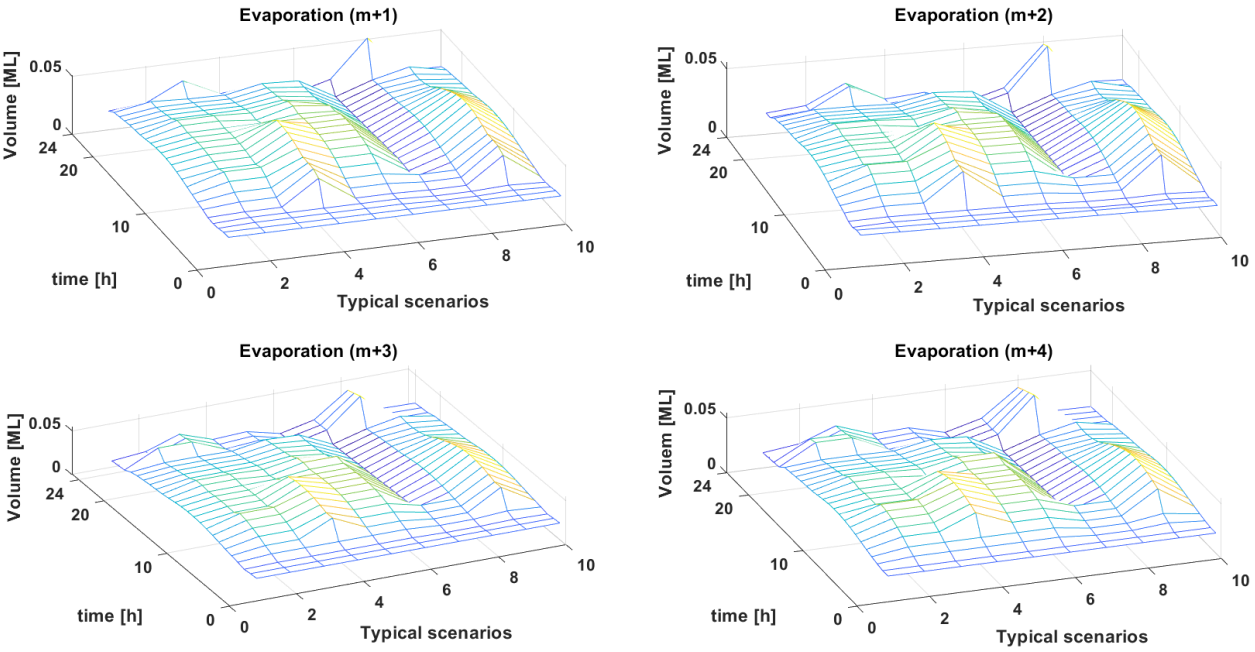

(b) Ten evaporation typical scenarios after reduction in 4 consecutive MPC iterations

Figure 5.8: Dynamic scenario generation and reduction by using the future 14-day data

III. Scenario-based MPC operation results for grid-connection microgrid

With the help of the scenario generation and reduction method for the historical dataset, we implement the close-loop MPC to optimize the operation of each pump during the whole irrigation period. The hourly control variables (x_i and x_i^{in}) can be obtained by solving (5.19) and (5.22). Figure 5.9a shows the on/off status of MG bore pump #1 (turned on for 1,125 h), MG river pump #2 (turned on for 810 h) and the independent pump #1 (turned on for 176 h), which are controlled under the static scenario-based MPC. Figure 5.9b shows the pump's on/off status under the dynamic scenario-based MPC, where MG bore pump #1 worked for 1,031 h, MG river pump #2 worked for 1,137 h, and the independent pump #1 worked for 76 h. It can be observed from Figure 5.9 that the usage rate of the water pumps connected to the MG is higher than the independent pump. The utilization rate of the independent pump in the static scenario-based MPC is slightly higher than that in the dynamic scenario-based MPC. Table 5.5 shows the comparison of the proposed scenario-based MPC with the Baseline case and the standard MPC. The expected value of the operational cost for static scenario-based MPC is AU$ 22,595, which saves AU$ 16,985 compared with the Baseline

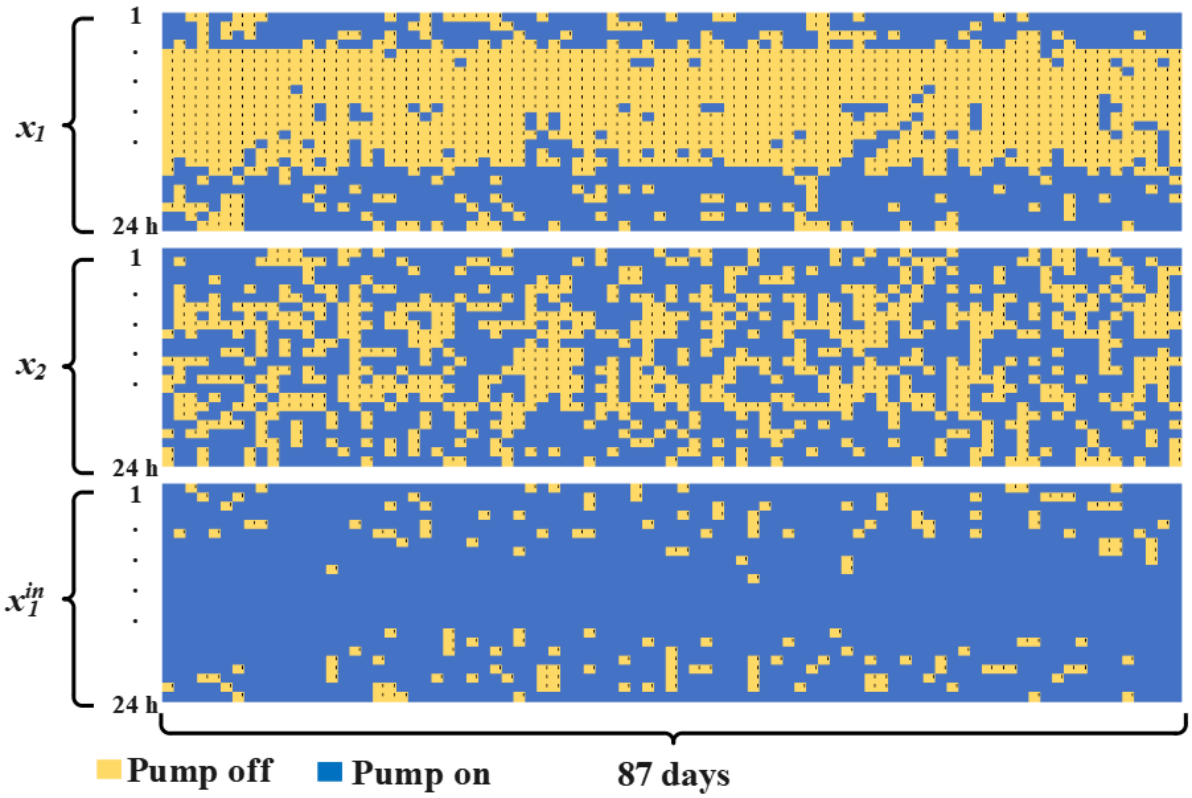

(a) Pump's on/off status under static scenario-based MPC

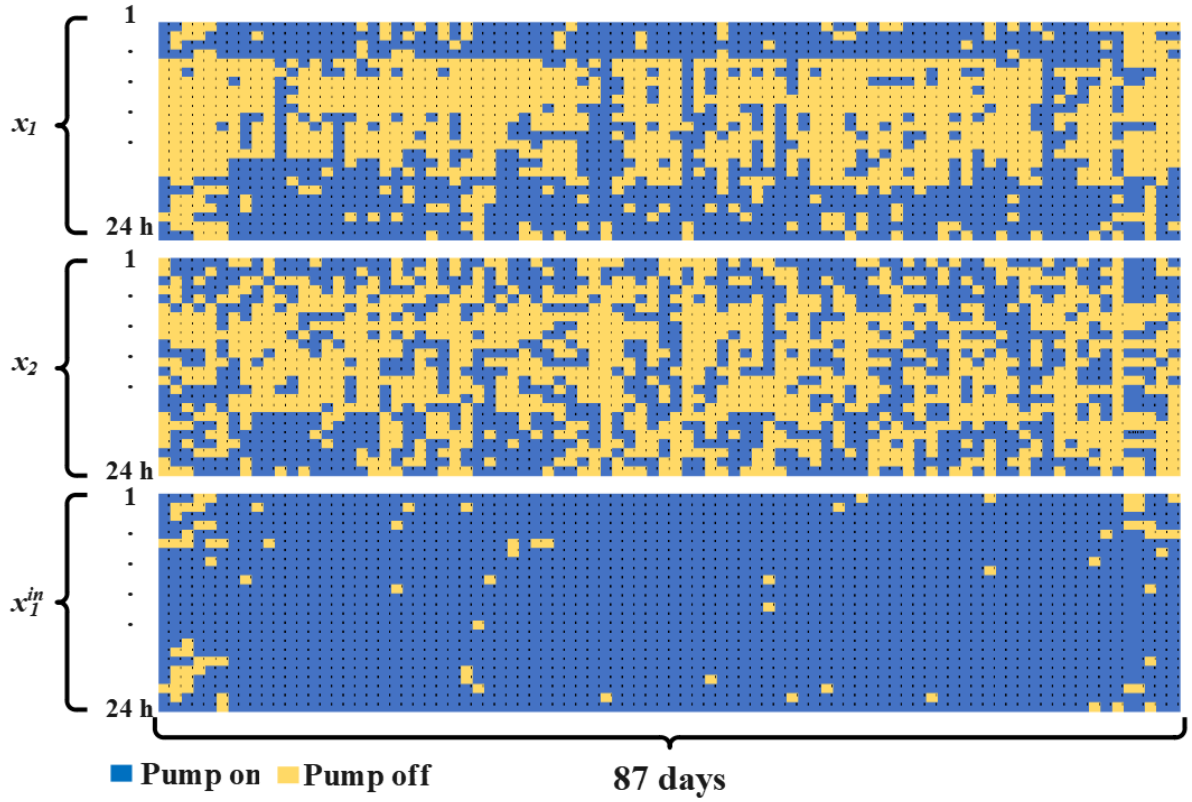

(b) Pump's on/off status under dynamic scenario-based MPC

Figure 5.9: Pump's on/off status for grid-connected microgrid

case and saves AU$ 4,961 compared with the standard MPC. Moreover, the expected operational cost value of the dynamic scenario-based MPC is AU$ 18,797, which is AU$ 20,783 less than the Baseline case and AU$ 8,759 less than the standard MPC.

Table 5.5: Operational result comparison of grid-connected microgrid

	Operational cost (AU$)	Total pumped water (ML)
Baseline case	39,580	1,224
Standard MPC	27,556	1,181
Static scenario-based MPC	22,595	1,233
Dynamic scenario-based MPC	18,797	1,238

IV. **Scenario-based MPC operation results for islanded microgrid**

Table 5.6: Pump's operational results of the scenario-based MPC for islanded microgrid

	Operation hours (h)	Pumped water (ML)
Static x_1	515	274
Static x_2	995	647
Static x_1^{in}	493	262
Dynamic x_1	381	203
Dynamic x_2	1,094	741
Dynamic x_1^{in}	507	270

In order to verify that the proposed approach is also suitable for islanded MG, we assume the same cotton farm parameters for the islanded MG with

Table 5.7: Operational result comparison of islanded microgrid

	Operational cost (AU$)	Total pumped water (ML)
Baseline case	40,902	1,181
Standard MPC	31,164	1,178
Static scenario-based MPC	27,416	1,214
Dynamic scenario-based MPC	24,443	1,210

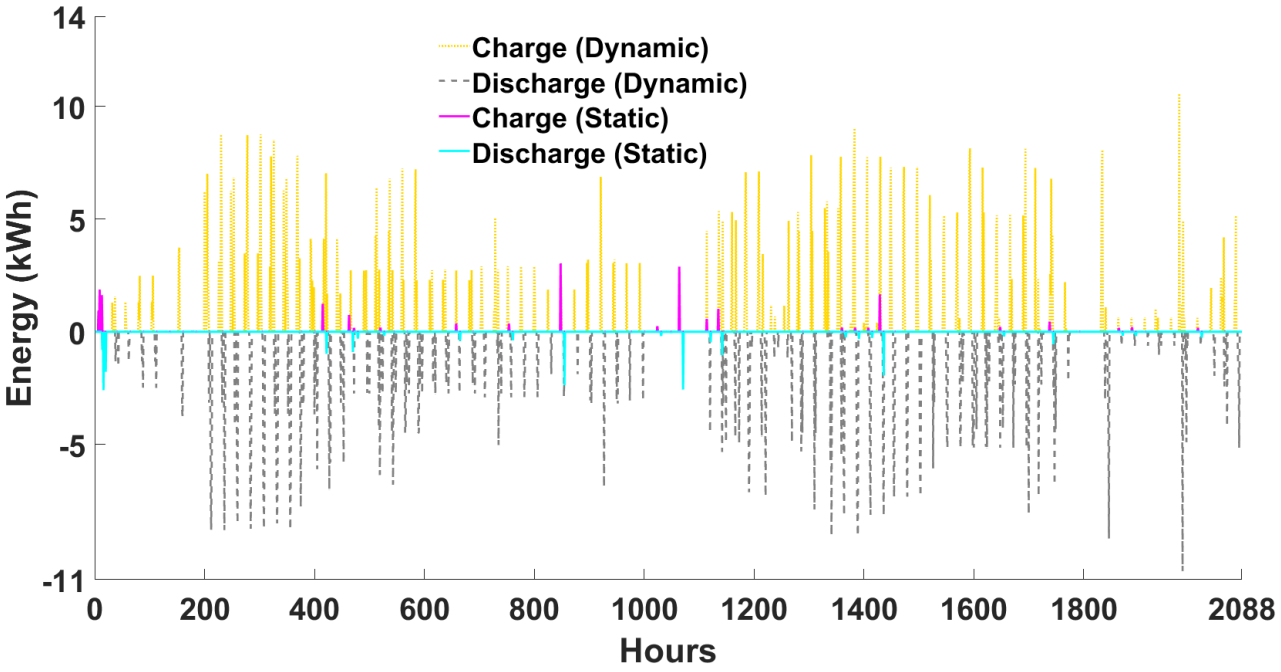

Figure 5.10: Battery charging and discharging pattern in islanded microgrid

Table 5.8: Operational results of the battery storage

	Static scenario	Dynamic scenario
Energy charge (kWh)	31.53	821.77
Energy discharge (kWh)	33.42	821.56
Saved cost (AU$)	10.35	254.62
Degradation cost (AU$)	6.61	167.38

diesel generators as a backup power source and a 25 kWh lead-acid battery storage equipped to store the excess energy. The scenario generation and reduction processes use the same dataset to facilitate the comparison with the Baseline case and the standard MPC for islanded MG. Based on (5.20) and (5.22), the pump control variables can be obtained and listed in Table 5.6. In addition, Table 5.7 shows the results of total pumped water volume and the operational cost for each islanded MG case. The expected value of operational cost from the static scenario-based MPC is AU$ 13,486 lower than the Baseline case and AU$ 3,748 lower than the standard MPC. For the dynamic scenario-based MPC, it has the lowest operational cost value AU$ 24,443, which is AU$ 16,459 lower than the Baseline case and AU$ 6,721 lower than the standard MPC. In the islanded MG system, the excess electrical energy is stored in the batteries and released to the pumps when needed. According to the battery pack parameters in Table 5.4, and the methodology in Section 5.2.3, the battery pack usage during the entire irrigation period can be obtained. Figure 5.10 shows the battery charging and discharging pattern for the static and dynamic scenario-based MPC. Meanwhile, Table 5.8 lists the operational results of the battery storage. We can observe from Figure 5.8 that the dynamic scenario-based MPC generates ten typical scenarios for each MPC iteration, and thus, the role of batteries can be clearly

reflected in the MG. The battery pack for the dynamic scenario-based MPC can reuse 821 kWh of excess energy to power the MG pumps. During the entire irrigation period, the energy cost savings from utilizing the battery storage is AU$ 87.24 more than the cost of battery pack degradation under the dynamic scenario-based MPC, which means using the battery to store and reuse the excess energy from the RES can save the operational cost of AU$ 87.24.

5.5 Summary

This study proposes two scenario-based approaches to model the uncertainties of environmental and demand factors on cotton farms by scenario generation and reduction under the MPC framework. Then, the MPC method is used to optimize the operation of the MG and cotton farm water pump under the obtained typical scenarios for the underlying uncertainties. The proposed method is validated by case studies on a cotton farm. It is found that the operational cost of the static and dynamic scenario-based MPC for the grid-connected MG are AU$ 22,595 and AU$ 18,797, which are AU$ 4,961 and AU$ 8,759 respectively, lower than that of the standard MPC. For the islanded MG, the operational cost of static and dynamic scenario-based MPC are AU$ 3,748 and AU$ 6,721, respectively, lower than the standard MPC.

Chapter 6

Conclusions and Future Work

This chapter summarizes the current studied results and provides suggestions for further work.

6.1 Summary of outcomes

In the literature review part of the thesis, the energy system of cotton farms and the irrigation method of cotton are investigated, and the traditional energy utilization methods of cotton farms are studied. The composition of current operational costs and their limitations are addressed. In addition, this part also reviews the MG's techno-economic requirements and the optimization algorithms. And then, the following optimization strategies are introduced for the MG of Australian cotton farms: optimal investment planning, optimal operation, and

optimal operation under uncertainties.

Chapter 3 proposes a novel MG optimal design method for Australian cotton farms. The design problem is formulated as a multi-objective optimization problem. It seeks the trade-off among those objective functions, which are related to the investment cost, operational cost and simple payback period. In the case study of a real cotton farm, a number of different MG scenarios are presented to illustrate the effectiveness of the proposed model. In addition, sensitivity analysis is explored by changing different parameters to explain the impact of the cost function's weighting factors, weather conditions and tariff selection on the MG design. In the studied cotton farm, the simulation results show that the operating cost can be reduced by 44.16% to 56.51% with the optimal MGs in different scenarios compared with the farm's existing energy consumption, and the simple payback period is 8.35 - 9.49 years. The grid-connected MG can feed the excess energy into the grid to accelerate the payback period, which depends on particular FIT tariffs. This case study provides a reference for cotton industry stakeholders to consider RES investment in cotton farms.

Chapter 4 introduces an MPC approach to the operating cost minimization problem for an Australian cotton farm MG. It also shows the robustness of the MPC algorithm under rainy and drought conditions for the grid-connected MG. The

case study results of the cotton farm in the Gunnedah show that the MPC approach reduces the operational cost of the grid-connected MG from AU$ 39,580 to AU$ 27,556, and using the MPC method for the islanded MG can reduce the operational cost from AU$ 40,902 to AU$ 31,164. Furthermore, in the case study of another cotton farm in Narromine, the large-scale MG with ESS can reduce the operational cost from AU$ 317,415 to AU$ 234,260, and if this MG has no ESS, the operational cost is reduced from AU$ 317,415 to AU$ 242,970. The MPC approach can be combined with future weather forecast data to achieve the MG's real-time operation in the cotton farm.

Chapter 5 presents two scenario-based approaches to model uncertainty in cotton farm environmental and demand factors through scenario generation and reduction under the MPC framework. Then, with the obtained typical scenarios, the MPC method is used to optimize the operation of the MG and cotton farm pumps. The proposed method is simulated through a case study of a cotton farm in Gunnedah. For the grid-connected MG, the static and dynamic scenario-based MPC approaches have operational costs of AU$ 22,595 and AU$ 18,797, respectively, which are lower than the standard MPC by AU$ 4,961 and AU$ 8,759, respectively. For the islanded MG, the operational costs of the static and dynamic scenario-based MPC approaches are AU$ 27,416 and AU$ 24,443, which

are AU$ 3,748 and AU$ 6,721 lower than that of the standard MPC.

6.2 Recommendations & future work

This thesis proposes methodologies for planning investment optimization, operation optimization and operation optimization under uncertainty for the RES-based MG in Australian cotton farms. These methods consider taking advantage of RES (especially solar) and battery energy storage to reduce the operational costs of cotton farm pumps. Meanwhile, more recommendations are proposed below that would extend the current research.

1. For chapter 3, only grid-connected cotton farms are considered. However, there is a number of cotton farms that are not grid-connected. Therefore, our future work will focus on the feasibility of MG designs for cotton farms where grid power is limited or unavailable.

2. For an immediate future study, artificial intelligence is a beneficial tool for agricultural technology development, and MPC can be combined with machine learning techniques to realize intelligent control. In addition, there is a need to evaluate and implement the proposed method at a real cotton farm in our future work.

3. In future work, the static scenario-based MPC approach for cotton farm MG control systems will use more years of historical data to improve its reliability. For the dynamic scenario-based MPC approach, we will investigate how to reduce the computation burden for real-time implementations.

Bibliography

[1] G. Chen and C. Baillie, "Development of a framework and tool to assess on-farm energy uses of cotton production," *Energy Conversion and Management*, vol. 50, no. 5, pp. 1256–1263, 2009.

[2] Australia Cotton, *Environment & People Social Impact*, https://australiancotton.com.au/social-impact, Retrieved October 8, 2022.

[3] Cotton Research and Development Corporation, *WATERpak - a guide for irrigation management in cotton and grain farming systems*, https://www.cottoninfo.com.au/sites/default/files/documents/WATERpak.pdf, 2012.

[4] E. F. Camacho and C. B. Alba, *Model predictive control*. Springer science & business media, 2013.

[5] A. Bemporad and M. Morari, "Robust model predictive control: A survey," in *Robustness in identification and control*, Springer, 1999, pp. 207–226.

[6] Cotton Australia, *The Australian cotton industry naturally world's best (Cotton Education Kit - Chapter 1)*, https://cottonaustralia.com.au/assets/general/Education-resources/CA-resources/Education-Kit/2021-Education-Kit/Educational_Kit_Cotton_Australia_Chapter01.pdf, Retrieved October 8, 2022.

[7] Cotton leads, *Water stewardship – Australia*, https://cottonleads.org/sustainable-production/water-stewardship-australia, Retrieved October 8, 2022.

[8] P. Szabo, J. Foley, G. Sandell, and C. Baillie, "Improving Energy Efficiency on Irrigated Australian Cotton Farms," CottonInfo, Tech. Rep., 2015.

[9] C. Baillie, "A Protocol for Assessing On-Farm Energy Use and Associated Greenhouse Gas Emissions," University of Southern Queensland, Tech. Rep., 2013.

[10] F. Gerry, H. David, R. Leigh, and S. Phil, *VSDs lead irrigation efficiency measures for Gunnedah cropping enterprise*, https://www.pumpindustry.com.au/vsds-lead-irrigation-efficiency-measures-for-gunnedah-cropping-enterprise/, 2017.

[11] C. Perry, E. Barnes, D. Munk, K. Fisher, and P. Bauer, "Cotton irrigation management for humid regions," *Cotton Incorporated, Cary, NC*, 2012.

[12] D. McJannet, F. Cook, J. Knight, and S. Burn, "Evaporation reduction by monolayers: Overview, modelling and effectiveness," *Urban Water Security Research Alliance Technical Report*, vol. 6, pp. 1–32, 2008.

[13] CottonInfo, *Energy case study - Energy-efficiency plan pays off for Gunnedah irrigator*, https://www.cottoninfo.com.au/sites/default/files/documents/WATERpak.pdf, 2015.

[14] Hydraulic Institute, "Improving the Performance of Existing Pumping Systems," Pumps & Systems, Tech. Rep., September 2008.

[15] R. Saidur, S. Mekhilef, M. B. Ali, A. Safari, and H. A. Mohammed, "Applications of variable speed drive (VSD) in electrical motors energy savings," *Renewable and sustainable energy reviews*, vol. 16, no. 1, pp. 543–550, 2012.

[16] J. Qian and F. C. Lee, "Charge pump power-factor-correction technologies. I. Concept and principle," *IEEE Transactions on power electronics*, vol. 15, no. 1, pp. 121–129, 2000.

[17] B. Jeff, "Farm-scale dam design and costs," Tech. Rep., 2018.

[18] CottonInfo, "WATER: Minimising storage evaporation and seepage," Tech. Rep., 2018.

[19] CottonInfo, "A Review of Centre Pivot and Lateral Move Irrigation Installations in the Australian Cotton Industry," Tech. Rep., 2014.

[20] A. David and T. Dave O'Donnell Chris, "Irrigation Equipment and Techniques," Tech. Rep., 2001.

[21] A. Simmons and G. Roth, "Smarter Irrigation for Profit 2," Tech. Rep., 2018.

[22] P. JW and W. JW, "Solar Energy – Policy setting and applications to cotton production," Tech. Rep., 2016.

[23] J. Li, P. Liu, and Z. Li, "Optimal design and techno-economic analysis of a solar-wind-biomass off-grid hybrid power system for remote rural electrification: A case study of west China," *Energy*, vol. 208, p. 118 387, 2020.

[24] S. Kichou, T. Markvart, P. Wolf, S. Silvestre, and A. Chouder, "A simple and effective methodology for sizing electrical energy storage (EES) systems based on energy balance," *Journal of Energy Storage*, vol. 49, p. 104 085, 2022.

[25] M. Riou, F. Dupriez-Robin, D. Grondin, C. Le Loup, M. Benne, and Q. T. Tran, "Multi-Objective Optimization of Autonomous Microgrids with Reliability Consideration," *Energies*, vol. 14, no. 15, p. 4466, 2021.

[26] N. Mousavi, G. Kothapalli, D. Habibi, C. K. Das, and A. Baniasadi, "A novel photovoltaic-pumped hydro storage microgrid applicable to rural areas," *Applied Energy*, vol. 262, p. 114 284, 2020.

[27] J. Powell and J. Welsh, *Integrating alternative Energy: A farm case study at Emerald, QLD*, https://www.agecon.com.au/media-and-publications/integrating-alternative-energy-a-farm-case-study-at-emerald-qld, 2019.

[28] J. Powell, J. Welsh, and R. Farquharson, "Investment analysis of solar energy in a hybrid diesel irrigation pumping system in New South Wales, Australia," *Journal of Cleaner Production*, vol. 224, pp. 444–454, 2019.

[29] T. Mtshali, G. Coppez, S. Chowdhury, and S. Chowdhury, "Simulation and modelling of PV-wind-battery hybrid power system," in *2011 IEEE Power and Energy Society General Meeting*, IEEE, 2011, pp. 1–7.

[30] A. Shahirinia, S. Tafreshi, A. H. Gastaj, and A. Moghaddomjoo, "Optimal sizing of hybrid power system using genetic algorithm," in *2005 International Conference on Future Power Systems*, IEEE, 2005, 6–pp.

[31] T. Ma, C. R. Lashway, Y. Song, and O. Mohammed, "Optimal renewable energy farm and energy storage sizing method for future hybrid power system," in *2014 17th International Conference on Electrical Machines and Systems (ICEMS)*, IEEE, 2014, pp. 2827–2832.

[32] G. Sandeep and V. Vakula, "Optimal combination and sizing of a standalone hybrid power system using HOMER," in *2016 International Conference on Electrical, Electronics, and Optimization Techniques (ICEEOT)*, IEEE, 2016, pp. 4141–4144.

[33] L. Olatomiwa, S. Mekhilef, A. N. Huda, and K. Sanusi, "Techno-economic analysis of hybrid PV-diesel-battery and PV-wind-diesel-battery power systems for mobile BTS: the way forward for rural development," *Energy Science & Engineering*, vol. 3, no. 4, pp. 271–285, 2015.

[34] S. Dhundhara, Y. P. Verma, and A. Williams, "Techno-economic analysis of the lithium-ion and lead-acid battery in microgrid systems," *Energy Conversion and Management*, vol. 177, pp. 122–142, 2018.

[35] M. L. Kolhe, K. I. U. Ranaweera, and A. S. Gunawardana, "Techno-economic sizing of off-grid hybrid renewable energy system for rural electrification in Sri Lanka," *Sustainable Energy Technologies and Assessments*, vol. 11, pp. 53–64, 2015.

[36] A. S. Ramya, N. Periyasamy, A. Vidhya, S. Sundrapandian, and P. Raja, "Design and development of a GUI for an optimal hybrid energy system," in *2014 Eighteenth National Power Systems Conference (NPSC)*, IEEE, 2014, pp. 1–6.

[37] O. Ekren and B. Y. Ekren, "Size optimization of a PV/wind hybrid energy conversion system with battery storage using simulated annealing," *Applied energy*, vol. 87, no. 2, pp. 592–598, 2010.

[38] G. Aghajani and N. Ghadimi, "Multi-objective energy management in a micro-grid," *Energy Reports*, vol. 4, pp. 218–225, 2018.

[39] A. R. Prasad and E. Natarajan, "Optimization of integrated photovoltaic–wind power generation systems with battery storage," *Energy*, vol. 31, no. 12, pp. 1943–1954, 2006.

[40] Z. Maheshwari, "A Study of Smart Integrated Renewable Energy Systems (SIRES)," Ph.D. dissertation, Oklahoma State University, 2017.

[41] T. Funabashi, T. Tanabe, T. Nagata, and R. Yokoyama, "An autonomous agent for reliable operation of power market and systems including microgrids," in *2008 Third International Conference on Electric Utility Deregulation and Restructuring and Power Technologies*, IEEE, 2008, pp. 173–177.

[42] M. F. Zia, E. Elbouchikhi, and M. Benbouzid, "Optimal operational planning of scalable DC microgrid with demand response, islanding, and battery degradation cost considerations," *Applied energy*, vol. 237, pp. 695–707, 2019.

[43] A. Hussain, V.-H. Bui, and H.-M. Kim, "Resilience-oriented optimal operation of networked hybrid microgrids," *IEEE Transactions on Smart Grid*, vol. 10, no. 1, pp. 204–215, 2017.

[44] H. Zhang, X. Xia, and J. Zhang, "Optimal sizing and operation of pumping systems to achieve energy efficiency and load shifting," *Electric Power Systems Research*, vol. 86, pp. 41–50, 2012.

[45] B. Aluisio, M. Dicorato, G. Forte, G. Litrico, and M. Trovato, "Integration of heat production and thermal comfort models in microgrid operation planning," *Sustainable Energy, Grids and Networks*, vol. 16, pp. 37–54, 2018.

[46] M. H. Imani, M. J. Ghadi, S. Ghavidel, and L. Li, "Demand response modelling in microgrid operation: A review and application for incentive-based and time-based programs," *Renewable and Sustainable Energy Reviews*, vol. 94, pp. 486–499, 2018.

[47] S. Tiwari, R. Naresh, and R. Jha, "Neural network predictive control of UPFC for improving transient stability performance of power system," *Applied Soft Computing*, vol. 11, no. 8, pp. 4581–4590, 2011.

[48] E. Khanmirza, A. Esmaeilzadeh, and A. H. D. Markazi, "Predictive control of a building hybrid heating system for energy cost reduction," *Applied Soft Computing*, vol. 46, pp. 407–423, 2016.

[49] P. M. Marusak, "Advantages of an easy to design fuzzy predictive algorithm in control systems of nonlinear chemical reactors," *Applied Soft Computing*, vol. 9, no. 3, pp. 1111–1125, 2009.

[50] A. Hajizadeh and M. A. Golkar, "Power flow control of grid-connected fuel cell distributed generation systems," *Journal of Electrical Engineering and Technology*, vol. 3, no. 2, pp. 143–151, 2008.

[51] H. Zhang, Z. Nie, X. Xiao, *et al.*, "Design and simulation of SMES system using YBCO tapes for direct drive wave energy converters," *IEEE transactions on applied superconductivity*, vol. 23, no. 3, pp. 5 700 704–5 700 704, 2012.

[52] S. K. Sahoo, "Comparison of SVM and DPC for reactive power control of DFIG based wind energy systems," *Journal of Renewable Energy and Smart Grid Technology*, vol. 11, no. 1, pp. 1–8, 2016.

[53] H. Liang and W. Zhuang, "Stochastic modeling and optimization in a microgrid: A survey," *Energies*, vol. 7, no. 4, pp. 2027–2050, 2014.

[54] D. R. Prabha, T. Jayabarathi, R. Mageshvaran, K. Kranthi Kumar, and M. Venkata Niveesh, "Economic dispatch with valve point effect using intelligent water drop algorithm," *Int J Appl Eng Res*, vol. 2, pp. 12–7, 2014.

[55] V. R. BHARADWAJ and G. SIDDHARTHA, "Invasive weed optimization for economic dispatch with valve point effects," *Journal of Engineering Science and Technology*, vol. 11, no. 2, pp. 237–251, 2016.

[56] D. R. Prabha, T. Jayabarathi, R. Umamageswari, and S. Saranya, "Optimal location and sizing of distributed generation unit using intelligent water drop algorithm," *Sustainable Energy Technologies and Assessments*, vol. 11, pp. 106–113, 2015.

[57] M. Preindl and S. Bolognani, "Model predictive direct torque control with finite control set for PMSM drive systems, Part 1: Maximum torque per ampere operation," *IEEE Transactions on Industrial Informatics*, vol. 9, no. 4, pp. 1912–1921, 2013.

[58] M. Preindl and S. Bolognani, "Model predictive direct torque control with finite control set for PMSM drive systems, part 2: Field weakening operation," *IEEE Transactions on Industrial Informatics*, vol. 9, no. 2, pp. 648–657, 2012.

[59] Q. Teng, J. Bai, J. Zhu, and Y. Sun, "Fault tolerant model predictive control of three-phase permanent magnet synchronous motors," *WSEAS Transactions on systems*, 2013.

[60] P. Mercorelli, "A multilevel inverter bridge control structure with energy storage using model predictive control for flat systems," *Journal of Engineering*, vol. 2013, 2013.

[61] J. Zhang and X. Xia, "A model predictive control approach to the periodic implementation of the solutions of the optimal dynamic resource allocation problem," *Automatica*, vol. 47, no. 2, pp. 358–362, 2011.

[62] M. B. Abdelghany, M. F. Shehzad, D. Liuzza, V. Mariani, and L. Glielmo, "Optimal operations for hydrogen-based energy storage systems in wind farms via model predictive control," *International Journal of Hydrogen Energy*, vol. 46, no. 57, pp. 29 297–29 313, 2021.

[63] E. Muhando, T. Senjyu, K. Uchida, H. Kinjo, and T. Funabashi, "Stochastic inequality constrained closed-loop model-based predictive control of MW-class wind generating system in the electric power supply," *IET renewable power generation*, vol. 4, no. 1, pp. 23–35, 2010.

[64] H. Zhao, Q. Wu, Q. Guo, H. Sun, and Y. Xue, "Distributed model predictive control of a wind farm for optimal active power control part I: Clustering-based wind turbine model linearization," *IEEE transactions on sustainable energy*, vol. 6, no. 3, pp. 831–839, 2015.

[65] F. Garcia-Torres and C. Bordons, "Optimal economical schedule of hydrogen-based microgrids with hybrid storage using model predictive control," *IEEE Transactions on Industrial Electronics*, vol. 62, no. 8, pp. 5195–5207, 2015.

[66] J. Hu, Y. Xu, K. W. Cheng, and J. M. Guerrero, "A model predictive control strategy of PV-Battery microgrid under variable power generations and load conditions," *Applied Energy*, vol. 221, pp. 195–203, 2018.

[67] F. Garcia-Torres, C. Bordons, and M. A. Ridao, "Optimal economic schedule for a network of microgrids with hybrid energy storage system using distributed model predictive control," *IEEE transactions on industrial electronics*, vol. 66, no. 3, pp. 1919–1929, 2018.

[68] Y. Jia, Z. Y. Dong, C. Sun, and G. Chen, "Distributed economic model predictive control for a wind–photovoltaic–battery microgrid power system," *IEEE Transactions on Sustainable Energy*, vol. 11, no. 2, pp. 1089–1099, 2019.

[69] J. Sachs and O. Sawodny, "A two-stage model predictive control strategy for economic diesel-PV-battery island microgrid operation in rural areas," *IEEE Transactions on Sustainable Energy*, vol. 7, no. 3, pp. 903–913, 2016.

[70] P. Kou, Y. Feng, D. Liang, and L. Gao, "A model predictive control approach for matching uncertain wind generation with PEV charging demand in a microgrid," *International Journal of Electrical Power & Energy Systems*, vol. 105, pp. 488–499, 2019.

[71] M. Nassourou, V. Puig, J. Blesa, and C. Ocampo-Martıénez, "Economic model predictive control for energy dispatch of a smart micro-grid system," in *2017 4th International Conference on Control, Decision and Information Technologies (CoDIT)*, IEEE, 2017, pp. 0944–0949.

[72] I. Aldaouab, M. Daniels, and R. Ordóñez, "Model predictive control energy dispatch to optimize renewable penetration for a microgrid with battery and thermal storage," in *2018 IEEE Texas Power and Energy Conference (TPEC)*, IEEE, 2018, pp. 1–6.

[73] A. Parisio, E. Rikos, G. Tzamalis, and L. Glielmo, "Use of model predictive control for experimental microgrid optimization," *Applied Energy*, vol. 115, pp. 37–46, 2014.

[74] A. Khodaei, S. Bahramirad, and M. Shahidehpour, "Microgrid planning under uncertainty," *IEEE Transactions on Power Systems*, vol. 30, no. 5, pp. 2417–2425, 2014.

[75] L. Luo, S. S. Abdulkareem, A. Rezvani, *et al.*, "Optimal scheduling of a renewable based microgrid considering photovoltaic system and battery energy storage under uncertainty," *Journal of Energy Storage*, vol. 28, p. 101 306, 2020.

[76] H. Jahangir, A. Ahmadian, and M. A. Golkar, "Optimal design of stand-alone microgrid resources based on proposed Monte-Carlo simulation," in *2015 IEEE Innovative Smart Grid Technologies-Asia (ISGT ASIA)*, IEEE, 2015, pp. 1–6.

[77] H. Bakhtiari, J. Zhong, and M. Alvarez, "Predicting the stochastic behavior of uncertainty sources in planning a stand-alone renewable energy-based microgrid using Metropolis–coupled Markov chain Monte Carlo simulation," *Applied Energy*, vol. 290, p. 116 719, 2021.

[78] S. S. Singh and E. Fernandez, "Modeling, size optimization and sensitivity analysis of a remote hybrid renewable energy system," *Energy*, vol. 143, pp. 719–731, 2018.

[79] Z. Li, C. Zang, P. Zeng, H. Yu, and H. Li, "Two-stage stochastic programming based model predictive control strategy for microgrid energy management under uncertainties," in *2016 International Conference on Probabilistic Methods Applied to Power Systems (PMAPS)*, IEEE, 2016, pp. 1–6.

[80] S. R. Cominesi, M. Farina, L. Giulioni, B. Picasso, and R. Scattolini, "A two-layer stochastic model predictive control scheme for microgrids," *IEEE Transactions on Control Systems Technology*, vol. 26, no. 1, pp. 1–13, 2017.

[81] A. Parisio and L. Glielmo, "Stochastic model predictive control for economic/environmental operation management of microgrids," in *2013 European Control Conference (ECC)*, IEEE, 2013, pp. 2014–2019.

[82] T. A. Nguyen and M. Crow, "Stochastic optimization of renewable-based microgrid operation incorporating battery operating cost," *IEEE Transactions on Power Systems*, vol. 31, no. 3, pp. 2289–2296, 2015.

[83] NSW Government, *Southern Cotton*, `https://www.industry.nsw.gov.au/development/why-sydney-and-nsw/invest-case-studies/southern-cotton`, 2014.

[84] Cotton Australia, *Australian cotton industry statistics*, `www.cottonaustralia.com.au`, 2018.

[85] A. López-González, B. Domenech, and L. Ferrer-Martıé, "Sustainability and design assessment of rural hybrid microgrids in Venezuela," *Energy*, vol. 159, pp. 229–242, 2018.

[86] A. Mariaud, S. Acha, N. Ekins-Daukes, N. Shah, and C. N. Markides, "Integrated optimisation of photovoltaic and battery storage systems for UK commercial buildings," *Applied energy*, vol. 199, pp. 466–478, 2017.

[87] E. Muh and F. Tabet, "Comparative analysis of hybrid renewable energy systems for off-grid applications in Southern Cameroons," *Renewable energy*, vol. 135, pp. 41–54, 2019.

[88] J. Kitson, S. J. Williamson, P. Harper, *et al.*, "Modelling of an expandable, reconfigurable, renewable DC microgrid for off-grid communities," *Energy*, vol. 160, pp. 142–153, 2018.

[89] A. Naderipour, H. Saboori, H. Mehrjerdi, S. Jadid, and Z. Abdul-Malek, "Sustainable and reliable hybrid AC/DC microgrid planning considering technology choice of equipment," *Sustainable Energy, Grids and Networks*, vol. 23, p. 100 386, 2020.

[90] F. Caballero, E. Sauma, and F. Yanine, "Business optimal design of a grid-connected hybrid PV (photovoltaic)-wind energy system without energy storage for an Easter Island's block," *Energy*, vol. 61, pp. 248–261, 2013.

[91] J. Kumar, B. Suryakiran, A. Verma, and T. Bhatti, "Analysis of techno-economic viability with demand response strategy of a grid-connected microgrid model for enhanced rural electrification in Uttar Pradesh state, India," *Energy*, vol. 178, pp. 176–185, 2019.

[92] Simply Energy, *Demand tariff*, `https://www.simplyenergy.com.au/business/electricity-and-gas/demand-tariff`, 2019.

[93] A. Middelberg, J. Zhang, and X. Xia, "An optimal control model for load shifting–with application in the energy management of a colliery," *Applied energy*, vol. 86, no. 7-8, pp. 1266–1273, 2009.

[94] A. J. Van Staden, J. Zhang, and X. Xia, "A model predictive control strategy for load shifting in a water pumping scheme with maximum demand charges," *Applied Energy*, vol. 88, no. 12, pp. 4785–4794, 2011.

[95] A. Anvari-Moghaddam, A. Rahimi-Kian, M. S. Mirian, and J. M. Guerrero, "A multi-agent based energy management solution for integrated buildings and microgrid system," *Applied energy*, vol. 203, pp. 41–56, 2017.

[96] R. K. Chauhan, C. Phurailatpam, B. Rajpurohit, F. Gonzalez-Longatt, and S. Singh, "Demand-side management system for autonomous DC microgrid for building," *Technology and Economics of Smart Grids and Sustainable Energy*, vol. 2, no. 1, pp. 1–11, 2017.

[97] K. S. El-Bidairi, H. D. Nguyen, S. Jayasinghe, T. S. Mahmoud, and I. Penesis, "A hybrid energy management and battery size optimization for standalone microgrids: A case study for Flinders Island, Australia," *Energy conversion and management*, vol. 175, pp. 192–212, 2018.

[98] J. Radosavljević, M. Jevtić, and D. Klimenta, "Energy and operation management of a microgrid using particle swarm optimization," *Engineering Optimization*, vol. 48, no. 5, pp. 811–830, 2016.

[99] X. Lin and R. Zamora, "Controls of hybrid energy storage systems in microgrids: Critical review, case study and future trends," *Journal of Energy Storage*, vol. 47, p. 103 884, 2022.

[100] Y. Shen, W. Hu, M. Liu, F. Yang, and X. Kong, "Energy storage optimization method for microgrid considering multi-energy coupling demand response," *Journal of Energy Storage*, vol. 45, p. 103 521, 2022.

[101] K. Zhou, S. Wei, and S. Yang, "Time-of-use pricing model based on power supply chain for user-side microgrid," *Applied energy*, vol. 248, pp. 35–43, 2019.

[102] F. Pallonetto, S. Oxizidis, F. Milano, and D. Finn, "The effect of time-of-use tariffs on the demand response flexibility of an all-electric smart-grid-ready dwelling," *Energy and Buildings*, vol. 128, pp. 56–67, 2016.

[103] M. Ruppert, M. Hayn, V. Bertsch, and W. Fichtner, "Impact of residential electricity tariffs with variable energy prices on low voltage grids with photovoltaic generation," *International Journal of Electrical Power & Energy Systems*, vol. 79, pp. 161–171, 2016.

[104] A. Azizivahed, M. Barani, S.-E. Razavi, S. Ghavidel, L. Li, and J. Zhang, "Energy storage management strategy in distribution networks utilised by photovoltaic resources," *IET Generation, Transmission & Distribution*, vol. 12, no. 21, pp. 5627–5638, 2018.

[105] N. J. Williams, P. Jaramillo, and J. Taneja, "An investment risk assessment of microgrid utilities for rural electrification using the stochastic techno-economic microgrid model: A case study in Rwanda," *Energy for Sustainable Development*, vol. 42, pp. 87–96, 2018.

[106] L. K. Gan, J. K. Shek, and M. A. Mueller, "Hybrid wind–photovoltaic–diesel–battery system sizing tool development using empirical approach, life-cycle cost and performance analysis: A case study in Scotland," *Energy Conversion and Management*, vol. 106, pp. 479–494, 2015.

[107] T. Ma, H. Yang, L. Lu, and J. Peng, "Pumped storage-based standalone photovoltaic power generation system: Modeling and techno-economic optimization," *Applied energy*, vol. 137, pp. 649–659, 2015.

[108] J. Lofberg, "YALMIP: A toolbox for modeling and optimization in MATLAB," in *2004 IEEE international conference on robotics and automation (IEEE Cat. No. 04CH37508)*, IEEE, 2004, pp. 284–289.

[109] Australia Government Clean Energy Regulator, *Small-scale systems eligible for certificates*, `http://www.cleanenergyregulator.gov.au/RET/Scheme-participants-and-industry/Agents-and-installers/Small-scale-systems-eligible-for-certificates`, 2019.

[110] Roth, G., Harris, G., Gillies, M., Montgomery, J., & Wigginton, D., "Water-use efficiency and productivity trends in Australian irrigated cotton: a review," *Crop and Pasture Science*, vol. 64(12), pp. 1033–1048, 2013.

[111] NSW Department of Primary Industries, *Example Irrigated Farm Water Use Efficiency Assessment (IFWUEA)*, `http://www.dpi.nsw.gov.au/`, 2016.

[112] NASA Surface meteorology, *NASA Surface meteorology and Solar Energy database*, `https://power.larc.nasa.gov/data-access-viewer/`, 2019.

[113] J. Powell and J. Welsh, *Solar Energy–policy setting and applications to cotton production*, CottonInfo reports and analyses, 2016.

[114] G. Chen, G. Sandell, T. Yusaf, C. Baillie, *et al.*, "Evaluation of alternative energy sources for cotton production in Australia," *Engineers Australia*, 2013.

[115] H. N. Afrouzi, A. Hassan, Y. P. Wimalaratna, *et al.*, "Sizing and economic analysis of stand-alone hybrid photovoltaic-wind system for rural electrification: A case study Lundu, Sarawak," *Cleaner Engineering and Technology*, vol. 4, p. 100 191, 2021.

[116] C. Chen, S. Duan, T. Cai, B. Liu, and G. Hu, "Smart energy management system for optimal microgrid economic operation," *IET renewable power generation*, vol. 5, no. 3, pp. 258–267, 2011.

[117] M. Naz, M. Bou-Rabee, S. Shukrullah, A. Ghaffar, A. Gungor, and S. Sulaiman, "A review of hybrid energy technologies tenets, controls and combinational strategies," *Cleaner Engineering and Technology*, vol. 5, p. 100 340, 2021.

[118] M. Nehrir, B. LaMeres, and V. Gerez, "A customer-interactive electric water heater demand-side management strategy using fuzzy logic," in *IEEE Power Engineering Society. 1999 Winter Meeting (Cat. No. 99CH36233)*, IEEE, vol. 1, 1999, pp. 433–436.

[119] G. McCormick and R. Powell, "Optimal pump scheduling in water supply systems with maximum demand charges," *Journal of water resources planning and management*, vol. 129, no. 5, pp. 372–379, 2003.

[120] J. Maciejowski, P. Goulart, and E. Kerrigan, "Constrained control using model predictive control," in *Advanced strategies in control systems with input and output constraints*, Springer, 2007, pp. 273–291.

[121] G. Li, J. Zhang, and H. He, "Battery SOC constraint comparison for predictive energy management of plug-in hybrid electric bus," *Applied energy*, vol. 194, pp. 578–587, 2017.

[122] W. R. Sultana, S. K. Sahoo, S. Sukchai, S. Yamuna, and D. Venkatesh, "A review on state of art development of model predictive control for renewable energy applications," *Renewable and sustainable energy reviews*, vol. 76, pp. 391–406, 2017.

[123] C. Shang, W.-H. Chen, A. D. Stroock, and F. You, "Robust model predictive control of irrigation systems with active uncertainty learning and data analytics," *IEEE transactions on control systems technology*, vol. 28, no. 4, pp. 1493–1504, 2019.

[124] B. Houska and M. E. Villanueva, "Robust optimization for MPC," in *Handbook of model predictive control*, Springer, 2019, pp. 413–443.

[125] S. V. Raković, "Model predictive control: Classical, robust, and stochastic," *IEEE Control Systems Magazine*, vol. 36, no. 6, pp. 102–105, 2016.

[126] C. E. Garcia, D. M. Prett, and M. Morari, "Model predictive control: Theory and practice—A survey," *Automatica*, vol. 25, no. 3, pp. 335–348, 1989.

[127] J. L. Svensen, C. Sun, G. Cembrano, and V. Puig, "Chance-constrained stochastic MPC of Astlingen urban drainage benchmark network," *Control Engineering Practice*, vol. 115, p. 104 900, 2021.

[128] S. V. Raković, "Robust Model Predictive Control," in *Encyclopedia of Systems and Control*, J. Baillieul and T. Samad, Eds. London: Springer London, 2019.

[129] J. Marquez, A. Zafra-Cabeza, C. Bordons, and M. A. Ridao, "A fault detection and reconfiguration approach for MPC-based energy management in an experimental microgrid," *Control Engineering Practice*, vol. 107, p. 104 695, 2021.

[130] S. Batiyah, R. Sharma, S. Abdelwahed, and N. Zohrabi, "An MPC-based power management of standalone DC microgrid with energy storage," *International Journal of Electrical Power & Energy Systems*, vol. 120, p. 105 949, 2020.

[131] C. Lozoya, C. Mendoza, L. Mejıéa, *et al.*, "Model predictive control for closed-loop irrigation," *IFAC Proceedings Volumes*, vol. 47, no. 3, pp. 4429–4434, 2014.

[132] C. Lozoya, C. Mendoza, A. Aguilar, A. Román, and R. Castelló, "Sensor-based model driven control strategy for precision irrigation," *Journal of Sensors*, vol. 2016, 2016.

[133] J. Passioura, "Increasing crop productivity when water is scarce—from breeding to field management," *Agricultural water management*, vol. 80, no. 1-3, pp. 176–196, 2006.

[134] R. Majumder, B. Chaudhuri, A. Ghosh, R. Majumder, G. Ledwich, and F. Zare, "Improvement of stability and load sharing in an autonomous microgrid using supplementary droop control loop," *IEEE transactions on power systems*, vol. 25, no. 2, pp. 796–808, 2009.

[135] H. Zhang, X. Xia, and J. Zhang, "Optimal sizing and operation of pumping systems to achieve energy efficiency and load shifting," *Electric Power Systems Research*, vol. 86, pp. 41–50, 2012.

[136] J. Foley, "Fundamentals of energy use in water pumping," *Irrigation Australia: The Official Journal of Irrigation Australia*, vol. 31, no. 1, pp. 8–9, 2015.

[137] Australia Government and NSW Department of Planning, Industry and Environment, *Water access licences*, `https://www.industry.nsw.gov.au/water/licensing-trade/licences/types/water-access`, 2021.

[138] F. Gerry, H. David, R. Leigh, and P. Shorten, *VSDs lead irrigation efficiency measures for Gunnedah cropping enterprise*, `https://www.pumpindustry.com.au`, 2013.

[139] NSW Farmers Association, NSW Office of Environment and Heritage, *Solar Powered Pumping Irrigation solutions*, 2015. [Online]. Available: `https://energy.nsw.gov.au/sites/default/files/2018-09/Solar%5C%20powered%5C%20irrigation%5C%20pumping_may-2015.pdf`.

[140] Australian Cotton Awards, *Case Study - Kensal Green*, http://www.australiancottonawards.com/, 2017.

[141] Cotton Research & Development Corporation (CRDC), *Broad Approach to Reducing Energy Costs*, http://www.crdc.com.au, 2015.

[142] Australian Government Bureau of Meteorology, *Daily rainfall- Gunnedah Airport AWS*, http://www.bom.gov.au/jsp/ncc/cdio/weatherData/av?p_nccObsCode=136&p_display_type=dailyDataFile&p_startYear=2016&p_c=-609448493&p_stn_num=055202, 2021.

[143] R. G. Allen, L. S. Pereira, D. Raes, and M. Smith, "Crop evapotranspiration-Guidelines for computing crop water requirements- FAO Irrigation and drainage paper 56," *Food and Agriculture Organization of the United Nations, Rome*, vol. 300, no. 9, p. D05109, 1998.

[144] Agriculture Victoria, *Determining the Evaporative Loss from a Farm Dam*, https://calculator.agriculture.vic.gov.au/fwcalc/information/determining-the-evaporative-loss-from-a-farm-dam, 2021.

[145] Australian Government Bureau of Meteorology, *Evapotranspiration Calculations - Gunnedah Airport*, http://www.bom.gov.au/watl/eto/tables/nsw/gunnedah_airport/gunnedah_airport.shtml, 2021.

[146] Agriculture Victoria, *Seepage Losses from Farm Dams*, https://calculator.agriculture.vic.gov.au/fwcalc/information/seepage-losses-from-farm-dams, 2021.

[147] Australia Government Department of the Environment and Energy, *Electricity feed-in tariff*, https://www.energy.gov.au/rebates/electricity-feed-tariff, 2019.

[148] REAQUA, *500kW Solar Diesel Hybrid Irrigation System.* [Online]. Available: https://reaqua.com.au/project/500kw-solar-diesel-hybrid-irrigation-system/ (visited on 10/24/2021).

[149] REAQUA, *REAQUAs largest solar diesel hybrid pumping system.* [Online]. Available: https://reaqua.com.au/australias-largest-solar-diesel-hybrid-pumping-system-set-to-be-installed/ (visited on 10/25/2021).

[150] K. Stark, *The dusty path to Australia's biggest solar-diesel irrigation system.* [Online]. Available: https://reaqua.com.au/australias-largest-solar-diesel-hybrid-pumping-system-set-to-be-installed/ (visited on 10/25/2021).

[151] J. Elder, *Solar Pumping at 'Waverleigh' Narromine.* [Online]. Available: https://assets.cleanenergycouncil.org.au/documents/events/Renewable-Agg-Conf/Jon-Elder-500kW-solar-diesel-pump.pdf (visited on 10/25/2021).

[152] NSW farmers, *Diesel versus electric pumps.* [Online]. Available: https://www.aginnovators.org.au/sites/default/files/Energy_Irrigation_Variable_speed_drives_on_pumps.pdf (visited on 10/25/2021).

[153] J. Kim, Y. Suharto, and T. U. Daim, "Evaluation of Electrical Energy Storage (EES) technologies for renewable energy: A case from the US Pacific Northwest," *Journal of Energy Storage*, vol. 11, pp. 25–54, 2017.

[154] J. Hu, Y. Shan, J. M. Guerrero, A. Ioinovici, K. W. Chan, and J. Rodriguez, "Model predictive control of microgrids – An overview," *Renewable and Sustainable Energy Reviews*, vol. 136, p. 110 422, 2021.

[155] A. Parisio, E. Rikos, and L. Glielmo, "A model predictive control approach to microgrid operation optimization," *IEEE Transactions on Control Systems Technology*, vol. 22, no. 5, pp. 1813–1827, 2014.

[156] W. Gu, Z. Wang, Z. Wu, Z. Luo, Y. Tang, and J. Wang, "An online optimal dispatch schedule for CCHP microgrids based on model predictive control," *IEEE transactions on smart grid*, vol. 8, no. 5, pp. 2332–2342, 2016.

[157] M. Kaut and S. Wallace, "Evaluation of scenario-generation methods for stochastic programming," *Pacific Journal of Optimization*, vol. 3, Jun. 2003.

[158] K. Høyland and S. W. Wallace, "Generating scenario trees for multistage decision problems," *Management science*, vol. 47, no. 2, pp. 295–307, 2001.

[159] J. Aghaei, T. Niknam, R. Azizipanah-Abarghooee, and J. M. Arroyo, "Scenario-based dynamic economic emission dispatch considering load and wind power uncertainties," *International Journal of Electrical Power & Energy Systems*, vol. 47, pp. 351–367, 2013.

[160] J. Yu, J.-H. Ryu, and I.-b. Lee, "A stochastic optimization approach to the design and operation planning of a hybrid renewable energy system," *Applied energy*, vol. 247, pp. 212–220, 2019.

[161] L. Luo, S. S. Abdulkareem, A. Rezvani, *et al.*, "Optimal scheduling of a renewable based microgrid considering photovoltaic system and battery energy storage under uncertainty," *Journal of Energy Storage*, vol. 28, p. 101 306, 2020.

[162] S. Mohammadi, S. Soleymani, and B. Mozafari, "Scenario-based stochastic operation management of microgrid including wind, photovoltaic, micro-turbine, fuel cell and energy storage devices," *International Journal of Electrical Power & Energy Systems*, vol. 54, pp. 525–535, 2014.

[163] D. Zhu and G. Hug, "Decomposed stochastic model predictive control for optimal dispatch of storage and generation," *IEEE Transactions on Smart Grid*, vol. 5, no. 4, pp. 2044–2053, 2014.

[164] M. Farina, L. Giulioni, and R. Scattolini, "Stochastic linear model predictive control with chance constraints–a review," *Journal of Process Control*, vol. 44, pp. 53–67, 2016.

[165] T. A. N. Heirung, J. A. Paulson, J. O'Leary, and A. Mesbah, "Stochastic model predictive control—how does it work?" *Computers & Chemical Engineering*, vol. 114, pp. 158–170, 2018.

[166] C. Shang and F. You, "A data-driven robust optimization approach to scenario-based stochastic model predictive control," *Journal of Process Control*, vol. 75, pp. 24–39, 2019.

[167] T. Pippia, J. Lago, R. De Coninck, and B. De Schutter, "Scenario-based nonlinear model predictive control for building heating systems," *Energy and Buildings*, vol. 247, p. 111 108, 2021.

[168] C. A. Hans, P. Sopasakis, A. Bemporad, J. Raisch, and C. Reincke-Collon, "Scenario-based model predictive operation control of islanded microgrids," in *2015 54th IEEE conference on decision and control (CDC)*, IEEE, 2015, pp. 3272–3277.

[169] LNesp, *Scenred*, `https://gitlab.com/supsi-dacd-isaac/scenred`, 2003.

[170] N. Growe-Kuska, H. Heitsch, and W. Romisch, "Scenario reduction and scenario tree construction for power management problems," in *2003 IEEE Bologna Power Tech Conference Proceedings,*, IEEE, vol. 3, 2003, 7–pp.

[171] T. Chen and W. Su, "Local energy trading behavior modelling with deep reinforcement learning," *IEEE access*, vol. 6, pp. 62 806–62 814, 2018.

[172] A. Jason, N. Eyre, J. Alexandra, R. Richards, and E. Swann, *The Water & Energy Nexus: A Multi-Factor Productivity Challenge*. 2014.

[173] Geoscience Australia, Canberra, *Australian energy resource assessment. Record 2010.* 2010. [Online]. Available: `https://pid.geoscience.gov.au/dataset/ga/70142`.

[174] NSW Department of Primary Industries, *Comparing running costs of diesel, LPG and electrical pumpsets*, https://www.dpi.nsw.gov.au/__data/assets/pdf_file/0011/665660/comparing-running-costs-of-diesel-lpg-and-electrical-pumpsets.pdf, 2016.

[175] Queensland Government, *Open Data Portal - SILO climate database - evaporation - synthetic*, https://www.data.qld.gov.au/dataset/silo-climate-database-evaporation-synthetic, 2022.